

**Some pages of this thesis may have been removed for copyright restrictions.**

If you have discovered material in AURA which is unlawful e.g. breaches copyright, (either yours or that of a third party) or any other law, including but not limited to those relating to patent, trademark, confidentiality, data protection, obscenity, defamation, libel, then please read our [Takedown Policy](#) and [contact the service](#) immediately

CONTRAST SENSITIVITY FOR COMPLEX AND RANDOM GRATINGS

OUTI IRENE UKKONEN

Doctor of Philosophy

THE UNIVERSITY OF ASTON IN BIRMINGHAM

May 1995

This copy of the thesis has been supplied on condition that anyone who consults it is understood to recognise that its copyright rests with its author and that no quotation from the thesis and no information derived from it may be published without proper acknowledgement.

The University of Aston in Birmingham

## CONTRAST SENSITIVITY FOR COMPLEX AND RANDOM GRATINGS

Outi Irene Ukkonen  
Doctor of Philosophy  
May 1995

### *Summary*

This thesis studied the effect of (i) the number of grating components and (ii) parameter randomisation on root-mean-square (r.m.s.) contrast sensitivity and spatial integration.

The effectiveness of spatial integration without external spatial noise depended on the number of equally spaced orientation components in the sum of gratings. The critical area marking the saturation of spatial integration was found to decrease when the number of components increased from 1 to 5-6 but increased again at 8-16 components. The critical area behaved similarly as a function of the number of grating components when stimuli consisted of 3, 6, or 16 components with different orientations and/or phases embedded in spatial noise. Spatial integration seemed to depend on the global Fourier structure of the stimulus. Spatial integration was similar for sums of two vertical cosine or sine gratings with various Michelson contrasts in noise. The critical area for a grating sum was found to be a sum of logarithmic critical areas for the component gratings weighted by their relative Michelson contrasts.

The human visual system was modelled as a simple image processor where the visual stimuli is first low-pass filtered by the optical modulation transfer function of the human eye and secondly high-pass filtered, up to the spatial cut-off frequency determined by the lowest neural sampling density, by the neural modulation transfer function of the visual pathways. The internal noise is then added before signal interpretation occurs in the brain. The detection is mediated by a local spatially windowed matched filter. The model was extended to include complex stimuli and its applicability to the data was found to be successful.

The shape of spatial integration function was similar for non-randomised and randomised simple and complex gratings. However, orientation and/or phase randomisation reduced r.m.s. contrast sensitivity by a factor of  $\sqrt{2}$ . The effect of parameter randomisation on spatial integration was modelled under the assumption that human observers change the observer strategy from cross-correlation (i.e., a matched filter) to auto-correlation detection when uncertainty is introduced to the task. The model described the data accurately.

### *Keywords*

Complex gratings  
Spatial integration  
Parameter randomisation  
Human image processing

## ACKNOWLEDGEMENTS

This work was carried out in the Department of Vision Sciences, University of Aston, and I thank the Head of Department, Mr Derek Barnes, and the personnel in the department for their help during this project.

I wish to thank my supervisor Dr Jyrki Rovamo for his support and continuous enthusiasm, Dr Risto Näsänen for his technical knowledge and useful discussions, my colleagues for their patient participation in the experiments, Nick Scott-Samuel for his technical advice and my family for their support.

The financial support from the Ministry of Education, the Association of Finnish Ophthalmic Opticians, the National Agency of Health and Welfare in Finland, the Association of Optometry in Finland, Iivari Smolander Foundation, and the Lions Club Tuusniemi is gratefully acknowledged.

## LIST OF CONTENTS

1.	INTRODUCTION	11
2.	GENERAL METHODS	15
2.1	<i>Apparatus 1</i>	15
2.1.1	Luminance response of the monitor	17
2.1.2	Contrast response of the monitor	18
2.2	<i>Apparatus 2</i>	19
2.3	<i>Apparatus 3</i>	19
2.4	<i>Stimulus generation</i>	20
2.5	<i>Threshold determination</i>	21
2.5.1	Staircase routine	22
2.6	<i>Additional calculations</i>	24
2.6.1	R.m.s. contrast and contrast energy threshold	24
2.6.2	Spectral density of external noise	26
2.6.3	Physical signal-to-noise ratio	28
2.6.4	Detection efficiency	30
2.6.5	Spectral density of equivalent noise	31
2.6.6	Goodness of fit	32
3.	MODELLING CONTRAST SENSITIVITY	34
3.1.	<i>Detection of visual signals known exactly</i>	35
3.2.	<i>Modelling contrast sensitivity and the energy threshold</i>	38
3.2.1.	Contrast sensitivity as a function of grating area	38
3.2.2.	Contrast energy threshold as a function of spatial frequency	41
3.3.	<i>Describing contrast sensitivity for a sum of orientations</i>	42

3.4.	<i>Describing contrast sensitivity for a sum of two spatial frequencies</i>	44
3.5.	<i>Detection of random visual signals</i>	46
4.	SPATIAL INTEGRATION	51
4.1	<i>Introduction</i>	51
4.1.1	Spatial integration for simple gratings without external spatial noise	51
4.1.2	Spatial integration for simple gratings with external spatial noise	53
4.1.3	Spatial integration for complex gratings	54
4.2	<i>Complex gratings with various orientation components without noise</i>	56
4.2.1	Introduction	56
4.2.2	Methods	57
4.2.3	Results	60
4.2.4	Discussion	70
4.3	<i>Complex gratings with various orientation components in noise</i>	74
4.3.1	Introduction	74
4.3.2	Methods	75
4.3.3	Results	82
4.3.4	Discussion	93
4.4	<i>Complex gratings with two spatial frequencies in noise</i>	95
4.4.1	Introduction	95
4.4.2	Methods	96
4.4.3	Results	101
4.4.4	Discussion	109
4.5	<i>Conclusions</i>	111

5.	PARAMETER UNCERTAINTY	113
5.1	<i>Introduction</i>	113
5.2	<i>Uncertainty of spatial location</i>	115
5.2.1	Introduction	115
5.2.1	Methods	117
5.2.3	Results	124
5.2.4	Discussion	135
5.3	<i>Uncertainty of orientation and/or phase</i>	139
5.3.1	Introduction	139
5.3.2	Methods	141
5.3.3	Results	146
5.3.4	Discussion	154
5.4	<i>Conclusions</i>	156
6.	OVERALL CONCLUSION	159
	PUBLICATIONS AND PRESENTATIONS	161
	REFERENCES	166
	APPENDIX 1	179

## LIST OF FIGURES

Figure 2.1	A typical pattern of trials for one threshold measurement	23
Figure 3.1	Model of the human visual system	35
Figure 4.1	The stimuli used in the experiments of Section 4.2	58
Figure 4.2	R.m.s. contrast sensitivity as a function of grating area at 0.25 c/deg	61
Figure 4.3	R.m.s. contrast sensitivity as a function of grating area at 1 c/deg	62
Figure 4.4	R.m.s. contrast sensitivity as a function of grating area at 4 c/deg	63
Figure 4.5	The critical area as a function of the number of components	65
Figure 4.6	The maximum contrast sensitivity as a function of the number of components	66
Figure 4.7	Energy threshold as a function of the normalised grating area	67
Figure 4.8	The estimates of $E_0$ as a function of spatial frequency	68
Figure 4.9	The estimates of $S_{\max}^{-2}A_c$ as a function of the number of components	69
Figure 4.10 A	Cosine, sine, and cosine+sine stimuli used in the experiments of Section 4.3.	77
Figure 4.10 B	Random orientation, random phase, and random orientation+phase stimuli used in the experiments of Section 4.3	78
Figure 4.11	R.m.s. contrast sensitivity as a function of the number of square cycles for sums of 3 simple gratings	83
Figure 4.12	R.m.s. contrast sensitivity as a function of the number of square cycles for sums of 6 simple gratings	84
Figure 4.13	R.m.s. contrast sensitivity as a function of the number of square cycles for sums of 16 simple gratings	85
Figure 4.14	The critical number of square cycles as a function of the number of components	87

Figure 4.15	The values of $S_{\max}^2 N_e f^2$ as a function of the stimulus type	88
Figure 4.16	Efficiency as a function of the number of square cycles for 3 components	90
Figure 4.17	Efficiency as a function of the number of square cycles for 6 components	91
Figure 4.18	Efficiency as a function of the number of square cycles for 16 components	92
Figure 4.19	The stimuli in the experiments of Section 4.4.	97
Figure 4.20 A-B	R.m.s. contrast sensitivity as a function of grating area for sums of two spatial frequency components in cosine or sine phase	101
Figure 4.20 C-E	R.m.s. contrast sensitivity as a function of grating area for sums of two spatial frequency components in cosine or sine phase	102
Figure 4.21	The critical area as a function of the relative contrast of the third harmonic	104
Figure 4.22	The maximum sensitivity as a function of the relative contrast of the third harmonic	105
Figure 4.23	Normalised r.m.s. contrast sensitivity for sums of two spatial frequency components added in cosine or sine phase as a function of square cycles for grating sums	106
Figure 4.24	Energy threshold as a function of the number of square cycles for grating sums	107
Figure 4.25	Efficiency as a function of the number of square cycles for grating sums	108
Figure 5.1	The stimuli of the experiments in Figures 5.4 and 5.5	118
Figure 5.2	Examples of the stimuli used in the experiments of Figures 5.6 - 5.8	119

Figure 5.3	Examples of the stimuli used in the experiments of Figures 5.9 - 5.11	120
Figure 5.4	R.m.s. contrast sensitivity for non-randomised and randomised gratings in noise as a function of exposure duration in spatial location uncertainty experiment in peripheral vision	124
Figure 5.5	Physical signal-to-noise ratio for non-randomised and randomised gratings as a function of exposure duration in spatial location uncertainty experiment in peripheral vision	125
Figure 5.6	R.m.s. contrast sensitivity for randomised gratings with and without noise as a function of randomisation range of spatial location in foveal vision	127
Figure 5.7	Physical signal-to-noise ratio as a function of randomisation range of spatial location in foveal vision	128
Figure 5.8	Equivalent noise as a function of randomisation range of spatial location in foveal vision	129
Figure 5.9	R.m.s. contrast sensitivity with and without noise as a function of randomisation range of aperture orientation at 0.5, 2, and 8 c/deg	131
Figure 5.10	Physical signal-to-noise ratio as a function of randomisation range of aperture orientation at 0.5, 2, and 8 c/deg	133
Figure 5.11	Equivalent noise as a function of randomisation range of aperture orientation at 0.5, 2, and 8 c/deg	134
Figure 5.12	The stimuli used in the experiments of Section 5.3	142
Figure 5.13	R.m.s. contrast sensitivity as a function of square cycles for non- randomised and randomised 1 component gratings at 0.5 c/deg	146
Figure 5.14	R.m.s. contrast sensitivity as a function of square cycles for non- randomised and randomised 1 component gratings at 2 c/deg	147

Figure 5.15	R.m.s. contrast sensitivity as a function of square cycles for non-randomised and randomised 1 component gratings at 8 c/deg	148
Figure 5.16	R.m.s. contrast sensitivity as a function of square cycles for non-randomised and randomised 4 component gratings at 0.5 c/deg	149
Figure 5.17	R.m.s. contrast sensitivity as a function of square cycles for non-randomised and randomised 4 component gratings at 2 c/deg	150
Figure 5.18	R.m.s. contrast sensitivity as a function of square cycles for non-randomised and randomised 4 component gratings at 8 c/deg	151
Figure 5.19	R.m.s. contrast sensitivity as a function of square cycles for non-randomised and randomised 16 component gratings at 0.5 c/deg	152
Figure 5.20	R.m.s. contrast sensitivity as a function of square cycles for non-randomised and randomised 16 component gratings at 2 c/deg	153
Figure 5.21	R.m.s. contrast sensitivity as a function of square cycles for non-randomised and randomised 16 component gratings at 8 c/deg	154

## 1. INTRODUCTION

During the last 25 years or so a popular way to describe the human visual system has been a multiple channel model, where the visual processing occurs in a large number of parallel channels (e.g. Campbell & Robson, 1968; Sach, Nachmias & Robson, 1971). Each channel is selectively sensitive to a limited range of spatial frequencies and orientations. One channel is represented by an array of filters whose receptive fields have a given type and they are distributed across the visual field. In the early versions of the model the output of the filters is passed to a threshold device which only responds if the output of one of the filters reaches a pre-determined threshold level. The subject reports the presence of the stimulus if any threshold device is activated.

The multiple channel model also takes into account the fact that stimulus information can be carried on more than one channel, for example when the spatial extent of the stimulus exceeds the receptive field of one filter and it excites several adjacent filters in different parts of the visual field. The statistical procedure of probability summation (e.g. Graham, 1989) is then used to combine the output of the filters. Probability summation means that when the number of stimulated filters and channels increases the probability that one of them exceeds the pre-determined threshold level increases.

There is a large amount of physiological evidence that these selectively sensitive cells exist in the primate visual cortex (e.g. Hubel & Wiesel, 1962; Movshon, Thompson & Tolhurst, 1978; De Valois, Albrecht & Thorell, 1982). Despite of all the evidence, it is nowadays a common view that the multiple channel model is as such too rigid to explain human detection performance. For example, the multiple channel model assumes that uncertainty of the stimulus parameters does not affect the performance. Studies concerning uncertainty have widely shown that uncertainty of the stimulus parameters decreases human performance (e.g. Lappin & Uttal, 1976; Burgess & Ghandeharian, 1984a, b). The

channels are now regarded as performing a preliminary coding of the signal and they are considered a convenient means of transmitting the visual information to the higher levels in the human brain (Burgess, 1990).

The human visual system is today seen as an image processing device followed by adaptive mechanisms, obtained by neural learning, which can use prior signal information. The model of Rovamo, Luntinen, and Näsänen (1993b) is based on the above idea. Visual signals, which can be embedded in external spatial noise, are first low-pass filtered by the optical modulation transfer function of the human eye (e.g. Campbell & Gubish, 1966; Santamaria, Artal & Bescos, 1987, Deeley, Drasdo & Charman, 1991) and subsequently high-pass filtered by the neural visual pathways reflecting the effects of lateral inhibition (e.g. Schade, 1956; Rovamo, Mustonen & Näsänen, 1995). After these filtering processes, internal neural noise is added to the signal (e.g. Barlow, 1956; Pelli 1981) before image interpretation occurs in the brain. At the image interpretation stage internal neural noise causes uncertainty, which is due to the difficulty in deciding whether the detected signal contains the visual signal or only noise. In the model (Rovamo et al., 1993b) the signal detection is mediated by the local matched filter (Hauske, Wolf & Lupp, 1976) whose sampling aperture, i.e. the area from which visual information is collected, has an upper limit (Burgess, 1990). This means that the human visual system is able to integrate visual information over only a limited area. Contrast sensitivity as a function of grating area thus increases up to the critical area and remains constant thereafter and this is due to a process called spatial integration (e.g. Savoy & McCann, 1975; Howell & Hess, 1978; Schober & Hilz, 1963; Virsu & Rovamo, 1979). The critical area which marks the saturation of spatial integration is signal dependent.

One of the aims of this thesis is to extend the above model (Rovamo et al., 1993b) by studying spatial integration for more complex spatial stimuli than simple sinusoidal gratings. Chapter 4 concentrates on how different complex stimuli with and without spatial noise affect spatial integration. All results in this thesis are expressed in terms of root-

mean-square (r.m.s.) contrast sensitivity, because this contrast sensitivity measure takes into account the random luminance distribution of complex stimuli; i.e. a complex stimulus has a vast number of intermediate luminances in addition to peak ones. The widely used Michelson contrast sensitivity which only takes into account the peak luminances of the stimulus does not describe complex stimuli accurately. Suprathreshold studies concerning complex stimuli have shown that the perceived contrast is described by r.m.s. contrast rather than by Michelson contrast (Moulden, Kingdom & Gatley, 1990; Tiippana, Näsänen & Rovamo, 1994).

Human performance is limited by the total noise in the visual system. Noise can be internal neural noise, external light-dependent noise, or external added spatial noise. The dominant source of noise varies in different conditions. At low luminance levels the magnitude of quantal (light-dependent) noise exceeds the magnitude of internal neural noise and unless the magnitude of external noise is sufficiently high human performance is limited by quantal noise. At high luminance levels without added external noise the magnitude of internal neural noise dominates over quantal noise. It has been shown that in absence of external noise contrast energy thresholds at high luminance levels are determined by internal neural noise (e.g. Pollen & Roehrig, 1970; Pelli, 1981; van Meeteren & Valeton, 1988). When the magnitude of external noise exceeds the magnitudes of other noise sources, external noise becomes the primary source of noise limiting the human performance.

The magnitude of noise is expressed by its spectral density, and when the magnitude is constant at all spatial frequencies the external noise is considered to be white. In the experiments of this thesis only white external spatial noise is used, which is due to the fact that the signal-to-noise ratio can be precisely defined as the square root of the ratio between the contrast energy threshold and the spectral density of external noise only if external noise is white. The spectral density of external noise has to exceed a certain value before it has any effect on the contrast energy threshold. Nagaraja (1964) showed that at low

spectral densities of external noise the contrast energy threshold remained constant, and it only started to increase in proportion to spectral density after it had exceeded the critical value. This finding implies that the signal-to-noise ratio is constant at threshold.

Chapter 5, the second major part of this thesis, concentrates on the effect of parameter randomisation on r.m.s. contrast sensitivity for simple and complex gratings with and without external spatial noise. It is a widely reported fact that signal parameter uncertainty ranging from spatial frequency to motion direction uncertainty decreases the detectability of simple stimuli (e.g. Burgess, 1985). The main reason to investigate the parameter uncertainty was that no references for the uncertainty effects on complex gratings were found. It is also unknown whether parameter randomisation affects the sampling aperture (Burgess, 1990) from which the contrast energy is collected and summed. For example, when the orientation or the phase of a simple grating is randomised it produces a change in the orientation or location of bars leaving the one-dimensional luminance distribution undisrupted. However, in a compound grating, the randomisation changes the internal structure of the grating by breaking down the original relationships between components, thus creating a completely new grating with a different appearance. Spatial integration for simple and compound gratings could therefore be affected differently by parameter randomisation.

The effect of parameter randomisation on spatial integration for simple and compound gratings was modelled under the assumption that human observers change the observer strategy from cross-correlation to auto-correlation detection when parameter uncertainty is introduced to the task (Kersten, 1983; Burgess & Ghandeharian, 1984b; Howard & Richardson, 1988). Both detectors are equally good at collecting contrast energy, but an auto-correlation detector is not as efficient at rejecting noise as a cross-correlator.

## 2. GENERAL METHODS

### 2.1 APPARATUS 1

Apparatus 1 was composed of a high-resolution 16 in. RGB monitor (Eizo Flexscan 9080i with a fast phosphor B22) and a VGA graphics board (Orchid's Pro Designer VGA plus) driven by an ALR Business Veisa 486/33 computer. The monitor could show 1280 x 800 pixels but the graphics board was used in a mode which only generated 640 x 480 pixels. The pixel size of 0.042 cm x 0.042 cm and the frame rate of 60 Hz enabled measurements at an adequate resolution in space and time. The monitor was used in the white mode. The average photopic luminance was set to 50 cd/m<sup>2</sup> and it was measured with a Minolta Luminance meter LS-110. The CIE 1931 (x, y) chromaticity coordinates of the display were (0.30, 0.31) measured with a Bentham spectroradiometer.

A VGA board can show 256 colours (8 bits) simultaneously from a palette of 262,144 colours (6+6+6 = 18 bits). The colour index value (0-255) corresponds to a certain combination of three colour channels. The index values are stored in the look up table (LUT) which provides the information about the index values and their corresponding colour channel combinations to the graphics board. Each of the three colour channels has a digital to analog converter (DAC) which transforms a digital signal to an analog one i.e. a numerical signal is transformed to electrical voltage. For one colour channel the maximum number of intensity, i.e. grey, levels is only 64 (6 bits).

A monochrome signal of 1,024 intensity levels (10 bits) available from a range of 65,536 intensity levels (4+4+6+2 = 16 bits) was obtained in the following way: the red, green, and blue outputs of the VGA board were combined by using a video summation device built according to Pelli and Zhang (1991). The green output was attenuated by a

factor of 1/13 and the blue by a factor of 1/182 in comparison to the red output and the attenuation was done by using suitable resistors. In order to obtain a single monochrome signal all the outputs were added together and as a result, an 8-bit signal from the palette of 14 bits (4+4+6) was produced. Only the four significant bits were used for red and green colour guns to avoid distortion in the contrast response caused by inaccurate voltages. The distortion in the contrast response decreases the more the output of the channel is attenuated. Because the blue gun was the most attenuated channel, it was safe to use its whole capacity (6 bits).

Two additional bits were obtained by adding a periodic dither signal to the visual image before intensity quantization (Näsänen, Kukkonen & Rovamo, 1993). If the size and the contrast of a periodic dither signal is kept small it is possible to increase the number of grey levels without the masking effect of the dither signal. The size of the dither was 2x2 pixels leading to the lowest spatial frequency of 11.9 c/cm on the screen which is 2.6 octaves higher than the highest spatial frequency of 2 c/cm used in the experiments of this thesis. The amplitude of the dither signal equals the amplitude of one step produced by a summation device. The contrast of the dither decreases with the contrast of the stimulus and, on the other hand, the amplitude of the dither increases with the luminance level.

The dither signal was  $d(0,0) = 0$ ,  $d(0,1) = 0.75$ ,  $d(1,0) = 0.5$ ,  $d(1,1) = 0.25$ . The dither increased the number of grey levels by four. The dithering algorithm was

$$g_q(x,y) = \text{int}[g(x,y) + d(x,y)] , \quad (2.1)$$

where  $\text{int}[\cdot]$  denotes rounding to the nearest integer,  $g_q(x,y)$  is the quantized signal with dither,  $g(x,y)$  is the continuous luminance signal, and  $d(x,y)$  is the dither signal.

The monochrome signal was connected to the red output and a switch in the monitor changed the colour of the monitor to white. The 10 bit signal within the range of 16 bits allowed measurements of contrast sensitivity for simple sinusoidal gratings consisting of

about 37 grey levels at a Michelson contrast of 0.001, which was the lowest contrast used in the experiments of this thesis (see Section Luminance Response of the Monitor for further details).

Apparatus 1 was used in the experiments described in Sections 4.2 and 5.3, and partly in the experiments of Sections 4.3, 4.4 and 5.2.

### 2.1.1 Luminance response of the monitor

The luminance response of the monitor in the white mode was measured with a Minolta Luminance Meter LS-110 as a function of 6-bit index values (0-63). The experimentally measured luminance increased from about 0.01 cd/m<sup>2</sup> to about 100 cd/m<sup>2</sup> when the index value increased from 0 to 63. The measured luminance and corresponding index values were plotted in double logarithmic coordinates in order to find a function to describe this relationship. The luminance response for Apparatus 1 was of form  $L(I) = 0.005298 I^{2.409}$ , where  $L$  is the luminance in cd/m<sup>2</sup> and  $I$  is the index value. As the luminance response of the display is non-linear, the gamma-correction was performed by using the inverse of the luminance response function  $I = (L(I) / 0.005298)^{1/2.409}$  when computing the stimulus images. In order to produce as accurate stimuli as possible it is necessary to choose the luminance range where the gamma-correction is most precise. Therefore, the mean luminance was set at 50 cd/m<sup>2</sup>, which was about in the middle of the linear luminance range of the display.

The luminance response of the monitor is described by the function  $L(I) = 0.005298 I^{2.409}$  when it is sampled with 64 index values (0-63). The total number of luminance steps in the 14 bit system is, however, 16,384 (14 bits). This means that each 64 step comprises 256 additional luminance steps. In order to calculate the total number of luminance steps in the 14 bit system, the function  $L(I) = 0.005298 I^{2.409}$  is transformed to  $L(I_e) = 0.005298 (I_e/256)^{2.409}$ , where  $I_e$  is the extended index value. We use the extended

gamma-function to estimate the total number of luminance steps: if we have the stimulus contrast of 0.001 at the mean luminance of 50 cd/m<sup>2</sup>, we first need to calculate the index values for the maximum (50.05 cd/m<sup>2</sup>) and the minimum (49.95 cd/m<sup>2</sup>) luminances. The extended index values ( $I_e$ ) were 11,439 for the maximum and 11,430 for the minimum luminance. Thus, there were 9 luminance levels which were produced using the summation box (Pelli & Zhang, 1991). The dither used added 3 more steps between each step and the total number of luminance levels was therefore 37. The number of grey levels increased at higher Michelson contrasts, reaching 1,024 at and above a Michelson contrast of 0.027. The number of grey levels was large enough to produce sinusoidal waveform with sufficiently small quantization errors at all Michelson contrasts used.

### **2.1.2 Contrast response of the monitor**

The contrast response of the monitor was measured for six sinusoidal gratings at spatial frequencies from 0.25 to 4 c/deg with a Minolta Luminance Meter LS-110. Three orientations (0°, 45°, and 90°) were tested and two contrast levels (0.1 and 0.5) were used. For each grating the minimum and maximum luminance was obtained by changing the phase of the grating from 0 degrees (maximum) to 180 degrees (minimum) and the luminance values were measured separately. At least three measurement of both luminances were recorded and their average provided the measured contrast of the displayed grating.

The measured contrast remained at first equal to the requested contrast as a function of spatial frequency. The contrast was independent of orientation and spatial frequency up to 2 c/cm, which was the highest spatial frequency used in the experiments of this thesis.

## 2.2 APPARATUS 2

Apparatus 2 consisted of a high-resolution 16" RGB monitor (Eizo Flexscan 9080i with a fast phosphor B22) and a VGA graphics board (Orchid's Pro Designer VGA plus) driven by a Dell PC-586 computer. The only differences between Apparatus 2 and Apparatus 1 were the attenuation factor for the blue colour gun, the pixel size and the luminance response of the display.

In order to display a monochrome signal of 1,024 intensity levels the red, green, and blue outputs of the VGA board were combined in the same way as described in Apparatus 1. In Apparatus 2 the blue output was attenuated by a factor 1/166 in comparison to the red output instead of the attenuation of 1/182 in Apparatus 1. The pixel size was 0.415 mm x 0.415 mm in Apparatus 2. The luminance response of the display was  $L(I) = 0.01176 I^{2.271}$  and the extended gamma-function was of form  $L(I_e) = 0.01176 (I_e/256)^{2.271}$ . At a contrast of 0.001 the extended index values for the maximum (50.05) and minimum (49.95) luminances were 10,144 and 10,135, respectively. The summation box thus produced 9 luminance levels and the total number of grey levels was 37. The number of grey levels was 1,024 at and above a Michelson contrast of 0.029.

All the other details in Apparatus 2 were the same as in Apparatus 1. Apparatus 2 was partly used in the experiments described in Sections 4.3 and 4.4.

## 2.3 APPARATUS 3

Apparatus 3 consisted of a high-resolution 16" RGB monitor (Eizo Flexscan 9070S), a VGA graphics board (Orchid's Pro Designer VGA plus) and a WYSE PC-386 computer.

Apparatus 3 had a different colour channel summation method, luminance response of the display, and number of grey levels compared to Apparatus 1.

To obtain a monochrome signal of 1,024 (10 bits) from a monochrome palette of 16,384 (6+6+2 = 14 bits), only the red and green outputs were added together. The green output of the VGA board was first attenuated by a factor of 1/64 and added to the red output. The sum was then fed to the red input of the display. The operation thus provided an 8-bit signal from a monochrome palette of 4,096 (6+6 = 12 bits) intensity levels. This means that each 64 step comprises 64 additional luminance steps. The luminance response of the display was  $L(I) = 0.177 (I-12)^{1.69}$  and the extended gamma-function was  $L(I_e) = 0.177 \left( \frac{I_e}{64} - 12 \right)^{1.69}$ . At a contrast of 0.001 the extended index values for the maximum (50.05) and minimum (49.95) luminances were 1,818 and 1,815, respectively. The summation box thus produced 3 luminance levels and the total number of grey levels was 13. The number of grey levels was 1,024 at and above a Michelson contrast of 0.12.

Apparatus 3 was partly used in the experiments described in Section 4.2.

## 2.4 STIMULUS GENERATION

Risto Näsänen developed the software which was used to create the stimuli. The software utilised the graphics subroutine library of a Professional HALO 2.0 developed by Media Cybernetics.

The stimuli were drawn on the screen with coordinates (x, y) varying between (0, 0) and (639, 479). The maximum diameter of the stimulus obtainable was 16 cm.

The required stimuli were stored on the hard disk of the computer. In order to equalise the search times of the required stimuli they were copied to the fast RAM disk which is part of the main 16 MB memory. The stimuli was returned to the VGA frame buffer upon

request. The stimulus was switched on and off by changing the colour look-up table during the vertical retrace period of the display.

### **2.5. THRESHOLD DETERMINATION**

The value at which the stimulus can be just detected is known as the detection threshold. In order to determine the contrast detection threshold the observer is shown the stimulus at different contrast levels and her/his correct responses can be plotted as a function of the variable (i.e. contrast). The probability of correct responses changes gradually as a function of the value and the ogive-shaped function is called a psychometric function. The probability of a correct answer increases up to 100 percent correct as the contrast increases. The threshold is thus determined as a value which produces a certain percentage of correct responses.

The detection thresholds in this thesis were determined by a forced-choice algorithm with a staircase routine. The used algorithm was a two-interval force-choice algorithm where the stimulus (e.g. signal+noise) and the comparison stimulus (e.g. noise alone) were presented in successive exposures. The algorithm produced a minimum of 50% of correct responses.

Each trial thus consisted of two exposures accompanied by sound signals and the observer indicated which exposure contained the stimulus by pressing one of two keys on a computer keyboard. The observer had an unlimited response time. The next trial began 250 msec after the observer's response. Feedback was provided to the observer by a sound signal which indicated the incorrectness of the response. The computer display was the only light source in the room. All the observers were experienced and motivated but usually naive about the aims of the experiments.

### 2.5.1 Staircase routine

The simple up-and-down (UD) rule means that one correct response reduces and one incorrect response increases the stimulus contrast by one step. The step size is constant. When e.g. two-interval forced-choice algorithm is used the 1-1 UD rule produces the same probability level of correct responses (50%) as pure guessing. When the number of incorrect responses is kept constant at one and the number of correct responses is varied, the probability of a correct response at any probability level  $x$  follows a function  $x^n = 0.50$ , where  $n$  is the number of required correct responses. The probability level is determined by the number of required correct responses

$$x = \sqrt[n]{0.5} . \quad (2.2)$$

The up-and-down transformed response (UDTR) rule introduced by Wetherill and Levitt (1965) is a modification of the simple UD rule, and was used to determine the contrast thresholds in this thesis. The UDTR rule allows us to change the level of probability by varying either the number of correct or incorrect responses or both. The UDTR rule in the thesis was used in a mode where four consecutive correct responses were needed to reduce the level of stimulus contrast by one step and one incorrect response increased the contrast level. According to equation 2.2 the probability of 0.84 ( $\sqrt[4]{0.50}$ ) was obtained. The size of one step was  $0.1 \log_{10}$  units.

The threshold determination happened in two consecutive phases in order to avoid the effect of the starting contrast on the threshold. The first phase started well above the threshold as we wanted to eliminate stimulus uncertainty. During the first phase each correct response reduced the stimulus contrast by  $0.1 \log_{10}$  units. The first incorrect response increased the contrast but it was not recorded as one of the turning points on which the threshold was based. The first phase continued until the second incorrect

response took place and it started the second and the final phase of the threshold determination.

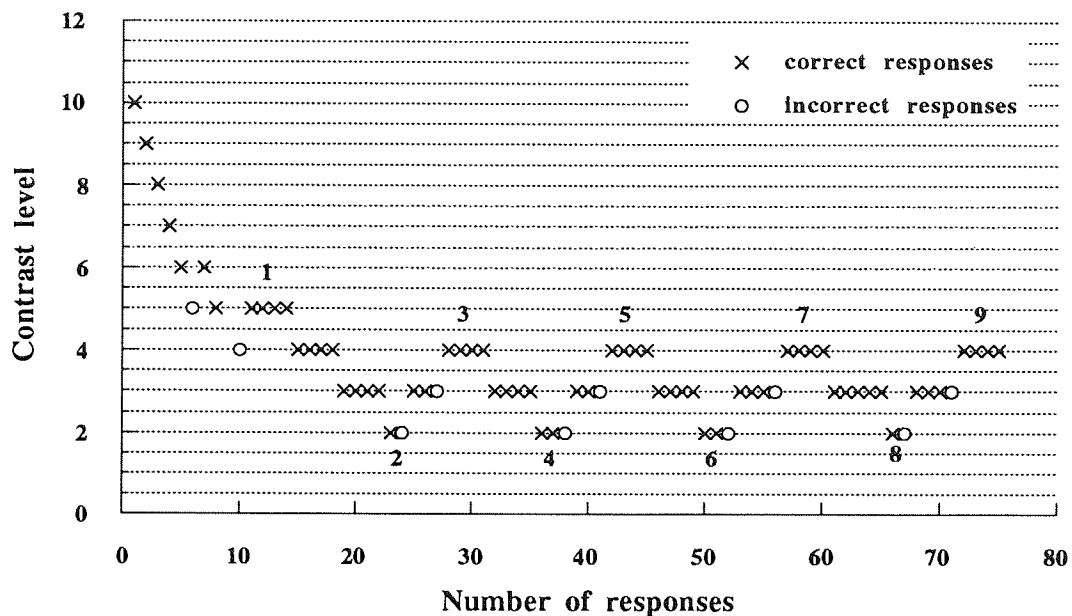


Figure 2.1. A typical pattern of trials for one threshold measurement.

During the final phase the 1-4 UDTR rule was applied. Four consecutive correct responses were needed to reduce the contrast level by one step and one incorrect response increased the contrast by the same amount. If the number of correct responses was smaller than four the contrast increased again by one step. The final phase lasted until nine reversals of the direction of the contrast change occurred. Thus, the threshold determination always finished in a sequence of four correct responses. The estimate of the threshold contrast was obtained as the arithmetic mean of eight reversals of the direction. The first reversal was not included in the mean because it could be substantially lower or higher than other reversal values due to the starting point of the final phase. Each data point in the

experiments of the thesis was based on the geometric mean of at least three threshold estimates.

## 2.6 ADDITIONAL CALCULATIONS

### 2.6.1 R.m.s. contrast and contrast energy threshold

Michelson contrast ( $c_{\text{Michelson}}$ ) is one of the most widely used contrast measures in the grating detection experiments of spatial vision. Michelson contrast is by definition

$$c_{\text{Michelson}} = \frac{L_{\text{max}} - L_{\text{min}}}{L_{\text{max}} + L_{\text{min}}}, \quad (2.3)$$

where  $L_{\text{max}}$  is the maximum and  $L_{\text{min}}$  the minimum luminance. Michelson contrast thus takes into account the peak luminances of the stimulus. For a simple periodic stimulus like a sinusoidal grating Michelson contrast is a convenient metric to express the contrast. Using Michelson contrast to express the contrasts for aperiodic stimuli, for example complex or randomised gratings, raises problems. Aperiodic stimuli contain, in addition to peak luminances, many intermediate ones, which Michelson contrast completely ignores. The contrast for aperiodic stimuli is more accurately described by the root-mean-square contrast ( $c_{\text{r.m.s.}}$ ) which is defined as

$$c_{\text{r.m.s.}} = \sqrt{\frac{1}{nm} \sum_{i=0}^{n-1} \sum_{j=0}^{m-1} c^2(i, j)}, \quad (2.4)$$

where the squares of local contrast [c (i,j)] are averaged across the stimulus area. R.m.s. contrast thus includes all the luminance fluctuations across the stimulus area. The local contrast is obtained by

$$c(i,j) = \frac{L(i,j) - L_0}{L_0} , \quad (2.5)$$

where L(i,j) is the local luminance (i.e., contrast) and L<sub>0</sub> is the mean luminance of the screen. R.m.s contrast is thus equal to the standard deviation of the luminance distribution calculated pixel by pixel across the stimulus area and divided by the average luminance. For simple cosine gratings r.m.s. contrast is approximately equal to Michelson contrast divided by  $\sqrt{2}$ .

The contrast energy of gratings was calculated by numerically integrating the square of the contrast waveform c(i,j) of the grating signal

$$E = \sum_{i=0}^{n-1} \sum_{j=0}^{m-1} c^2(i,j) p^2 , \quad (2.6)$$

where c(i,j) indicates the local contrast described in equation 2.4, and p<sup>2</sup> is the area of the image pixel in solid degrees.

The relationship between r.m.s. contrast and contrast energy threshold is thus given by

$$c_{r.m.s.} = \sqrt{\frac{E}{A}} , \quad (2.7)$$

where A = nmp<sup>2</sup> is grating area. The data in this thesis are expressed in terms of r.m.s. contrast sensitivity, which is the inverse of r.m.s. contrast.

### 2.6.2 Spectral density of external noise

Two-dimensional static white spatial noise was used in the experiments of this thesis. Spatial noise which was produced on the computer screen consists of square shaped picture elements called pixels. The luminance varied randomly from one pixel to another and luminances of the neighbouring pixels were uncorrelated. Spatial noise is one- or two-dimensional depending on whether the luminance varies randomly in one or two spatial dimensions. In one-dimensional noise the luminance is constant in one dimension (e.g. individual pixels form a row with the same luminance) and random luminance fluctuations occur in the other dimension (e.g. two neighbouring rows of pixels have a different luminance). In two-dimensional noise each individual pixel has a random luminance. If the luminance of a pixel or a row of pixels varies randomly in time, noise is called dynamic spatio-temporal noise. In static spatial noise the random luminance variations occur only in the spatial dimension.

The magnitude of noise is expressed by spectral density. In theory, noise is considered to be white if the spectral density is constant at all spatial frequencies. In the spatial domain this would require that the pixel size is extremely small and the luminances of the neighbouring pixels are uncorrelated. The Fourier transform of a stimulus impulse has the same value at all spatial frequencies if the spatial size of an impulse is infinitely small. As it is not possible to produce an infinitely small pixel, pixel noise has always a limited bandwidth in practise. The bandwidth depends on the pixel size and, therefore, pixel noise is white at spatial frequencies lower than a cut-off frequency, where the spectral density of noise ceased to be constant.

The spectral density function of one-dimensional static noise can be computed as (e.g. Legge, Kersten & Burgess, 1987)

$$N(f_x) = p_x c_n^2 \left( \frac{\sin[\pi f_x p_x]}{\pi f_x p_x} \right)^2, \quad (2.8)$$

where  $p_x$  is the pixel width in degrees of visual field,  $c_n$  is the r.m.s. contrast of noise,  $f_x$  is the spatial frequency along the horizontal spatial frequency axis.

The spectral density function of two-dimensional noise is an extension of the one-dimensional condition given by

$$N(f_x, f_y) = p_x p_y c_n^2 \left( \frac{\sin[\pi f_x p_x]}{\pi f_x p_x} \right)^2 \left( \frac{\sin[\pi f_y p_y]}{\pi f_y p_y} \right)^2, \quad (2.9)$$

where  $p_x$  and  $p_y$  are the noise pixel width and height, and  $f_x$  and  $f_y$  the spatial frequencies along the horizontal and vertical axis, respectively.

The spectral density function is first constant and then it dies out oscillating according to equations 2.8 and 2.9. The latter part of equation 2.9 approximately equals one at the lowest spatial frequencies

$$\left( \frac{\sin[\pi f_x p_x]}{\pi f_x p_x} \right)^2 \left( \frac{\sin[\pi f_y p_y]}{\pi f_y p_y} \right)^2 \approx 1. \quad (2.10)$$

The noise spectral density function is constant at these low spatial frequencies where pixel noise is, thus, white. Consequently, the spectral density of white two-dimensional pixel noise can be defined with an adequate accuracy

$$N_e = c_n^2 p_x p_y, \quad (2.11)$$

where  $c_n$  is the r.m.s. contrast of noise, and  $p_x p_y$  is the noise pixel area.

### 2.6.3 Physical signal-to-noise ratio

In a signal-known-exactly detection task, the ideal detector is the matched filter (see Chapter 3) which is a template  $[m(x,y)]$  with the signal to be detected. The response at the matched filter is computed as

$$R = \int_{-x/2}^{x/2} \int_{-y/2}^{y/2} m(x,y) s(x,y) dx dy , \quad (2.12)$$

where  $m(x,y)$  is the detection filter and  $s(x,y)$  is the signal. As the matched filter is a replica of the signal, we can thus express equation 2.12 in form

$$R = \int_{-x/2}^{x/2} \int_{-y/2}^{y/2} s^2(x,y) dx dy , \quad (2.13)$$

which equals the energy of the signal ( $E$ ).

Noise causes variance in the response of the detection filter. The spectral density of noise expresses its variance per unit frequency. The variance of the filter ( $\sigma^2$ ) in the presence of white noise can thus be computed as

$$\sigma^2 = N_e \iint |M(u,v)|^2 du dv , \quad (2.14)$$

where  $N_e$  is the spectral density of external noise,  $M(u,v)$  is the Fourier transform of the detection filter. As external noise is white in the experiments of this thesis, its spectral density is constant and thus  $N_e(u,v) = N_e$ . As the matched filter equals the signal, its Fourier transform can be replaced by the Fourier transform of the signal:

$$\sigma^2 = N_e \iint |S(u,v)|^2 du dv , \quad (2.15)$$

where  $S(u,v)$  is the Fourier transform of the signal. According to the Rayleigh's Theorem (Bracewell, 1978)

$$\iint |S(u,v)|^2 du dv = \iint s^2(x,y) dx dy . \quad (2.16)$$

Consequently, by combining equations 2.13, 2.15, and 2.16 we get

$$\sigma^2 = N_e \iint s^2(x,y) dx dy = N_e E . \quad (2.17)$$

According to signal detection theory (Green & Swets, 1966) the signal-to-noise ratio, which is believed to be constant at threshold, determines the detection threshold for any detector. Therefore, the signal-to-noise ratio for the matched filter is defined

$$\frac{R^2}{\sigma^2} = \frac{E^2}{N_e E} = \frac{E}{N_e} = d'^2 . \quad (2.18)$$

As  $E$  is the energy of the signal, it is thus the energy threshold of the matched filter i.e. the ideal detector ( $E_{ideal}$ ) in the experiments of this thesis.

Physical signal-to-noise ratio ( $d' = \text{s.n.r.}$ ) refers to the ratio between signal contrast energy ( $E$ ) and the spectral density of external noise ( $N_e$ )

$$\text{s.n.r.} = \sqrt{\frac{E}{N_e}} . \quad (2.19)$$

### 2.6.4 Detection efficiency

The human performance is limited by the spectral density of the total noise ( $N$ ) in the visual system. If the images are viewed in bright light the spectral density of the total noise consists of internal neural noise ( $N_i$ ) and external spatial noise ( $N_e$ ). The energy threshold ( $E_{\text{human}}$ ) is a sum of internal and external spectral densities weighted by a stimulus dependent constant  $k$

$$E_{\text{human}} = k (N_i + N_e) . \quad (2.20)$$

$E_{\text{human}}$  is equal to  $N_i$  if there is no external noise and  $N_i$  can be replaced by a term  $E_0$ , which is the energy threshold without external noise

$$E_{\text{human}} = E_0 + k N_e . \quad (2.21)$$

If the effect of internal noise is small compared to external noise ( $E_0 \ll N_e$ ) we can ignore the effect of internal noise and write

$$E_{\text{human}} = k N_e . \quad (2.22)$$

The r.m.s. contrast threshold with external noise was always at least 3 times higher than the r.m.s. contrast threshold without noise. Consequently, the energy threshold with noise ( $E_{\text{human}}$ ) was at least 9 times the energy threshold without noise ( $E_0$ ) (see Section 2.6.1.). The error in equation 2.22 is hence maximally 11%.

The detection efficiency ( $\eta$ ) refers to the ratio of the contrast energy thresholds of the ideal ( $E_{\text{ideal}}$ ) and human ( $E_{\text{human}}$ ) observers (Tanner & Birdsall, 1958)

$$\eta = \frac{E_{\text{ideal}}}{E_{\text{human}}} . \quad (2.23)$$

According to equation 2.18  $E_{\text{ideal}} = d'^2 N_e$ . The detectability index ( $d'$ ) is task dependent (Elliot, 1964). The threshold estimates in the two-alternative forced-choice experiments of this thesis correspond to the probability level of 0.84 of correct responses. According to Elliot's (1964) force-choice tables the value of  $d'$  is 1.4 and thus,  $d'$  squared is 2. The energy threshold for the ideal detector is consequently

$$E_{\text{ideal}} = 2N_e . \quad (2.24)$$

Detection efficiency was calculated in the experiments of this thesis by combining equations 2.23 and 2.24

$$\eta = \frac{2N_e}{E_{\text{human}}} , \quad (2.25)$$

where  $E_{\text{human}}$  was determined experimentally.

### 2.6.5 Spectral density of equivalent noise

In the model described in detail in Chapter 3 when there is additive external noise ( $N_e$ ) in the images and they are viewed in bright light, the spectral density of the total noise ( $N$ ) in the visual system consists of internal neural noise ( $N_i$ ) and external spatial noise, i.e.  $N = N_e + N_i$ . When images are viewed in bright light in the absence of external noise the spectral density of the total noise in the visual system is  $N = N_i$ . The spectral density of internal neural noise is expressed in terms of external noise equivalent to internal noise ( $N_{\text{eq}}$ ). Thus, by replacing  $N_i$  with  $N_{\text{eq}}$  the total noise  $N$  in the presence of external noise is

$N_e + N_{eq}$  and in the absence of external noise the total noise (N) in the visual system is  $N_{eq}$ . With and without external spatial noise the signal-to-noise ratio described in equation 2.17 is constant at detection threshold (Cornsweet, 1970; Rovamo, Kukkonen, Tiippana & Näsänen, 1993a)

$$\frac{E}{N_e + N_{eq}} = \frac{E_0}{N_{eq}} , \quad (2.26)$$

where E is the contrast energy threshold with external noise and  $E_0$  the contrast energy threshold without external noise. The spectral density of equivalent noise is thus calculated

$$N_{eq} = \frac{E_0 N_e}{E - E_0} . \quad (2.27)$$

#### 2.6.6 Goodness of fit

We expressed the goodness of the fit of the model to the experimental data by calculating first the root-mean-square (r.m.s.) error on the  $\log_{10}$  scale

$$e_{r.m.s.} = \sqrt{\frac{1}{n} \sum_{i=1}^n (\log_{10} Y_i - \log_{10} Y_{i_{est}})^2} , \quad (2.28)$$

where n is the total number of data points,  $\log_{10} Y_i$  refer to the logarithmic values of the experimental data, and  $\log_{10} Y_{i_{est}}$  the logarithmic value of the corresponding predictions of the model. The goodness of the fit (G) expressed in percentages was then calculated

$$G = 100 \times (1 - [k e_{r.m.s.}]) . \quad (2.29)$$

The value of  $k$  is 1 for contrast sensitivity ( $S$ ), but 0.5 for energy threshold and efficiency because they are proportional to  $S^{-2}$  and  $S^2$ , respectively. The value of  $k$  is also 0.5 for the critical area because it is proportional to the maximum contrast sensitivity squared (Section 4.4.). For contrast sensitivity the goodness of fit is 85%, when the average difference between experimental data points and the fit of least squares is 0.15 logarithmic units, whereas the same goodness of fit is reached when the difference for energy thresholds, efficiencies, and spectral densities of noise is 0.3 logarithmic units.

### 3. MODELLING CONTRAST SENSITIVITY

Visual stimuli, which can be embedded in external spatial noise ( $N_e$ ), are filtered by the ocular optics and neural visual pathways before being interpreted by the human brain. The human visual system can be modelled as an image processor (Rovamo et al., 1993b). It contains the following consecutive stages. Low-pass filtering (i.e. filtering attenuates high spatial frequencies relatively more than low spatial frequencies) is due to the optical modulation transfer function ( $O_{MTF}$ ) of the eye.  $O_{MTF}$  is assumed to contain all the optical attenuation that occurs in the human eye between the front surface of the cornea and the event of quantal absorption in the outer segments of the photoreceptors. Image degradation is mainly caused by ocular aberrations, and intraocular as well as retinal light scatter. The effect of quantal noise ( $N_q$ ) is added at this stage if stimuli are viewed in dim light. Then comes neural high-pass filtering, up to the spatial cut-off frequency determined by the lowest neural sampling density (Rovamo et al., 1995), due to the neural modulation transfer function of the neural visual pathways ( $P_{MTF}$ ).  $P_{MTF}$  attenuates low spatial frequencies relatively more than high spatial frequencies, thus enhancing contours. Addition of internal neural noise ( $N_i$ ) occurs before signal interpretation (detection, discrimination, recognition etc.) takes place in the brain.

In the model the signal is detected by a local matched filter. Its limited sampling aperture is in agreement with the fact that the size of human sampling aperture (i.e., the area from where visual information is collected) seems to have an upper limit (Burgess, 1990) which is signal dependent.

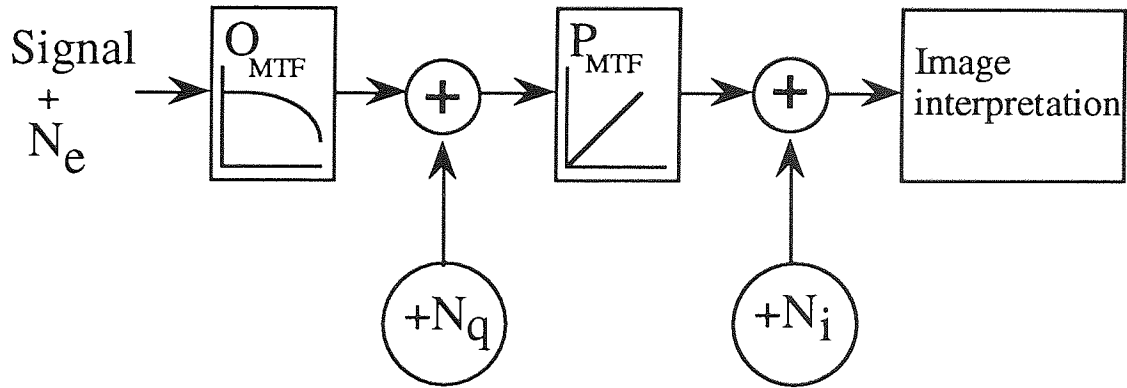


Figure 3.1 Model of the human visual system.

### 3.1 DETECTION OF VISUAL SIGNALS KNOWN EXACTLY

After being filtered by the optical modulation transfer function ( $O_{MTF}$ ) of the eye and neural modulation transfer function ( $P_{MTF}$ ) of the visual pathways, the input to the image interpretation device can be defined as

$$i_1(x, y) = s'(x, y) + n_1(x, y) , \quad (3.1)$$

where  $s'(x, y)$  is the signal  $s(x, y)$  filtered by the eye optics and neural visual pathways and  $n_1(x, y)$  is the spatial component of the white additive internal spatiotemporal neural noise.

On each trial of a two-alternative forced-choice experiment (2AFC) the observer must choose between two exposures: one that contains the contrast signal and another that is blank ( $b(x, y) = 0$ ), because its contrast is zero. If the exposure is blank, the input to the image interpretation device is only

$$i_2(x,y) = n_2(x,y) . \quad (3.2)$$

Let's now assume that the visual stimulus is detected, i.e., discrimination between the two exposures consisting of the signal and blank is mediated by the sampled response of a filter  $h(x,y)$ .

If signal is known exactly (e.g. a stationary grating, whose location, spatial frequency, phase, orientation, and area are known) the detector  $h(x,y)$  is the matched filter, i.e. the replica of the input signal  $s'(x,y)$  (e.g. Hauske et al., 1976). We assume that the detecting filter is created by averaging across several exposures, because a typical 2AFC procedure starts with a signal that is clearly above detection threshold, and thus easily discriminable from the blank exposure.

The sampled responses of the detector  $h(x,y)$  to the two exposures are calculated as

$$R_1 = \iint h(x,y) i_1(x,y) dx dy , \quad (3.3)$$

and

$$R_2 = \iint h(x,y) i_2(x,y) dx dy . \quad (3.4)$$

By combining equations 3.1 and 3.3, and 3.2 and 3.4 we get

$$R_1 = \iint s'(x,y) [s'(x,y) + n_1(x,y)] dx dy , \quad (3.5)$$

and

$$R_2 = \iint s'(x,y) n_2(x,y) dx dy . \quad (3.6)$$

The difference  $\Delta R = R_1 - R_2$  is used as a decision variable by which it is possible to decide which exposure contained the signal: if  $\Delta R > 0$  then the first exposure contained the signal and if  $\Delta R < 0$  then it was the second exposure during which the signal was shown. However, the internal neural noise of the human brain limits the accuracy of the decision. Hence, in order to compute the detection threshold at a desired probability level, we have to take into account the variance ( $\sigma^2$ ) of the mean response difference.

If the signal is known exactly, then the two mean responses are

$$R_1 = \iint s'^2(x,y) + s'(x,y) n_1(x,y) dx dy = \iint s'^2(x,y) dx dy + \iint s'(x,y) n_1(x,y) dx dy , \quad (3.7)$$

and

$$R_2 = \iint s'(x,y) n_2(x,y) dx dy . \quad (3.8)$$

The mean response difference is  $\Delta R = \iint s'^2(x,y) dx dy = E'$  , where  $E'$  is the contrast energy of the filtered signal  $s'(x,y)$ , because the noise terms are reduced to zero when response difference is averaged across several trials. The variance ( $\sigma^2$ ) of each mean response is due to the term  $\left[ \iint s'(x,y) n(x,y) dx dy \right]$  from the two exposures, because  $\iint s'(x,y) n_1(x,y) dx dy$  is approximately equal to  $\iint s'(x,y) n_2(x,y) dx dy$  . The variance is calculated as

$$\sigma^2 = \iint H^2(u,v) N_i(u,v) du dv = N_i \iint S'^2(u,v) du dv = N_i E' , \quad (3.9)$$

where  $N_i(u,v)$  is the variance (spectral density) of internal neural noise in the Fourier space, and  $H(u,v) = S'(u,v)$  is the Fourier transform of the detection filter (the matched filter which is the replica of the signal). Thus, according to equation 3.9, the variance ( $\sigma^2$ )

of the mean response difference is calculated by integrating the power spectrum of noise  $N_i(u,v)$  weighted by the power spectrum of the detector  $H^2(u,v)$  across Fourier space. As internal neural noise is white, its spectral density is constant, i.e.,  $N_i(u,v) = N_i$ . The expression  $\iint [H(u,v)]^2 du dv$  indicates the energy ( $E'$ ) of the signal, which is the same irrespective of whether it is calculated in Fourier space or in the visual field.

The signal-to-noise ratio squared ( $d'^2$ ) is then calculated as

$$d'^2 = \frac{\Delta R^2}{\sigma^2} = \frac{E'}{N_i} . \quad (3.10)$$

### 3.2 *MODELLING CONTRAST SENSITIVITY AND THE ENERGY THRESHOLD*

#### 3.2.1 *Contrast sensitivity as a function of grating area*

The grating contrast energy in the ideal detection filter at threshold is

$$E_{\text{ideal}} = d'^2 N , \quad (3.11)$$

where the ideal detector refers to a global matched filter, which in Gaussian white noise produces the best possible signal-to-noise ratio for a signal known exactly (Tanner & Birdsall, 1958). In equation 3.11  $d'$  is the detectability index (Tanner & Birdsall, 1958) indicating the signal-to-noise ratio (see Section 2.6.3) at the output of the detection filter. The threshold estimation algorithm used in the experiments of this thesis gives threshold estimates at the probability level of 0.84 of correct responses in a two-alternative forced-

choice task. From Elliot's (1964) forced-choice tables, the value of  $d'$  is therefore 1.4. In equation 3.11  $N$  is the spectral density of the total noise in the visual system.

The contrast energy at the input to the human detection filter at threshold is

$$E_{\text{human}} = O_{\text{MTF}}^2(f) P_{\text{MTF}}^2(f) c_{\text{r.m.s.}}^2 A, \quad (3.12)$$

where  $O_{\text{MTF}}$  is the optical transfer function of the human eye,  $P_{\text{MTF}}$  is the modulation transfer function of the neural visual pathways,  $f$  is spatial frequency,  $A$  is the grating area,  $c_{\text{r.m.s.}} = \sqrt{\frac{E}{A}}$  is the experimentally measured r.m.s. contrast of a grating at threshold, and  $E$  is the corresponding contrast energy.

Next we assume that image quality is very good and images are viewed in bright light (for the effect of quantal noise, see Rovamo, Mustonen & Näsänen, 1994a) so that the total noise of the visual system is equal to the internal neural noise, i.e.  $N = N_i$ . The efficiency (Tanner & Birdsall, 1958) of the human detection filter is  $\eta = \frac{E_{\text{ideal}}}{E_{\text{human}}}$  derived in Section

2.6.4. By combining equations 3.11 and 3.12 we then get

$$\eta = \frac{d'^2 N_i}{O_{\text{MTF}}^2(f) P_{\text{MTF}}^2(f) c_{\text{r.m.s.}}^2 A}. \quad (3.13)$$

From equation 3.13 we get r.m.s. contrast sensitivity ( $S_{\text{r.m.s.}}$ ) as the inverse of  $c_{\text{r.m.s.}}$

$$S_{\text{r.m.s.}}^2 = \frac{O_{\text{MTF}}^2(f) P_{\text{MTF}}^2(f) A \eta}{d'^2 N_i}. \quad (3.14)$$

In the model (Rovamo et al., 1993b) it is assumed that the human detection filter is a local matched filter, the efficiency ( $\eta$ ) of which is constant up to a critical grating area  $A_c$  but then decreases in proportion to increasing area. Thus,

$$\eta = \frac{\eta_{\max}}{1 + A/A_c} . \quad (3.15)$$

Its limited aperture is in agreement with the fact that the size of the human sampling aperture, the area from which visual information is collected, seems to have an upper limit (Burgess, 1990).

For simple cosine gratings  $A_c f^2$  increases with spatial frequency at low spatial frequencies but remains constant at medium and high spatial frequencies (Rovamo et al., 1993b). Hence, on the basis of equation 3.15, the efficiency of detection is constant for gratings with a constant number of square cycles ( $Af^2$ ) at medium and high spatial frequencies, in agreement with Banks, Geisler and Bennet (1987). However, at low spatial frequencies the efficiency of detection decreases with decreasing spatial frequency. On the other hand, according to Rovamo et al. (1993b)  $P_{\text{MTF}}(f) = f$  up to the spatial cut-off frequency determined by the lowest neural sampling density (Rovamo et al., 1995). Therefore, on the basis of equation 3.14, contrast sensitivity at medium and high spatial frequencies is directly proportional to the modulation transfer function  $O_{\text{MTF}}(f)$  of the eye optics, because  $P_{\text{MTF}}^2(f) A = Af^2$  is constant. This is again in complete agreement with Banks et al. (1987).

By combining equations 3.14 and 3.15 we get by simple algebra the following equations

$$S_{\text{r.m.s.}} = \frac{S_{\max}}{\sqrt{1 + A_c/A}} , \quad (3.16)$$

where

$$S_{\max}^2 = \frac{\eta_{\max} A_c O_{\text{MTF}}^2(f) P_{\text{MTF}}^2(f)}{d'^2 N_i} . \quad (3.17)$$

Equation 3.16 says that contrast sensitivity for large gratings ( $A \gg A_c$ ) is equal to the maximum contrast sensitivity  $S_{\max}$  and independent of grating area. However, for small gratings ( $A \ll A_c$ ), contrast sensitivity increases in proportion to  $\sqrt{A}$ , in agreement with Piper's (1903) law. When  $A = A_c$ ,  $S$  is equal to  $S_{\max}$  divided by  $\sqrt{2}$ .

In equation 3.17 variables  $A_c$ ,  $O_{\text{MTF}}$ , and  $P_{\text{MTF}}$  depend on spatial frequency but parameters  $\eta_{\max}$ ,  $d'$ , and  $N_i$  are constants. Thus, at all spatial frequencies  $S_{\max}$  is proportional to the product of  $\sqrt{A_c}$ ,  $O_{\text{MTF}}$ , and  $P_{\text{MTF}}$ .

### 3.2.2. Contrast energy threshold as a function of spatial frequency

Contrast energy is defined as the product of stimulus area and r.m.s. contrast squared. The r.m.s. contrast at threshold is equal to the inverse of r.m.s. contrast sensitivity ( $S_{\text{r.m.s.}}$ ). Hence, the contrast energy at threshold is

$$E_{\text{th}} = \frac{A}{S_{\text{r.m.s.}}^2} . \quad (3.18)$$

On the basis of equation 3.16 we get by simple algebra the following equation

$$E_{\text{th}} = E_0 (1 + A/A_c) , \quad (3.19)$$

where  $E_0 = S_{\max}^{-2} A_c$  refers to the contrast energy at threshold for grating areas much smaller than the critical area of spatial integration. On the basis of equation 3.17 we get

$$E_0 = \frac{d'^2 N_i \eta_{\max}^{-1}}{O_{\text{MTF}}^2(f) P_{\text{MTF}}^2(f)} . \quad (3.20)$$

Equation 3.20 means that at all spatial frequencies  $E_0$  is proportional to

$[O_{MTF}(f) P_{MTF}(f)]^{-2}$ , because the parameters  $\eta_{max}$ ,  $d'$ , and  $N_i$  are constants. At low spatial frequencies, where the optical modulation transfer function is close to unity (Deeley et al., 1991),  $E_0$  is inversely proportional to spatial frequency squared, because according to Rovamo et al. (1993b)  $P_{MTF}(f) = f$ .

### 3.3 DESCRIBING CONTRAST SENSITIVITY FOR A SUM OF ORIENTATIONS

On the basis of equation 3.16 the following equation for r.m.s. contrast sensitivity as a function of square cycles ( $Af^2$ ) was derived

$$S(f) = \frac{S_{max}(f)}{\sqrt{1 + A_c(f)/A}} = \frac{S_{max}(f)}{\sqrt{1 + A_c(f)f^2/Af^2}}, \quad (3.21)$$

where

$$S_{max}^2(f) = \frac{\eta_{max} A_c(f) O_{MTF}^2(f) P_{MTF}^2(f)}{d'^2 N}. \quad (3.22)$$

When there is additive external noise ( $N_e$ ) in the image, the total noise in the visual system is, according to the model, calculated as

$$N = N_i + O_{MTF}^2(f) P_{MTF}^2(f) N_e. \quad (3.23)$$

By substituting equation 3.23 to 3.22 under the assumption that  $N_e$  is the dominant source of noise, i.e.  $N \approx O_{MTF}^2(f) P_{MTF}^2(f) N_e$ , we get

$$S_{\max}^2(f) = A_c(f) \left( \frac{\eta_{\max}}{d'^2 N_e} \right) = A_c(f) f^2 \left( \frac{\eta_{\max}}{d'^2 N_e f^2} \right). \quad (3.24)$$

For simple gratings at spatial frequencies  $f \geq 0.5$  c/deg (Rovamo et al., 1993b)

$$A_c(f) = \frac{Z_0}{f^2}, \quad (3.25)$$

where  $Z_0$  is the critical number of square cycles marking the saturation of spatial integration.

For a sum of cosine gratings with equally spaced orientations ( $n = 1$  to 16) and the same contrast, spatial frequency, and zero phase at the centre of rotation,  $A_c(f)$  first decreases with increasing number of components, reaching a minimum at  $n = 5$  to 6, and increases thereafter. This can be formulated as

$$A_c(f, n) = \frac{Z_0(n)}{f^2} = \frac{Z_0 g(n)}{f^2}, \quad (3.26)$$

where  $g(n)$  varies as a function of the number of components as described above.

According to equation 3.15 described in Section 3.2.2 detection efficiency

$$\eta = \frac{\eta_{\max}}{1 + A/A_c}. \text{ Thus, on the basis of equation 3.26 we get}$$

$$\eta = \frac{\eta_{\max}}{1 + (Af^2 g(n)^{-1}/Z_0)}. \quad (3.27)$$

On the other hand, when external noise ( $N_e$ ) is the dominant source of noise, as in our experiments, efficiency is  $\eta = \frac{d'^2 N_e}{E_{th}}$  (Kukkonen, Näsänen & Rovamo, 1994), where

contrast energy ( $E_{th}$ ) at threshold is equal to the stimulus area divided by r.m.s. contrast sensitivity squared  $\left(\frac{A}{S^2}\right)$ .

### 3.4 DESCRIBING CONTRAST SENSITIVITY FOR A SUM OF TWO SPATIAL FREQUENCIES

Describing r.m.s. contrast sensitivity as a function of square cycles for sums of two spatial frequencies is identical to contrast sensitivity for sums of orientations described in equations 3.21 to 3.25 in Section 3.3.

For a sum of two simple vertical gratings with the same contrast and spatial frequencies  $f_1$  and  $f_2$  we assume that its critical area is the geometric mean of the critical areas of the component frequencies. By analogy, when the relative contrasts are  $(1-a)$  and  $(a)$  we assume that

$$A_c = A_{c_1}^{1-a} A_{c_2}^a \quad \text{i.e.} \quad \log A_c = (1-a)\log A_{c_1} + a\log A_{c_2} . \quad (3.28)$$

Let  $f_1 = f$  and  $f_2 = nf$ . By substituting equation 3.25 described in Section 3.3 at spatial frequencies  $f_1$  and  $f_2$  to equation 3.28 we obtain the following

$$A_c(f, n, a) = \frac{Z_0}{n^{2a} f^2} , \quad (3.29)$$

where  $n$  refers to the ratio of the lower and higher spatial frequencies and  $a$  indicates the relative contrast of the higher spatial frequency. In the experiments of Section 4.4

$a = 0, 0.25, 0.5, 0.75,$  or  $1$  and  $n = 3$  which means that the higher spatial frequency is the third harmonic of the lower (fundamental) spatial frequency. Equation 3.29 is equivalent to equation 3.25 described in Section 3.3 when the contrast of the  $n^{\text{th}}$  harmonic is zero. By substituting equation 3.29 to 3.21 described in Section 3.3 we get by simple algebra the following equation

$$S n^a f = \frac{S'_{\max}}{\sqrt{1 + \frac{Z_0}{n^{2a} A f^2}}}, \quad (3.30)$$

where

$$S'_{\max} = S_{\max} n^a f. \quad (3.31)$$

In equation 3.30 the expression  $n^{2a} A f^2$  is the number of square cycles ( $Z$ ) valid for simple gratings and the sums of two gratings ( $f$  and  $nf$ ) irrespective of phase. When  $a = 0$ , the grating comprises only the lower spatial frequency ( $f$ ), and  $Z = A f^2$ , but when  $a = 1$ , the grating comprises only the higher spatial frequency ( $nf$ ), and  $Z = A (nf)^2$ . Thus, the number of square cycles ( $A f^2$ ) is a good descriptor of complexity for simple gratings but to make it valid both for simple gratings and for sums of two gratings it has to be multiplied by the term  $n^{2a}$ .

Contrast energy at threshold is equal to stimulus area divided by r.m.s. contrast sensitivity squared (Rovamo et al., 1993b). On the basis of the model the following equation was derived

$$E_{\text{th}} = E_0 (1 + A/A_c), \quad (3.32)$$

where  $E_0 = \frac{A_c}{S_{\max}^2}$  refers to the contrast energy threshold for grating areas smaller than the critical area of spatial integration. By substituting equation 3.29 to 3.32 we obtain

$$E_{\text{th}} = E_0 \left( 1 + \frac{n^{2a} A f^2}{Z_0} \right), \quad (3.33)$$

where  $E_0 = \frac{Z_0}{S_{\max}^2}$ . Efficiency is  $\eta = \frac{d'^2 N_e}{E_{\text{th}}}$ , because  $N_e$  is the dominant source of noise.

Thus, on the basis of equation 3.33 we get

$$\eta = \frac{\eta_{\max}}{1 + (n^{2a} A f^2 / Z_0)}, \quad (3.34)$$

where  $\eta_{\max} = \frac{S_{\max}^2 d'^2 N_e}{Z_0}$ .

### 3.5 DETECTION OF RANDOM VISUAL SIGNALS

Equations 3.1 to 3.6 described in Section 3.1 are also valid for unknown signals in which one or several of the grating parameters are randomised. However, for an unknown signal the detector  $h(x,y)$  is the input  $[i_1(x,y)$  or  $i_2(x,y)]$  during each trial. The sampled responses of the detector  $h(x,y)$  to the two exposures are calculated as

$$R_1 = \eta \iint h(x,y) i_1(x + \varepsilon, y + \varepsilon) dx dy, \quad (3.35)$$

and

$$R_2 = \eta \iint h(x,y) i_2(x + \varepsilon, y + \varepsilon) dx dy , \quad (3.36)$$

where  $\eta$  is the sampling efficiency and  $\varepsilon$  is a small error in the superposition of the detection filter and input. The sampling efficiency  $\eta = \eta_{\max} (1+A/A_c)^{-1}$  is described in equation 3.15 in Section 3.2.1.

The difference  $\Delta R = R_1 - R_2$  is used as a decision variable by which it is possible to decide which exposure contained the signal: if  $\Delta R > 0$  then the first exposure contained the signal and if  $\Delta R < 0$  then it was the second exposure during which the signal was shown. However, the internal neural noise of the human brain limits the accuracy of the decision. Hence, in order to compute the detection threshold at a desired probability level, we have to take into account the variance ( $\sigma^2$ ) of the mean response difference. If the signal is unknown, two responses are

$$R_1 = \eta \iint [s'(x,y) + n_1(x,y)] [s'(x,y) + n_1(x + \varepsilon, y + \varepsilon)] dx dy , \quad (3.37)$$

and

$$R_2 = \eta \iint [n_2(x,y)] [n_2(x + \varepsilon, y + \varepsilon)] dx dy , \quad (3.38)$$

because  $s'(x+\varepsilon,y+\varepsilon)$  is approximately equal to  $s'(x,y)$ . The mean response difference is again  $\Delta R = \eta \iint s'^2(x,y) dx dy = \eta E'$ . Also,  $\left[ \iint s'(x,y) n(x,y) dx dy \right]$  is approximately equal to  $\left[ \iint s'(x,y) n(x + \varepsilon, y + \varepsilon) dx dy \right]$  and  $\left[ \iint n_1(x,y) n_1(x + \varepsilon, y + \varepsilon) dx dy \right]$  to  $\left[ \iint n_2(x,y) n_2(x + \varepsilon, y + \varepsilon) dx dy \right]$ . Thus the variance ( $\sigma^2$ ) of the mean response is due to the terms  $\left[ \eta \iint s'(x,y) n(x,y) dx dy \right]$  and  $\left[ \eta \iint n(x,y) n(x + \varepsilon, y + \varepsilon) dx dy \right]$  from the two exposures. The variance due to the term  $\left[ \eta \iint s'(x,y) n(x,y) dx dy \right]$  is calculated

$$\sigma^2 = \eta \iint H^2(u, v) N_i(u, v) du dv = \eta N_i \iint S'^2(u, v) du dv = \eta N_i E' \quad , (3.39)$$

where  $N_i(u, v)$  is the variance (spectral density) of internal neural noise in the Fourier space and  $H(u, v) = S'(u, v)$  is the Fourier transform of the detection filter (the matched filter which is the replica of the signal). Thus, according to equation 3.39 the variance ( $\sigma^2$ ) of the mean response difference is calculated by integrating the power spectrum of noise  $N_i(u, v)$  weighted by the power spectrum of the detector  $H^2(u, v)$  across Fourier space. As internal neural noise is white, its spectral density is constant, i.e.,  $N_i(u, v) = N_i$ . The expression  $\iint [H(u, v)]^2 du dv$  indicates the energy ( $E'$ ) of the signal, which is the same irrespective of whether it is calculated in the Fourier space or in the visual field.

The variance due to the term  $\left[ \eta \iint n(x, y) n(x + \epsilon, y + \epsilon) dx dy \right]$  is calculated as follows.

The above integral is first presented in discrete form

$$R_n = \sum_{x=1}^X \sum_{y=1}^Y n(x, y) n'(x, y) \quad , \quad (3.40)$$

where  $XY$  is the size of the signal  $s'(x, y)$  in pixels. The pixel size is assumed to be equal to unity. Let  $q(x, y) = n(x, y) n'(x, y)$ . The means of  $n(x, y)$  and  $n'(x, y)$  are equal to zero and their variances are equal to  $c_n^2$ , which is the square of r.m.s. contrast of noise. Hence,  $\sigma_q^2 = c_n^4$ , because the variance of the product of two random variables is equal to the product of their variances provided that the means of the two random variables are equal to zero. The variance of  $R_n$  is then calculated as

$$\sigma_{R_n}^2 = \sum_{x=1}^X \sum_{y=1}^Y \sigma_q^2 = XY \sigma_q^2 = XY c_n^4 \quad , \quad (3.41)$$

because the variance of a sum of random variables is equal to the sum of their variances.

Because pixel size ( $p$ ) was assumed to equal to unity,

$$c_n^2 = c_n^2 p^2 = N_i , \quad (3.42)$$

according to Legge et al., (1987), and

$$XY = XY p^2 = A , \quad (3.43)$$

where  $A$  is the area of the signal  $s'(x,y)$ . Then

$$c_n^2 XY = c_n^2 A = E_n , \quad (3.44)$$

which refers to the contrast energy of noise superimposed on the signal  $s'(x,y)$ . By combining equations 3.41, 3.42, and 3.44 we get

$$\sigma_{R_n}^2 = N_i E_n . \quad (3.45)$$

Thus,  $N_i E_n$  is the variance due to the term  $\left[ \eta \iint n(x,y) n(x+\epsilon, y+\epsilon) dx dy \right]$ .

The signal-to-noise ratio squared ( $d'^2$ ) is then calculated as

$$d'^2 = \frac{\Delta R^2}{\sigma^2} = \frac{\eta E'^2}{N_i E' + N_i E_n} . \quad (3.46)$$

Next we assume that  $E_n = E'$ , i.e. the contrast energies of both the signal and internal neural noise are equal at detection threshold for randomised stimuli. This also means that

$c_n = c_{th}$ , i.e. the contrast of internal neural noise is equal to signal contrast at threshold.

Consequently,  $d'^2 = \frac{\eta E'}{2N_i}$  for randomised stimuli. The threshold estimates in our 2AFC

experiments performed without external noise correspond to the probability level of 0.84 of correct responses. Thus,  $d'^2 = 2$  (Elliot, 1964) and the spectral density of internal neural noise is the only source of additive noise in the human visual system.

According to the model of Rovamo et al. (1993b) the contrast energy of a grating signal at the input to the image interpretation device in the human brain is

$$E' = O_{MTF}^2(f) P_{MTF}^2(f) E, \quad (3.47)$$

where  $E$  is the contrast energy of the grating signal in the visual field. Hence, in the experiments of Section 5.3. contrast energy threshold for an unknown signal should be twice the energy threshold for a signal known exactly. Contrast energy at detection threshold is calculated as  $E_{th} = \frac{A}{S^2}$ , where  $S$  refers to r.m.s. contrast sensitivity and  $A$  to grating area in  $\text{deg}^2$  of the visual field. This means that contrast sensitivity for a signal with randomised orientation and/or phase should be  $1/\sqrt{2} = 0.71$  times the contrast sensitivity for the signal with known orientation and phase.

## 4. SPATIAL INTEGRATION

### 4.1 INTRODUCTION

#### 4.1.1 Spatial integration for simple gratings without external spatial noise

Spatial integration for foveal simple grating stimuli in contrast detection refers to human observers' ability to integrate visual information over space so that contrast sensitivity increases with grating area. However, human observers are able to integrate information only over a limited area in the visual field. Contrast sensitivity thus increases with grating area up to a critical area after which the increase ceases. This increase of grating area can result from an increase in the number of grating cycles (e.g. Hoekstra, van der Goot, van den Brink & Bilsen, 1974; Savoy & McCann, 1975; Howell & Hess, 1978), length of bars (Howell & Hess, 1978), or both (Schober & Hilz, 1965; Cohen, 1978; Howell & Hess, 1978; Virsu & Rovamo, 1979; Rovamo et al., 1993b).

Hoektra et al. (1974) studied the range of spatial frequencies between 1 and 7 c/deg at different luminances and concluded that contrast sensitivity for sinewave modulated fields saturated with the same the number of grating bars at all spatial frequencies.

Howell and Hess (1978) measured contrast thresholds for sine wave gratings at spatial frequencies from 0.5 to 20 c/deg and found that contrast thresholds were determined by the spatial extent of the grating in both horizontal and vertical dimensions. The number of grating bars and the length of bars thus had a similar effect on contrast threshold. The critical size after which the threshold remained constant was found to be inversely related to the spatial frequency, i.e. the saturation point decreased with increasing spatial frequency.

Rovamo et al. (1993b) measured contrast sensitivity as a function of grating area for simple cosine gratings at spatial frequencies 0.125 to 32 c/deg. They found that at small grating areas contrast sensitivity increased in proportion to the square-root of grating area, obeying Piper's law (1903). The critical grating area marking the saturation of spatial integration and cessation of Piper's law (1903) was about 100 in solid degrees of the visual field at 0.125 to 1 c/deg (Rovamo et al., 1993b). However, the critical area decreased with increasing spatial frequency at medium and high spatial frequencies so that it remained inversely proportional to spatial frequency squared at and above 1 c/deg, in agreement with Howell and Hess (1978). Thus the gratings with critical area are scaled versions of each other at 1 to 32 c/deg, which support the view that human vision is scale invariant.

Scale invariance is demonstrated by the fact that the detection threshold is determined by the relative grating area or the amount of detail and contour in the image rather than the absolute grating area in degrees of visual angle. This implies that the magnification or the viewing distance do not affect the detection threshold of the grating provided that the spatial frequency is not so high that grating contrast is attenuated by the modulation transfer function of the eye optics (Artal & Navarro, 1990; Deeley et al., 1991; Ijspeert, van den Berg & Spekreijse, 1993; Rovamo, Mustonen & Näsänen, 1994b) and sampling limitations of the retina (Curcio, Sloan, Packer, Henricson & Kalina, 1987; Virsu & Rovamo, 1979). Relative grating area can be expressed as the number of square cycles, first introduced by Virsu and Rovamo (1979). The number of square cycles ( $Af^2$ ) is calculated by multiplying grating area ( $A$ ) by spatial frequency ( $f$ ) squared. The square cycle is a square with a side length equal to one cycle of the grating. For a constant number of square cycles, spatial frequency is low when grating area is large, and vice versa. Multiplication by spatial frequency squared normalises grating area in the sense that the cessation of Piper's law (1903) and saturation of spatial integration occur at the same number of square cycles (Howell & Hess, 1978).

The above studies suggest that spatial integration without external noise is determined by the number of square cycles, and the critical value of grating cycles was found to vary between 8 to 20 grating cycles.

### **4.1.2 Spatial integration for simple gratings with external spatial noise**

Coltman and Anderson (1960) measured detection thresholds for a constant sized sinewave pattern in white external noise as a function of viewing distance, which varied from 25 to 700 cm. They found thresholds to be constant at the viewing distances used. They also measured detection thresholds as a function of line pairs (cycles) and found that the threshold decreased up to the critical number of line pairs after which threshold stayed constant.

Rovamo, Franssila, and Näsänen (1992) studied sinusoidal gratings with and without two-dimensional external spatial noise as a function of viewing distance. They kept the size of the grating constant on the screen. Consequently, the spatial frequency increased and grating area decreased with increasing viewing distance. The ratio of grating area and noise spectral density and, thus their physical signal-to-noise ratio, remained constant because the decrease of spectral density and grating area are parallel with increasing viewing distance. Contrast sensitivity without noise was first constant and later decreased. They found that in external noise contrast sensitivity for gratings with constant number of square cycles and constant signal-to-noise ratio was independent of viewing distance as long as contrast sensitivity was lower with noise than without. After that, contrast sensitivity decreased identically for stimuli with and without noise due to the attenuating effect of the eye optics at the higher spatial frequencies (e.g. Deeley et al., 1991; Ijspeert et al., 1993). The finding that contrast sensitivity is constant irrespective of viewing distance implies that spatial integration is also determined by the number of square cycles in external spatial noise, in agreement with Coltman & Anderson (1960).

Luntinen, Rovamo, and Näsänen (1995) measured r.m.s. contrast sensitivity at spatial frequencies from 0.125 to 16 c/deg as a function of spectral density of external noise for vertical cosine gratings with various grating areas. They found that the greater the magnitude of spatial noise the lower the sensitivity but the shape of contrast sensitivity function was similar with and without noise. The finding implies that detection which is limited by internal noise in absence of external noise is replaced by external noise in noise conditions. Internal noise does not disappear in the visual system when external noise is present but the magnitude of external noise becomes dominant and detection is thus limited by external noise.

Van Meeteren and Barlow (1981) formed sinewave gratings by modulating average random dot density and they measured detection efficiencies described in Section 2.6.4. as a function of the number of square cycles in static dot noise. They showed that efficiency first remained constant and then decreased monotonically. Their result suggests that detection efficiency is also determined by the number of square cycles. Similar dependence of the number of square cycles on efficiency was reported by Kersten (1984) who used sinusoidal gratings with Gaussian spatial and temporal envelopes in one-dimensional dynamic noise.

According to the studies described above, spatial integration also seems to be determined by the number of square cycles in external spatial noise. The critical value of square cycles was found to vary between 1 and 9 grating cycles. The range of various findings might be due to different ways of defining the point of saturation, as well as the fact that different types of noise were used in the experiments.

### **4.1.3 Spatial integration for complex gratings**

The number of grating bars or square cycles seems to be a good descriptor of relative grating area for simple gratings, but it is more difficult to find a suitable metric for

expressing the amount of detail and contour in complex gratings which often have ambiguous grating areas. Näsänen, Kukkonen, and Rovamo (1994) introduced the number of square cycles to complex gratings by defining image complexity ( $Z$ ) as a product of spatial spread of contrast energy ( $\alpha$ ) multiplied by centre frequency squared ( $f_c$ ). They measured detection efficiencies for uniform and patched stimuli in external noise. Patched stimuli comprised nine separate patches with a size of one square cycle each and the distance between the patches was changed in order to match the varying size of the uniform gratings. They found that detection efficiency for both stimuli was a decreasing function of image complexity. Kukkonen et al. (1994) studied spatial integration for bandpass-filtered point stimuli whose spatial frequency bandwidths were kept constant while areas were increased by modifying the phase spectra. They showed that detection efficiency for point spread stimuli was determined equally well by the spatial spread of contrast energy ( $\alpha$ ) and image complexity ( $Z$ ) introduced in their earlier study (Näsänen et al., 1994). Even though detection efficiencies for uniform and patched cosine gratings in the previous study (Näsänen et al., 1994) and irregular patterns with random phase spectra in the present study were determined by image complexity, the efficiency of spatial integration decreased faster for irregular patterns.

Even though the human visual system has to deal with complex patterns in everyday life, only a few previous studies have investigated the visual processing of complex gratings. The aim of this chapter is to reveal more about higher levels of visual processing by studying spatial integration for complex gratings with and without external noise.

## 4.2 *COMPLEX GRATINGS WITH VARIOUS ORIENTATION COMPONENTS WITHOUT NOISE*

### 4.2.1 Introduction

At small grating areas foveal contrast sensitivity for simple cosine gratings increases with grating area but the process of spatial integration saturates at large areas (Hoekstra et al., 1974; Savoy & McCann, 1975; Howell & Hess, 1978). The increase is at all spatial frequencies proportional to the square root of grating area (Rovamo et al., 1993b), in agreement with Piper's (1903) law. The critical area marking the saturation of spatial integration decreases with increasing spatial frequency (Howell & Hess, 1978).

Virsu and Rovamo (1979) have shown that at 1 to 32 c/deg spatial integration in grating detection obeys a single function of the number of square cycles calculated by multiplying grating area ( $A$ ) by spatial frequency ( $f$ ) squared. On this basis they suggested that spatial integration is determined by the amount of contour and detail within the grating. This hypothesis is in agreement with the finding that the span of attention is limited to a constant number of elements (Verghese & Pelli, 1992). The amount of contour and detail per unit area is greater in a sum of cosine gratings of different orientations than in a simple cosine grating. This suggests that spatial integration might become less effective and saturate at smaller stimulus areas when the stimulus to be detected is a sum of cosine gratings of different orientations than when it is a simple cosine grating.

Rovamo et al. (1993b) have recently modelled the human visual system as an image processor comprising (i) low-pass filtering due to optical modulation transfer function of the eye, (ii) high-pass filtering (lateral inhibition) due to the neural modulation transfer function of visual pathways, (iii) addition of internal neural noise, and (iv) detection by a matched filter (Hauske et al., 1976) modified so that, in agreement with Burgess (1990), its sampling aperture is limited. For simple cosine gratings the detection efficiency of this

local matched filter is first constant at small stimulus areas but then decreases in proportion to increasing area.

In the experiments of this section the applicability of the model to spatial integration was tested by measuring r.m.s. contrast sensitivity as a function of grating area for sums of cosine gratings with different orientations. The orientation difference between  $n$  components ( $n = 1, 2, 3, 4, 5, 6, 8$  or  $16$ ) was  $180/n$  but the components had the same contrast, phase (zero at the centre of rotation) and spatial frequency (0.25, 1 or 4 c/deg). The experiments were performed at spatial frequencies  $\leq 4$  c/deg because at high spatial frequencies contrast sensitivity for simple cosine gratings depends on grating orientation (Campbell, Kulikowski & Levinson, 1966).

### 4.2.2 Methods

#### *Apparatus*

The experiments were carried out using Apparatus 1 and Apparatus 3 described in Sections 2.1 and 2.3, respectively.

#### *Stimuli*

The stimuli consisted of sharp-edged circular grating fields (diameters 1, 2, 4, 8, and 16 cm). Their equiluminous surround was limited to a circular field of 20 cm by a black cardboard. The stimuli were sums of various numbers of cosine gratings ( $n = 1, 2, 3, 4, 5, 6, 8$ , or  $16$ ) with the same contrast, phase (0 deg at the centre of rotation), and spatial frequency (0.25, 1, or 4 c/deg) but with an orientation difference of  $180/n$  between components. Thus, the orientation difference between components decreased when the number of components increased. One of the grating components was always vertical.

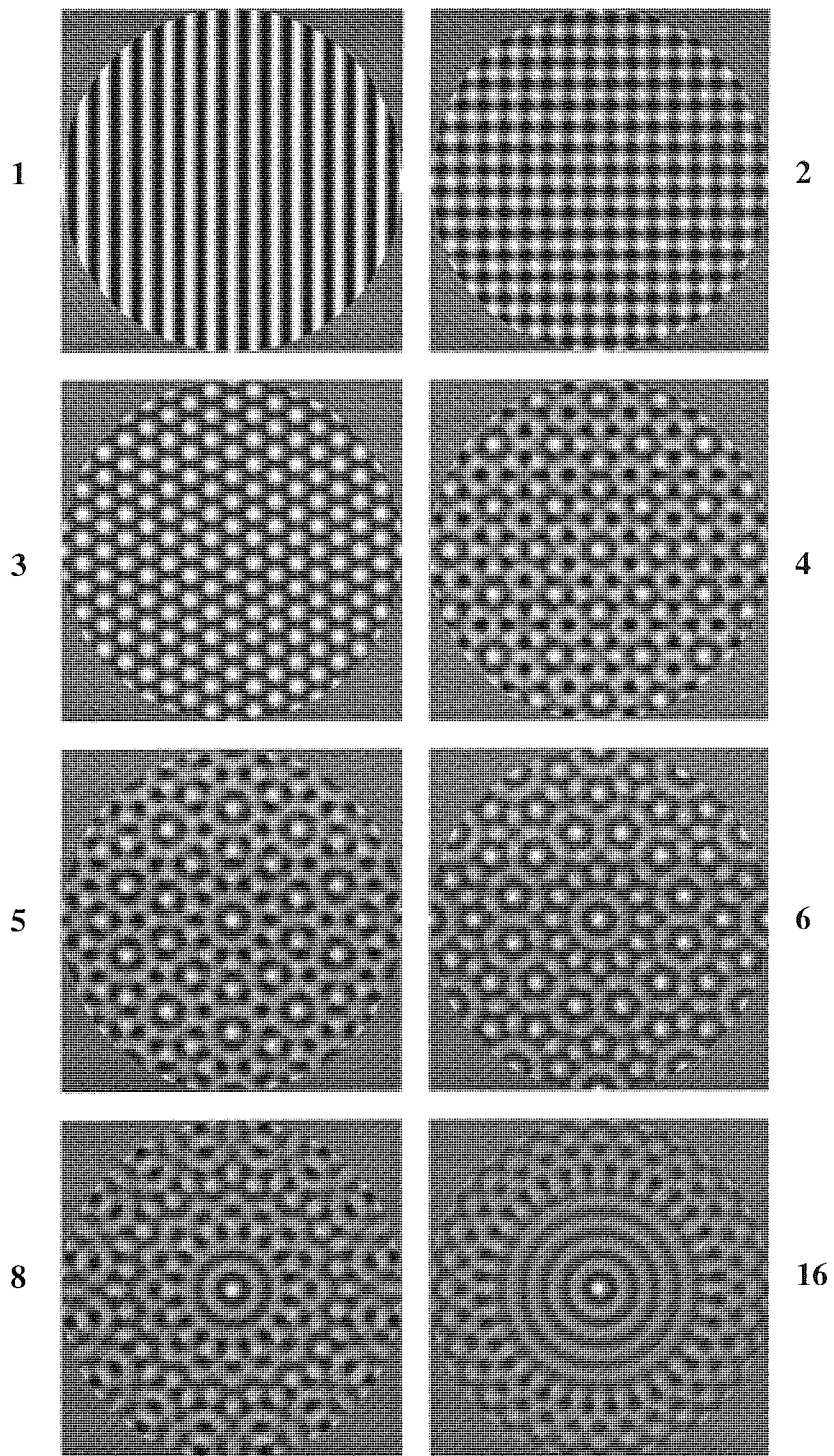


Figure 4.1 The stimuli used in the experiments of Section 4.2.

Thus, for example, when  $n = 1$ , the stimulus was a simple vertical grating, when  $n = 2$ , the stimulus was the sum of a vertical and horizontal grating, and when  $n = 3$ , the three component gratings had an orientation difference of  $60^\circ$  between each of them.

The stimuli are shown in Figure 4.1. The numbers close to the gratings refer to the number of components. The gratings fields shown had a diameter of 16 cm on the screen. All stimuli are unchanged by certain rotations. For  $n = 1$  to 3 they are also unchanged for certain translations. When  $n$  increases from 4 to 16, an increasing part of the centre of the stimulus approaches a  $J_0$  target (Kelly & Magnuski, 1975), where the radial luminance distribution of the stimulus is the zero order Bessel function of the first kind.

### *Procedure*

Contrast thresholds which are the inverses of contrast sensitivity were determined by using the forced-choice algorithm at the probability of 0.84 correct responses described by in detail in Section 2.5. All data points shown are based on geometric means of at least three threshold estimates.

The stimuli were viewed binocularly with natural pupils. Their diameters increased with viewing distance from 3.5 to 6 mm. The range of retinal illuminance was thus 480 - 1,400 phot. td.

The exposure duration was 500 msec. Each trial consisted of two exposures which were separated by about 600 msec. The observer indicated, which exposure contained the stimulus by pressing one of the two keys on a computer keyboard. Between two exposures the observer saw only the equiluminous field. A new trial began 250 msec after the observer's response. Sound signals provided the feedback indicating whether the observer's response was correct or incorrect. The experiments were performed in a dark room and the only light source was the display. The subject's head was stabilised using a chin rest. Fixation was binocular and directed to the centre of the stimulus field. No

fixation point was used and free eye movements were allowed within the central region of the stimulus field.

### *Subjects*

Three experienced subjects, aged 27 - 32 years, served as observers. Subject CT was an emmetrope, OU was a corrected non-astigmatic myope/hyperope (od. -0.75 DS / os. +0.75 DS) and JM was a corrected astigmatic myope (od. -1.5 DS / os. -0.5 / -0.5 x 180). Binocular Snellen acuity at 6 m was 1.6 for CT, 1.5 for OU and 1.7 for JM.

### *R.m.s. contrast and energy thresholds*

Contrast energy and r.m.s contrast were calculated by equations 2.6 and 2.7 respectively and they are described in Section 2.6.1.

### **4.2.3 Results**

In the experiments of Figures 4.2 - 4.4 we measured binocular r.m.s. contrast sensitivity as a function of area for compound gratings consisting of sums of cosine gratings with different number of orientation components. Spatial frequencies 0.5 (Figure 4.2), 1 (Figure 4.3), and 4 c/deg (Figure 4.4) were studied. Stimulus area ( $A$ ) varied from 0.049 to 770 deg<sup>2</sup>. The number of square cycles, calculated as  $Af^2$ , varied from 0.79 to 200 at 1 and 4 c/deg but only to 50 at 0.25 c/deg, because at low spatial frequencies the number of square cycles was limited by the largest stimulus size available (diameter 16 cm) in the apparatus. The numbers close to the curves on the left in Figures 4.2 - 4.4 refer to the number of components. For clarity of presentation the curves and data points have been shifted vertically. In each frame the uppermost curve and data are in their correct place but

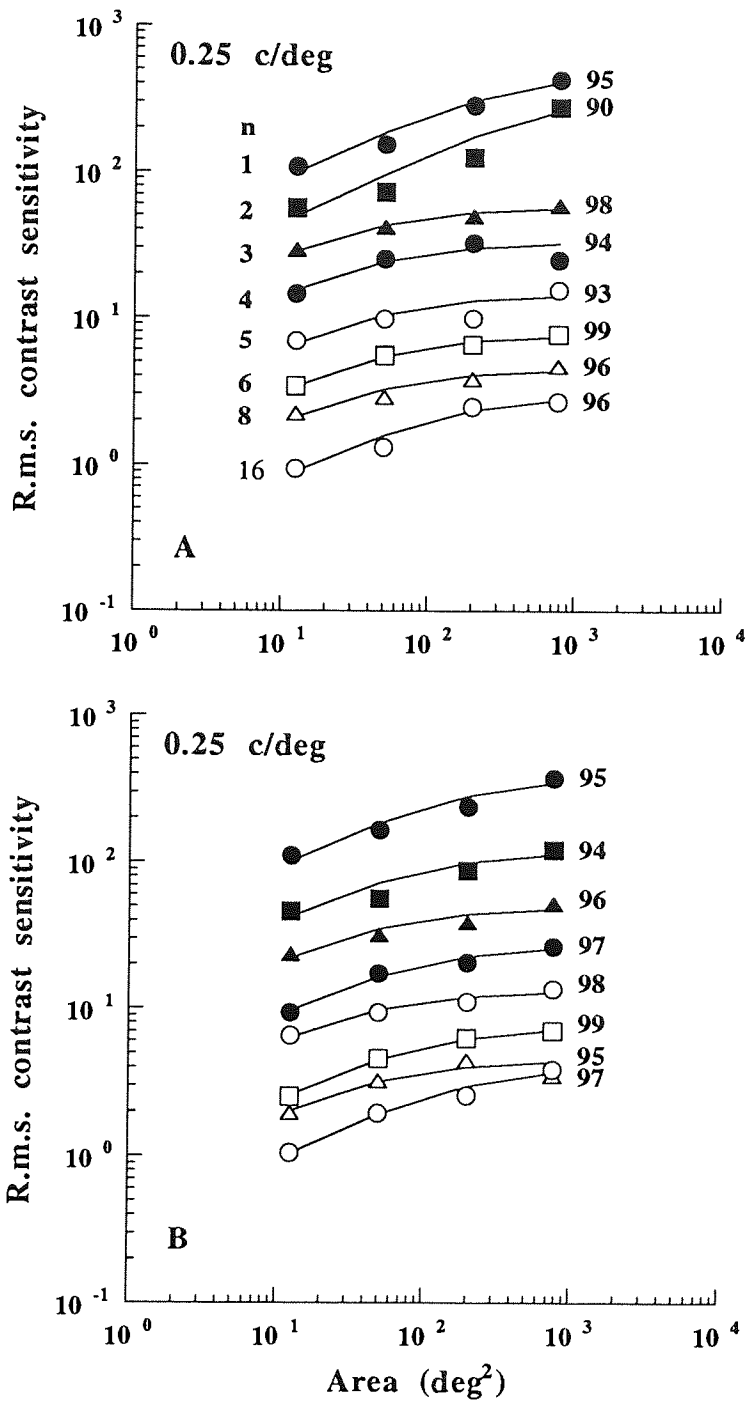


Figure 4.2 R.m.s. contrast sensitivity as a function of grating area at 0.25 c/deg. Subjects were JM (A), and OU (B).

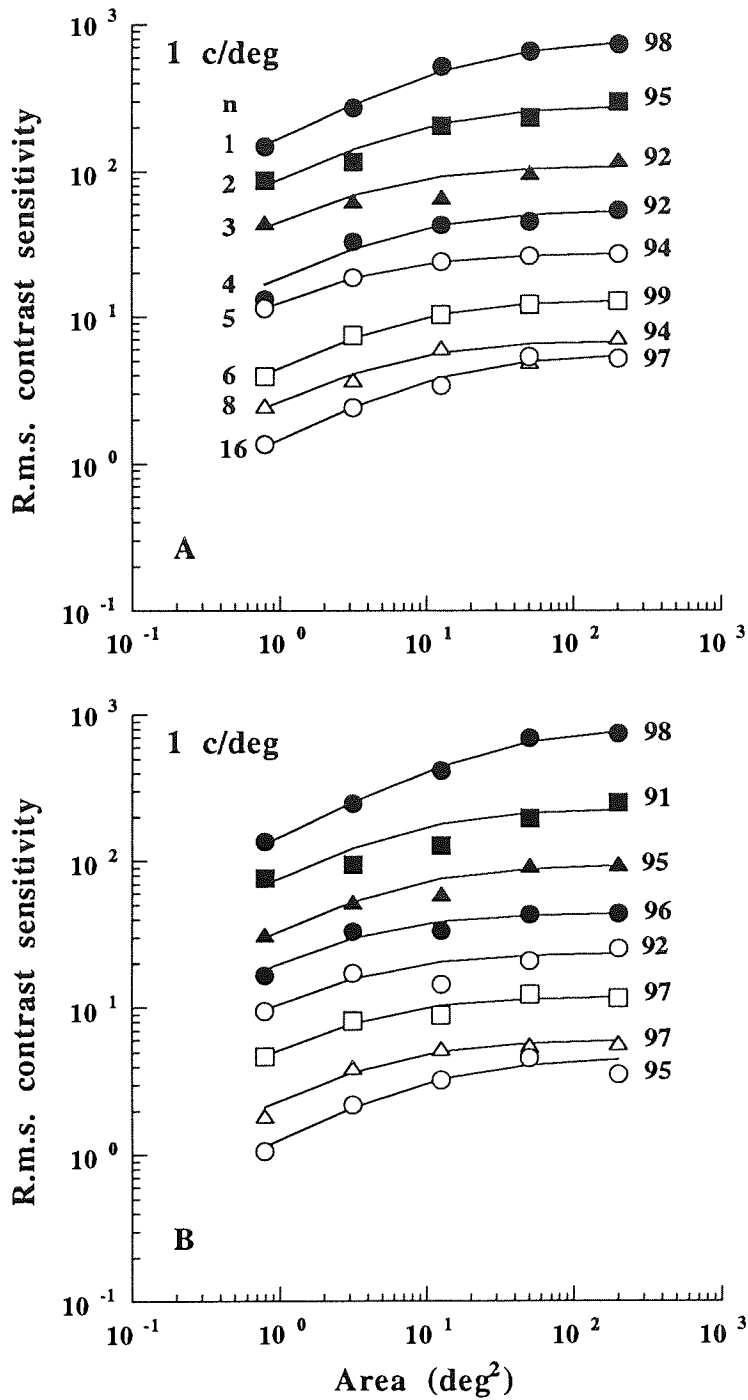


Figure 4.3 R.m.s. contrast sensitivity as a function of grating area at 1 c/deg. Subjects were CT (A), and OU (B).

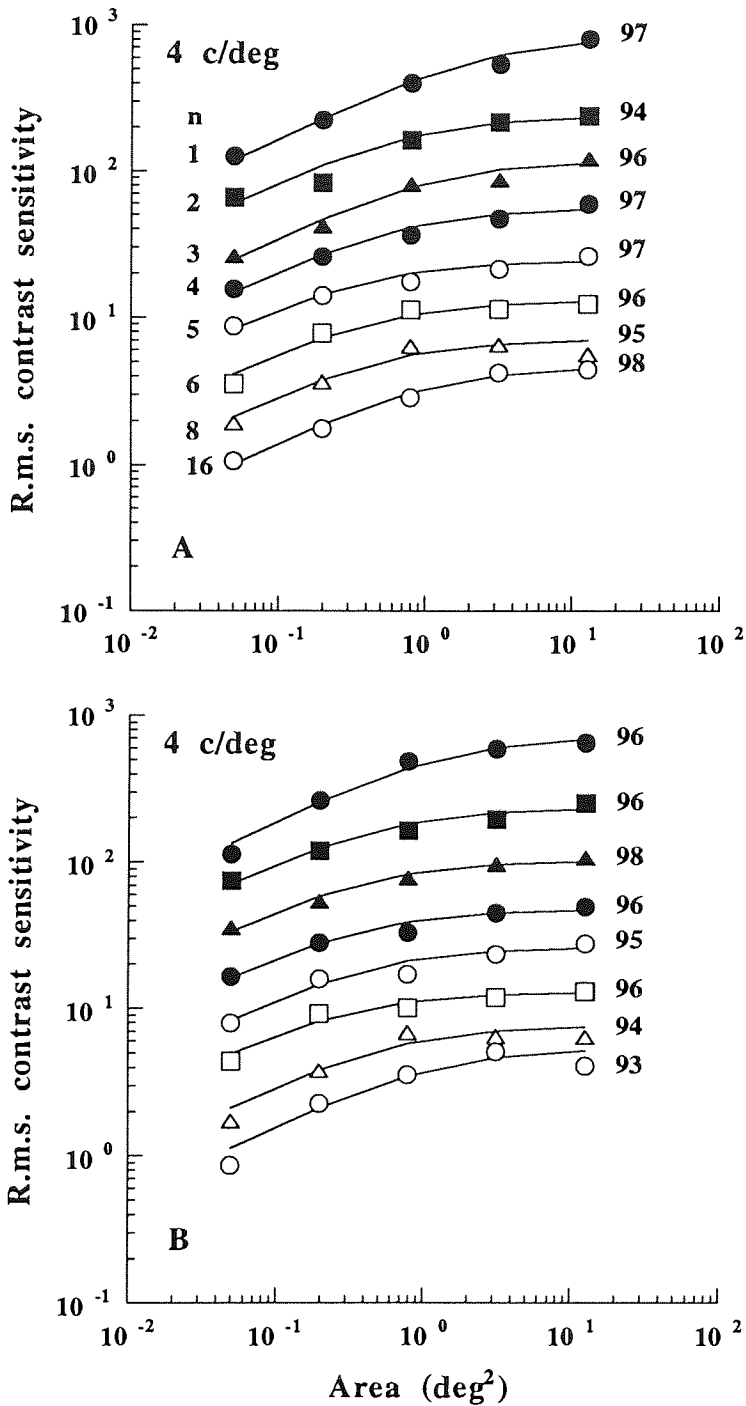


Figure 4.4 R.m.s. contrast sensitivity as a function of grating area at 4 c/deg. Subjects were CT (A), and OU (B).

the others have been shifted downwards by a factor of 2, 4, 8, 16, 32, 64, and 128, respectively. The numbers on the right in Figures 4.2 - 4.4 refer to the goodness of the fit calculated by equation 2.29 described in Section 2.6.6.

In Figure 4.2 the viewing distance was 28.6 cm and the spatial frequency on the screen was 0.5 c/cm. The stimulus diameter had the range of 2 to 16 cm. In Figures 4.3 and 4.4 the spatial frequency was 1 c/cm on the screen and the range of diameters was 1 to 16 cm. Viewing distance was 57.3 cm in Figure 4.3 and 229 cm in Figure 4.4.

As Figures 4.2 - 4.4 show, r.m.s. contrast sensitivity increased with area. However, scrutiny revealed that the increase became less steep and saturated at smaller areas when the number of components increased from 1 to 5 - 6. At greater values of  $n = 8$  to 16 the deterioration of spatial integration ceased, and the increase of contrast sensitivity with area again became steeper and saturated at larger areas, starting to resemble the contrast sensitivity function at  $n = 1$ . The results of Figures 4.2 - 4.4 mean that the effectiveness of spatial integration depended on the number of orientation components in the sum of gratings. In Figures 4.2 - 4.4 the critical area marking the saturation of spatial integration decreased with increasing spatial frequency, in agreement with Howell and Hess (1978).

Smooth curves of least squares in Figures 4.2 - 4.4 were calculated by separately fitting equation 3.16 described in Section 3.2.1 to the data of each subject, spatial frequency and number of components. Equation 3.16 is  $S = \frac{S_{\max}}{\sqrt{1 + A/A_c}}$ , where  $S$  is r.m.s. contrast sensitivity,  $A$  is grating area,  $S_{\max}$  is the maximum contrast sensitivity obtainable by spatial integration, and  $A_c$  is the critical area marking the saturation of spatial integration. The goodness of the fit calculated by equation 2.29 described in Section 2.6.6 was on average 96%, ranging from 90 to 99%. The applicability of equation 3.16 to the data means that all contrast sensitivity functions were, in fact, similar in shape but shifted along both the vertical and horizontal axes.

In Figure 4.5 the critical area ( $A_c$ ) of spatial integration was plotted as a function of the number of orientation components in double logarithmic coordinates. The estimates of  $A_c$

were obtained when equation 3.16 described in Section 3.2.1 was fitted to the data of Figures 4.2 - 4.4 The solid lines show the geometric mean of the data points at each spatial frequency.

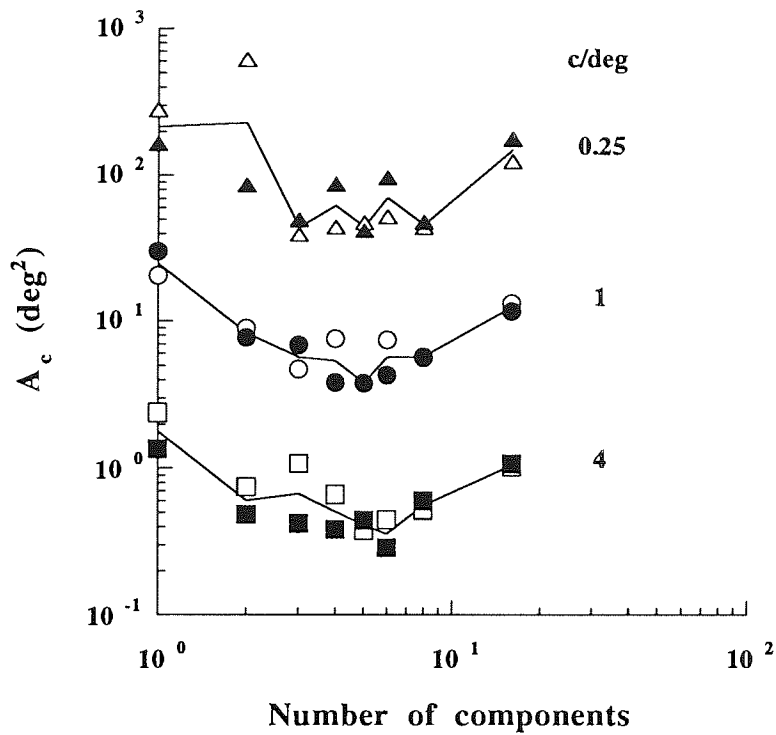


**Figure 4.5** The critical area ( $A_c$ ) as a function of the number of components. Open symbols refer to subject JM at 0.25 c/deg, and subject CT at 1 and 4 c/deg. Solid symbols refer to subject OU at all spatial frequencies.

As Figure 4.5 shows, critical area  $A_c$  first decreased with increasing number of components reaching a minimum at  $n = 5$  or  $6$  but increased thereafter. The only exception was the value of  $A_c$  when  $n = 2$  at 0.25 c/deg for subject JM. In Figure 4.5 the dependence of  $A_c$  on the number of components was fairly similar at all spatial frequencies studied. In addition,  $A_c$  decreased in approximate proportion to spatial frequency squared at all values of  $n$ . This means that the critical number of square cycles, calculated as  $A_c f^2$ , was

independent of spatial frequency at each number of components.

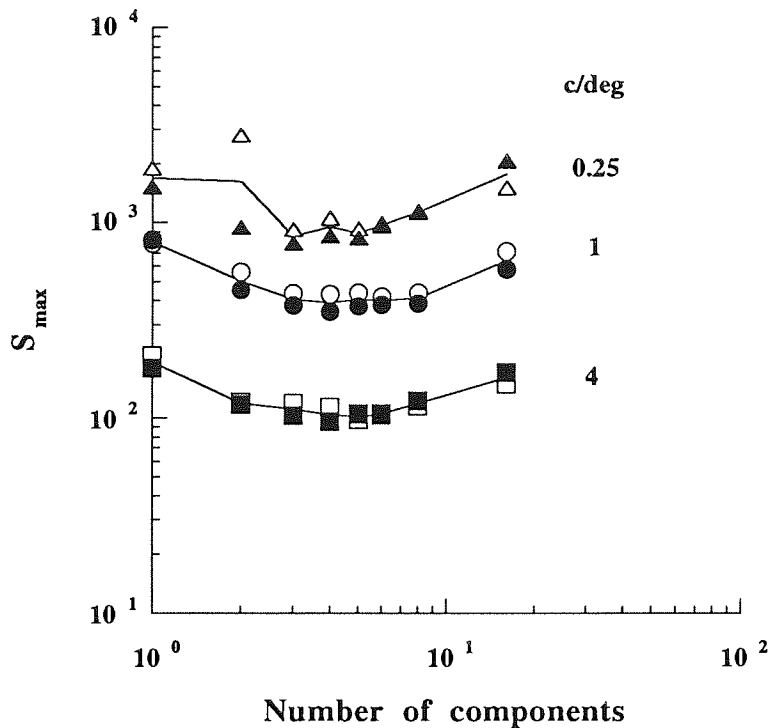


**Figure 4.6** The maximum contrast sensitivity ( $S_{max}$ ) as a function of the number of components. Symbols and subjects were the same as in Figure 4.5.

In Figure 4.6 the maximum sensitivity ( $S_{max}$ ) obtainable by spatial integration was plotted as a function of the number of orientation components in double logarithmic coordinates. The estimates of  $S_{max}$  were obtained when equation 3.16 described in Section 3.2.1 was fitted to the data of Figures 4.2 - 4.4. For clarity of presentation the curves and data for 0.25 and 4 c/deg have been shifted by a factor of four up- and downwards, respectively. Again, the solid lines show the geometric mean of the data points at each spatial frequency.

As Figure 4.6 shows, the maximum sensitivity  $S_{max}$  first decreased with increasing number of components reaching a minimum and increased thereafter. The dependence of

$S_{\max}$  on the number of components was similar at all spatial frequencies studied. Again, the only exception was the value of  $S_{\max}$  when  $n = 2$  at  $0.25$  c/deg for subject JM. In addition, close inspection revealed that  $S_{\max}$  was almost independent of spatial frequency at all numbers of components.

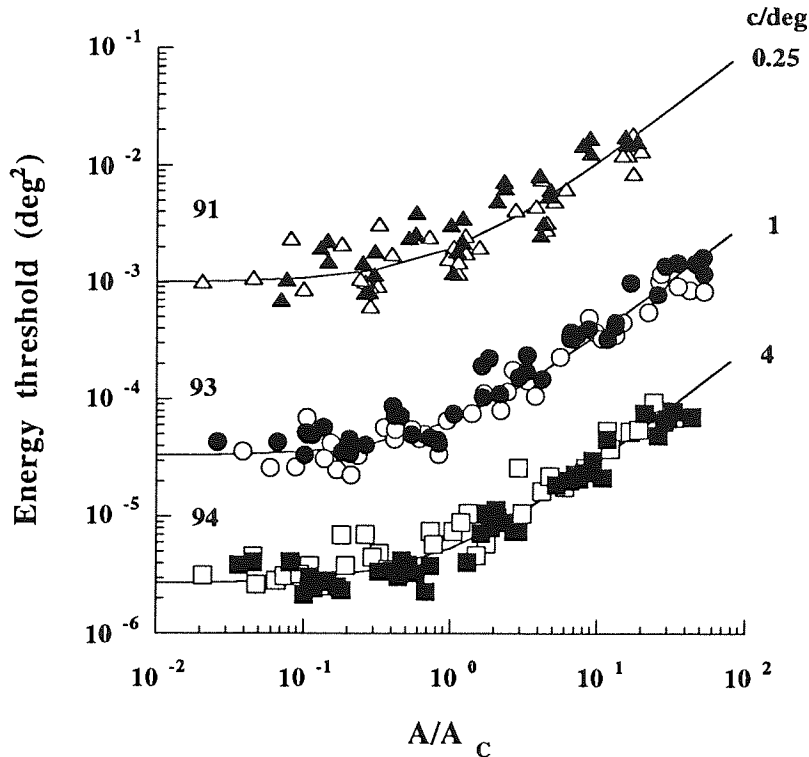


**Figure 4.7** Energy threshold as a function of the normalised grating area ( $A/A_c$ ). Symbols and subjects were the same as Figure 4.5.

Next the contrast sensitivity data of Figures 4.2 - 4.4 at each spatial frequency was transformed to contrast energy thresholds ( $E_{th}$ ) by means of equation 3.18 described in Section 3.2.2, which is  $E_{th} = AS_{r.m.s.}^{-2}$ . Then  $E_{th}$  was plotted as a function of the normalised grating area, calculated as  $A/A_c$ , in double logarithmic coordinates. The numbers on the left refer to the goodness of the fit calculated by equation 2.29 described in Section 2.6.6.

As Figure 4.7 shows, contrast energy threshold was constant at small values of  $A/A_c$  but then it started to increase with  $A/A_c$ . Smooth curves were calculated using equation 3.19 described in Section 3.2.2. Equation 3.19 means that  $E_{th}$  is constant at small values of  $A/A_c$  but increases in double logarithmic coordinates linearly with a slope of 1 at large values of  $A/A_c$ . The estimate of  $E_0$  at each spatial frequency was calculated in the following way. The values of  $E_{th}$  at each spatial frequency were first divided by  $(1+A/A_c)$ . Their geometric mean then provided an estimate  $E_0$  at each spatial frequency. The goodness of the fit to the data calculated by equation 2.29 described in Section 2.6.6 was on average 93%, ranging from 91 to 94% at spatial frequencies of 0.25 - 4 c/deg.

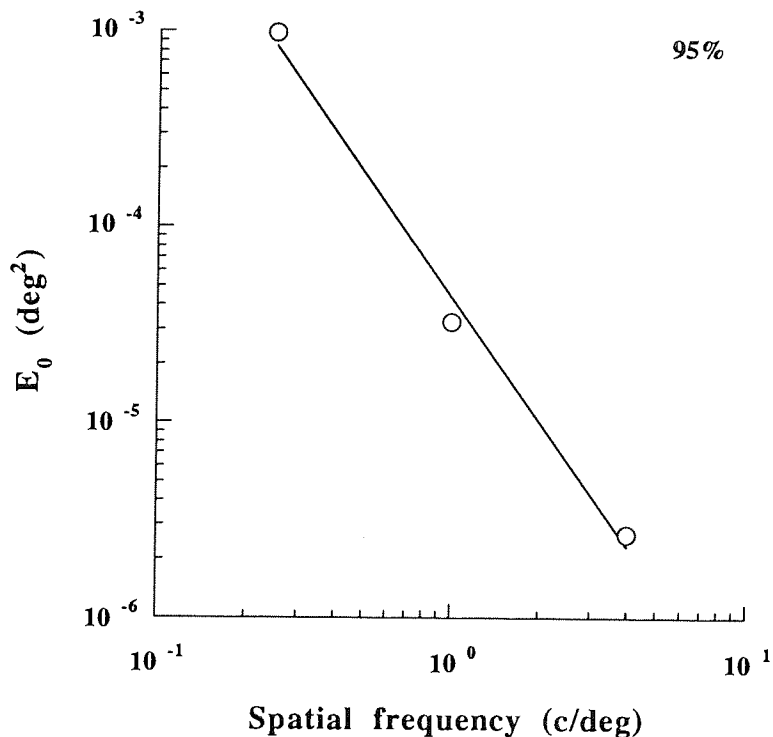


**Figure 4.8** The estimates of  $E_0$  as a function of spatial frequency.

In Figure 4.8 the estimates of  $E_0$  were plotted as a function of spatial frequency in double logarithmic coordinates. The estimates of  $E_0$  were obtained when equation 3.19 described in Section 3.2.2 was fitted to the data of Figure 4.7. As Figure 4.8 shows,  $E_0$  decreased linearly with increasing spatial frequency when plotted in double logarithmic coordinates. The slope of decrease was -2, which means that  $E_0$  was inversely proportional ( $r^2 = 95\%$ ) to spatial frequency squared ( $f^2$ ).

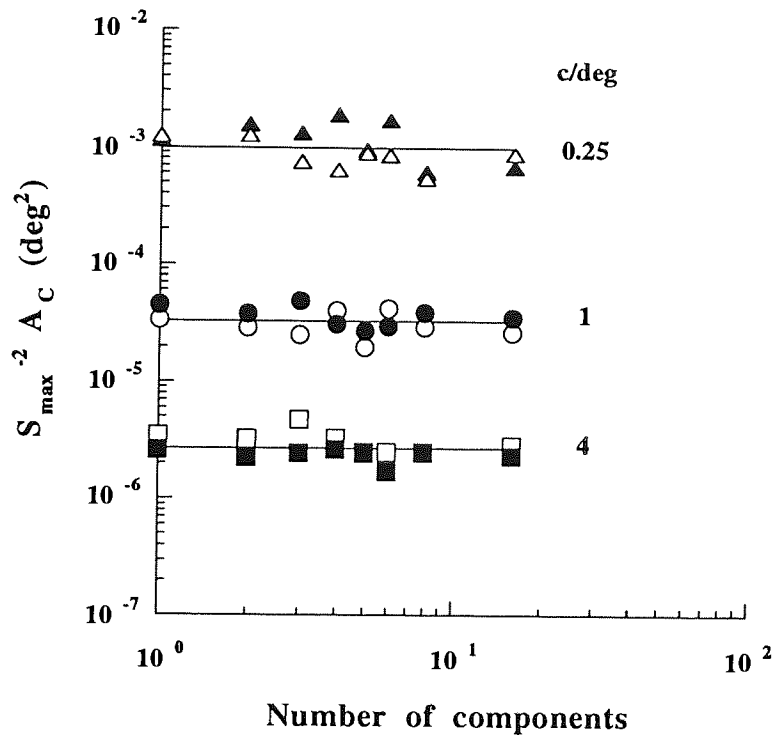


**Figure 4.9** The estimates of  $S_{\max}^{-2} A_c$  as a function of the number of components. The symbols and subjects were the same as in Figure 4.5.

In Figure 4.9 the product of the inverse of maximum r.m.s. contrast sensitivity ( $S_{\max}$ ) squared and critical area ( $A_c$ ) i.e.  $S_{\max}^{-2} A_c$  was plotted as a function of the number of orientation components in double logarithmic coordinates. The estimates of  $S_{\max}$  and  $A_c$  were obtained when equation 3.16 described in Section 3.2.1 was fitted to the data of Figures 4.2 - 4.4. Horizontal solid lines refer to the estimates of  $E_0$  shown in Figure 4.8.

As Figure 4.9 shows, the product  $S_{\max}^{-2} A_c$  was independent of the number of orientation components at all spatial frequencies studied. The horizontal lines in Figure 4.9 refer to the estimates of  $E_0$  shown in Figure 4.8 and obtained when equation 3.19 described in Section 3.2.2 was fitted to the data of Figure 4.7. Figure 4.9 is in agreement with relationship  $E_0 = S_{\max}^{-2} A_c$  derived when equations 3.16 described in Section 3.2.1 and 3.18 described in Section 3.2.2 were combined to produce equation 3.19. The estimates of  $S_{\max}^{-2} A_c$  as a function of the number of components at spatial frequencies 0.25, 1, and 4 c/deg. Horizontal lines refer to the estimates of  $E_0$  shown in A.

#### 4.2.4 Discussion

The experiments with sums of various numbers ( $n = 1$  to 16) of cosine gratings having the same contrast, phase (zero at the centre of rotation) and spatial frequency (0.25, 1 or 4 c/deg) but an orientation difference of  $180/n$  between components showed that the increase of r.m.s. contrast sensitivity with grating area was described by  $S_{r.m.s.} = S_{\max} (1 + A_c/A)^{-0.5}$ , where  $S_{r.m.s.}$  is r.m.s. contrast sensitivity,  $A$  is grating area,  $S_{\max}$  is the maximum r.m.s. contrast sensitivity obtainable by spatial integration, and  $A_c$  is the critical area marking the saturation of spatial integration. The goodness of the fit calculated by equation 2.29 described in Section 2.6.6 was on average 96%, ranging from 90 to 99%. Both  $A_c$  and  $S_{\max}$  decreased with increasing number of components reaching a minimum at  $n = 5$  or 6 but increased thereafter.  $A_c$  was found to decrease in approximate proportion to increasing spatial frequency squared whereas  $S_{\max}$  was almost independent

of spatial frequency.

When the contrast sensitivities were transformed to energy thresholds the increase of threshold with grating area could be described by  $E_{th} = E_0 (1 + A/A_c)$ , where  $E_{th}$  is energy threshold and  $E_0$  is the energy threshold at grating areas much smaller than  $A_c$ . The goodness of the fit calculated by equation 2.29 described in Section 2.6.6 was on average 93%, ranging from 91 to 94%.  $E_0$  was found to be independent of the number of components but decreased in proportion to increasing spatial frequency squared. At all spatial frequencies studied the product  $S_{max}^{-2} A_c$  was equal to  $E_0$ . The product was thus independent of the number of components but decreased in proportion to increasing spatial frequency squared.

All the above findings are compatible with the model (Rovamo et al., 1993b) that describes the human visual system as an image processor comprising (i) low-pass filtering due to ocular optics, (ii) neural high-pass filtering due to lateral inhibition, (iii) addition of internal neural noise, and (iv) signal detection by a local matched filter which integrates contrast information from a limited area. The matched filter approach has previously been shown to explain the perceived suprathreshold contrasts of sums of cosine gratings with 1-4 orientation components (Tiippana et al., 1994).

According to channel models pattern thresholds are determined by detectors which are selectively sensitive to particular spatial frequencies and orientations (Quick, Hamerley & Reichert, 1976; Graham, 1989). In such models the detection of all but the simplest patterns depends upon probability summation or some equally inefficient non-linear pooling of the outputs of many detectors (Graham & Robson, 1987). However, within the framework of the local matched filter model (Rovamo et al., 1993b) the dependency of contrast sensitivity on the grating area and number of orientation components results from the decrease in the efficiency of contrast energy collection, which is probably due to the increasing amount of contour and detail in the stimulus to be detected. The dependence of  $A_c$  on the number of orientation components is not predicted by the model but suggests that

the sampling aperture of the local matched filter as well as its efficiency at each grating size depends on the number of orientation components in the grating sum. This is in agreement with the fact that the human sampling aperture has a signal-dependent upper limit (Burgess, 1990).

The decrease of critical area ( $A_c$ ) of spatial integration with increasing spatial frequency in an approximate proportion to  $f^{-2}$  irrespective of the number of components implies that  $A_c$  covers the same amount of contour and detail at all spatial frequencies studied. This scale invariance of spatial integration is in agreement with Howell and Hess (1978) as well as with Virsu and Rovamo (1979) who showed that for simple cosine gratings spatial integration saturates at the same number of square cycles ( $Af^2$ ) irrespective of spatial frequency within 1-32 c/deg.

The experiments described in this section with sharp-edged circular apertures at the fovea showed that spatial integration for grating sums could be modelled by equation 3.16 described in Section 3.2.1 irrespective of the number of components. In addition, the experiments of Rovamo et al. (1993b) with simple cosine gratings have shown that aperture shape, the phase at which contrast is abruptly reduced to zero, aperture location in the visual field and edge type (smooth or sharp) has no qualitative effect on contrast sensitivity as function of area. This suggests that spatial integration for grating sums can also be modelled by equation 3.16 irrespective of aperture shape, edge type, cut-off phase, or eccentricity.

The finding that both  $A_c$  and  $S_{max}$  decrease with increasing number of components reaching a minimum at  $n = 5$  or  $6$  but increasing thereafter means that the effectiveness of spatial integration within the detection mechanism depends on the number of orientation components. The finding also supports the hypothesis (Virsu & Rovamo, 1979) that the area of spatial integration is determined by the amount of contour and detail within the grating, because in a sum of cosine gratings of different orientations the amount of contour and detail per unit area at and around the stimulus centre increases with the number of

components reaching a maximum at  $n = 5$  or  $6$  and decreases thereafter (see Figure 4.1.). This variation in the amount of contour and detail is, however, not taken into account by the measures of image complexity introduced recently (Kelly & Magnuski, 1975; Näsänen et al., 1994).

Although the integration area depends on the number of components,  $E_0 = S_{\max}^{-2} A_c$  does not, because it represents the energy threshold for very small stimuli, whose detection efficiency is not limited by the integration area or sampling aperture at any number of components.

On the basis of equation 3.20 described in Section 3.2.2  $E_0$  is proportional to  $[O_{\text{MTF}}(f) P_{\text{MTF}}(f)]^{-2}$ , where  $f$  is spatial frequency. Thus, the finding that  $E_0$  is proportional to  $f^{-2}$  at  $0.25$  to  $4$  c/deg indicates that the neural modulation transfer function is proportional to  $f$ , because the optical modulation transfer function of the human eye is close to unity at low and medium spatial frequencies (Deeley et al., 1991). The finding that  $P_{\text{MTF}}(f)$  is proportional to spatial frequency is in agreement with Rovamo et al. (1993b) and Banks et al. (1987) (see Section 3.2) and means that neural visual pathways attenuate low spatial frequencies relatively more than high spatial frequencies. Equally well the finding that  $P_{\text{MTF}}(f)$  is proportional to spatial frequency means that high spatial frequencies are relatively more amplified than low spatial frequencies. In any case the direct proportionality between  $P_{\text{MTF}}(f)$  and spatial frequency is in agreement with the proposal (Schade, 1956; Nachmias, 1968) that lateral inhibition (Ratliff & Hartline, 1959) reduces contrast sensitivity more at low than high spatial frequencies.

In conclusion, the experiments of this section have demonstrated that the contrast energy threshold for a sum of cosine gratings with different orientations decreases in proportion to increasing spatial frequency ( $0.25$ - $4$  c/deg) squared but increases as the same linear function of grating area normalised i.e. divided by the critical area for each number of components. These findings are compatible with the local matched filter model proposed by Rovamo et al. (1993b), although area normalisation is not predicted by the model.

### 4.3 *COMPLEX GRATINGS WITH VARIOUS ORIENTATION COMPONENTS IN NOISE*

#### 4.3.1 Introduction

For simple gratings without external spatial noise contrast sensitivity first increases with small numbers of square cycles ( $Af^2$ ), calculated as a product of the absolute grating area ( $A$ ) and spatial frequency squared ( $f^2$ ), but then the increase of contrast sensitivity ceases at larger numbers of square cycles (e.g. Virsu & Rovamo, 1979). The same result has been found in external spatial noise in contrast sensitivity studies (Coltman & Anderson, 1960; Luntinen et al., 1995) and in detection efficiency studies (e.g. van Meeteren & Barlow, 1981; Kersten, 1984; Näsänen et al., 1993). In agreement with Virsu and Rovamo (1979), van Meeteren and Barlow (1981) showed that in external spatial noise energy thresholds for sinewave gratings formed by modulating average dot density are determined by the number of cycles. Furthermore, Rovamo et al. (1992) found that contrast sensitivity in external spatial noise is independent of viewing distance and magnification. Thus, spatial integration for simple gratings is scale invariant both with and without external noise.

There are only a few studies concerning spatial integration for complex stimuli. Kukkonen et al. (1994) studied spatial integration in noise for bandpass-filtered point stimuli whose spatial frequency bandwidths were kept constant while areas were increased by modifying the phase spectra. They showed that detection efficiency for point spread stimuli is determined by stimulus area expressed in terms of spatial spread of contrast energy.

In this section spatial integration for sums of simple gratings ( $n = 3, 6, \text{ or } 16$ ) with the same Michelson contrast and spatial frequency, but different orientations and/or phases, was studied. Six different types of stimuli embedded in external additive spatial noise were used. Two different spatial frequencies within the range 0.5 to 4 c/deg were tested at each

number of components. The aim was to find out whether different stimulus configuration has any effect on spatial integration. R.m.s. contrast sensitivity and detection efficiency for sums of simple gratings with different orientations and/or phases was modelled, thus extending the model of human spatial vision (Rovamo et al., 1993b).

### 4.3.2 Methods

#### *Apparatus*

The experiments were carried out by using Apparatus 1 and Apparatus 2 described in Sections 2.1 and 2.2, respectively.

#### *Stimuli*

The stimuli consisted of sharp-edged circular grating fields (diameters 1, 2, 4, 8, or 16 cm on the screen) with an equiluminous surround limited to a circular field (diameter 20 cm) by a black cardboard. The stimuli were sums of various numbers of simple gratings ( $n = 3, 6, \text{ or } 16$ ) with the same Michelson contrast and spatial frequency (1 c/cm). Cosine stimuli consisted of equally spaced orientation components ( $180^\circ/n$ ) added in cosine phase. In sine stimuli the orientation components were added in sine phase. In cosine+sine stimuli even orientation components ( $[2k] 180^\circ/n, k = 1, 2, 3, \dots, 8$ ) were added in cosine phase and odd orientations ( $[2k-1] 180^\circ/n$ ) in sine phase. The random orientation stimuli consisted of a sum of simple cosine gratings with randomly chosen orientations ranging from  $0^\circ$  to  $180^\circ$ . Random phase stimuli consisted of a sum of equally spaced orientation components with randomly chosen phases between  $0^\circ$  and  $360^\circ$ . Random orientation+phase stimuli consisted of a sum of simple gratings with randomly chosen orientations and phases.

The stimuli are shown without noise in Figures 4.10 A and B although they were embedded in external spatial noise in the experiments. The numbers on the top refer to the number of components. In Figure 4.10 A cosine stimuli are shown on the top row, sine stimuli on the middle row, cosine+sine stimuli on the bottom row. In Figure 4.10 B random orientation stimuli are shown on the top row, random phase stimuli on the middle row, and random orientation+phase stimuli on the bottom row. The grating fields shown had a diameter of 16 cm on the screen. Figure 4.10 shows that four stimuli without orientation randomisation looked fairly similar when the number of components was 3 or 6. On the other hand, all three randomised stimuli looked fairly similar when the number of components was 16.

The gratings were embedded in white external noise. The circular noise fields had always the same diameter as the grating. Two-dimensional stationary spatial noise was produced by adding to each noise check within the noise field a random number drawn independently from a Gaussian distribution with zero mean. The distribution was truncated at  $\pm 2.5$  SD units. The r.m.s. contrast of spatial noise was varied by changing the standard deviation of the Gaussian luminance distribution. Neighbouring noise check luminances were uncorrelated. Check noise can be regarded as white if there are at least four noise checks per grating cycle at all spatial frequencies (Kukkonen, Rovamo & Näsänen, 1995). Each noise check consisted of 1x1, 2x2, or 3x3 image pixels. Thus, the two-dimensional spatial noise was regarded as white because there were 8-24 checks per cycle at the spatial frequency (1 c/cm) used in the experiments.

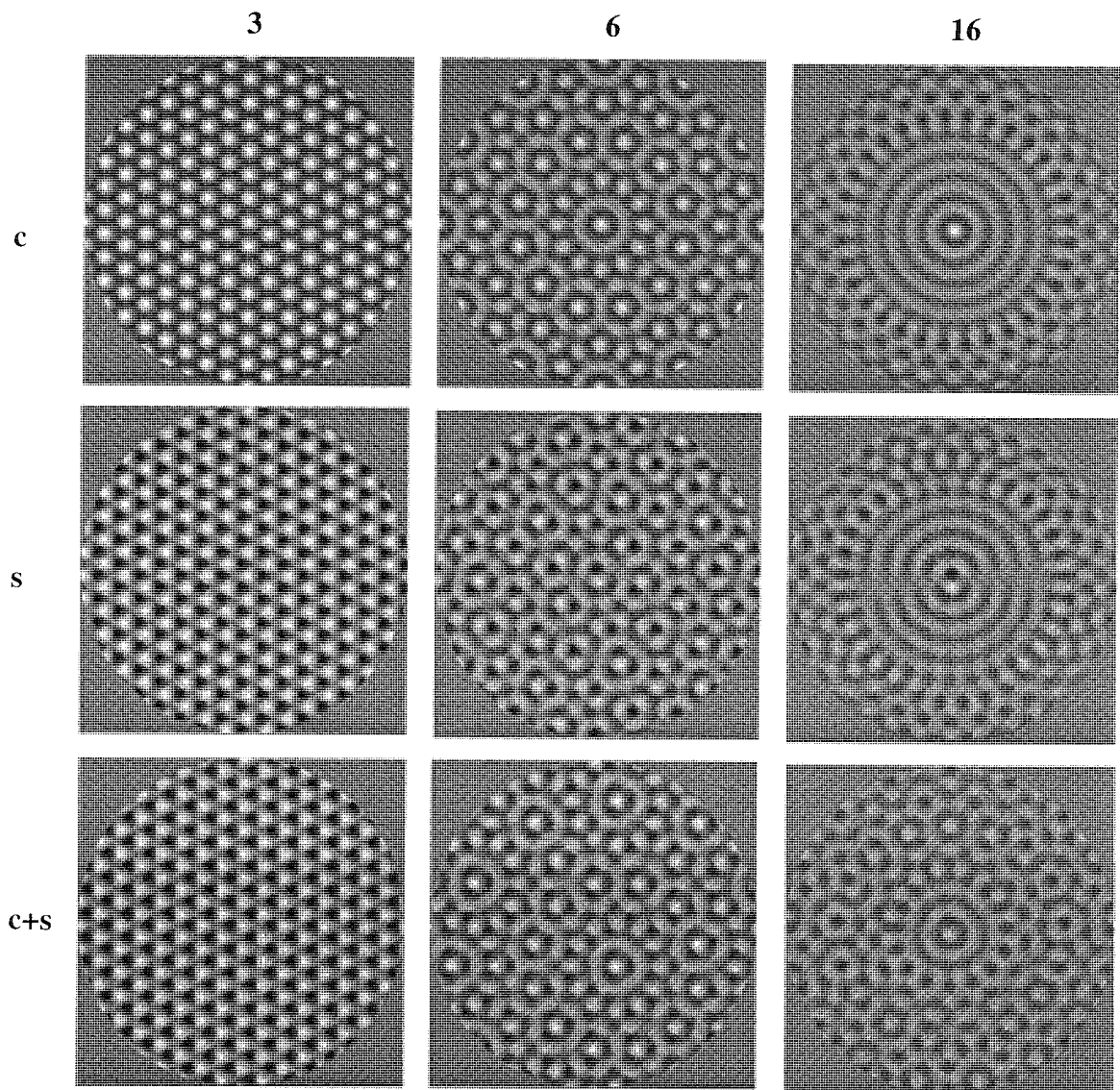
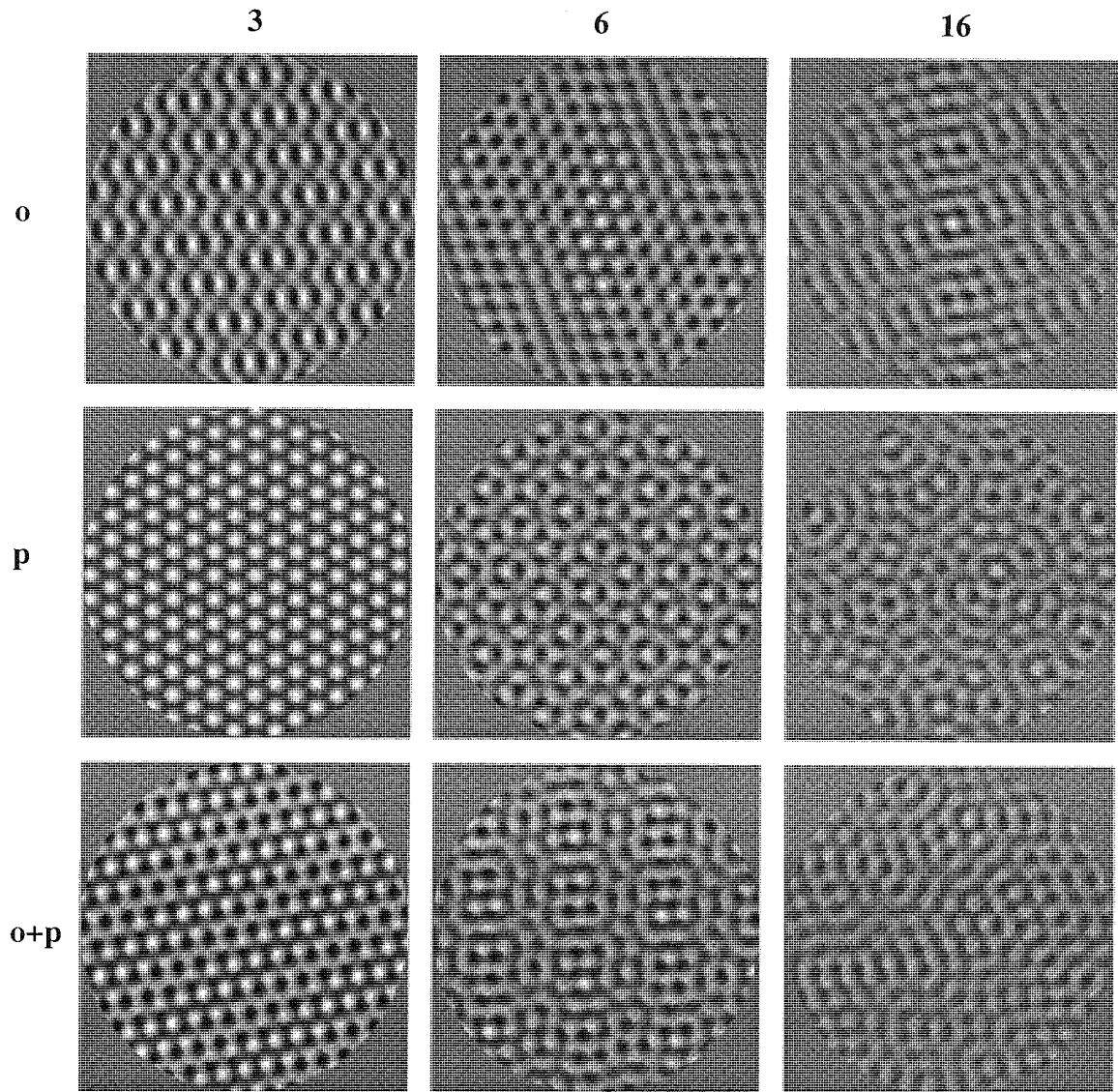


Figure 4.10 A Cosine, sine, and cosine+sine stimuli used in the experiments of Section 4.3.



**Figure 4.10 B** Random orientation, random phase, and random orientation+phase stimuli used in the experiments of Section 4.3.

## Spatial integration

In the three component condition the noise check size was 0.084 cm x 0.084 cm at 1 c/deg but 0.126 cm x 0.126 cm at 4 c/deg, whereas the r.m.s. contrast of noise was 0.25 in both. Thus, the spectral density of external noise calculated by equation 2.11 described in Section 2.6.2 was  $4.4 \times 10^{-4} \text{ cm}^2$  at 1 c/deg and  $9.9 \times 10^{-4} \text{ cm}^2$  at 4 c/deg.

In the six component condition the size of noise checks was 0.042 cm x 0.042 cm at 1 c/deg. The r.m.s. contrast of noise was 0.25 for cosine+sine, random phase, and random orientation+phase stimuli, but 0.3 for cosine, sine, and random orientation stimuli. The corresponding spectral densities of external noise were thus 1.1 and  $1.6 \times 10^{-4} \text{ cm}^2$ . At 2 c/deg the size of noise checks was 0.042 cm x 0.042 cm for random phase stimuli, but 0.084 cm x 0.084 cm for the other stimuli. The r.m.s. contrast of noise was 0.25 at 2 c/deg. Thus, the spectral density of external noise calculated by equation 2.11 described in Section 2.6.2 was  $1.1 \times 10^{-4} \text{ cm}^2$  for random phase stimuli and  $4.4 \times 10^{-4} \text{ cm}^2$  for all the others.

In the sixteen component condition the size of noise checks was 0.084 cm x 0.084 cm at 0.5 c/deg. The r.m.s. contrast of noise was 0.2 for all random stimuli, but 0.25 for cosine, sine, and cosine+sine stimuli. The corresponding spectral densities of external noise were 2.8 and  $4.4 \times 10^{-4} \text{ cm}^2$ . At 1 c/deg the size of noise checks was 0.042 cm x 0.042 cm and the r.m.s. contrast of noise was 0.2. Thus, the spectral density of external noise calculated by equation 2.11 described in Section 2.6.2 was  $7.1 \times 10^{-5} \text{ cm}^2$ .

### *Procedure*

Contrast thresholds for gratings with noise were determined by using the forced-choice algorithm at the probability of 0.84 correct responses described in Section 2.5. All data points of contrast sensitivity shown are the inverses of the geometric means of at least three threshold estimates.

## Spatial integration

Because the gratings in the experiment were embedded in noise, there were 5 samples of the stimuli (grating+noise) at each stimulus contrast level and one of them was chosen randomly for each exposure. The comparison stimulus (noise only) was chosen randomly from a set of 21 different noise stimuli. A new set of comparison stimuli was generated each time stimulus configuration or noise check size on the screen was changed.

Viewing was binocular with natural pupils and their diameter increased from 5 to 6.5 mm with viewing distances of 28.6 - 228 cm. The corresponding retinal illuminance was 980 - 1,660 phot.td.

The duration of grating exposure was 500 msec. Each trial consisted of two exposures separated by 600 msec and the observer indicated, which exposure contained the grating by pressing one of the two keys on a computer keyboard. Sound signal provided the feedback indicating whether the observer's response was correct or incorrect. A chin-rest was used to stabilise the head. The only light source was the display, otherwise the room was dark. No fixation point was used. The main experiments were performed in external spatial noise. Control experiments showed that the spectral densities of noise used reduced contrast sensitivity at least by a factor of three for each subject, which guarantees that external spatial noise is the principal source of noise determining the contrast threshold.

### *Subjects*

Three experienced subjects, aged 25 - 29 years, served as observers. Subject TH was a corrected astigmatic myope (od. -1.75 DS / os. -1.5/-0.25 x 155), OU was a corrected non-astigmatic myope/hyperope (od. -0.75 DS / os. +0.75 DS), and HK was an uncorrected hyperope (+0.5 DS oa.). Their accommodation had a range of at least 6 D. Hence, they were emmetropes at the viewing distances used in the experiments. Binocular Snellen acuity at 6 meters was 1.6 for TH, 1.5 for OU and 1.3 for HK.

*Contrast energy and r.m.s. contrast*

Contrast energy and r.m.s contrast were calculated by equations 2.6 and 2.7 respectively and they are described in Section 2.6.1.

*Spectral density of external noise*

Spectral density of external noise was calculated by equation 2.11 described in Section 2.6.2.

*Detection efficiency*

Detection efficiency was calculated by equation 2.25 described in Section 2.6.4.

*Spectral density of equivalent noise*

Spectral density of equivalent noise was calculated by equation 2.27 described in Section 2.6.5.

### 4.3.3 Results

In Figures 4.11 - 4.13 r.m.s. contrast sensitivity as a function of grating area expressed in terms of square cycles ( $Af^2$ ) was measured for sums of three (Figure 4.11), six (Figure 4.12), and sixteen (Figure 4.13) simple gratings with the same Michelson contrast and spatial frequency using six different stimulus types. Two different spatial frequencies within 0.5-4 c/deg were tested at each number of components. They were obtained by changing the viewing distance. Cosine, sine, cosine+sine, random orientation, random phase, and random orientation+phase stimuli were used (for further information see Stimuli in Methods). In Figure 4.11 viewing distance was 57 cm in A and 228 cm in B. In Figure 4.12 viewing distance was 57 cm in A and 114 cm in B and it was 28.6 cm in A, and 57 cm in B in Figure 4.13.

Cosine data and curve are in its original place, but for clarity of presentation the others have been shifted downwards by a factor of 3 (sine), 9 (cosine+sine), 27 (random orientation), 81 (random phase), and 243 (random orientation+phase). The numbers on the left refer to the spatial frequency studied, and percentages on the right to goodness of fit calculated by equation 2.29 described in Section 2.6.6.

As Figures 4.11 - 4.13 show, r.m.s. contrast sensitivity first increased with the number of square cycles but then the increase saturated at larger number of square cycles. At each number of orientation components spatial integration was found to be similar for all types of stimuli used and the two spatial frequencies tested. The increase of contrast sensitivity at small number of square cycles had a slope of 0.5 in double logarithmic coordinates but the slope decreased approaching zero at large number of square cycles areas suggesting that contrast sensitivity increase saturates at even larger numbers. Scrutiny revealed that the increase of contrast sensitivity with the number of square cycles was greatest at  $n = 16$  and smallest at  $n = 6$ . This means that the extent of spatial integration depends on the number of components.

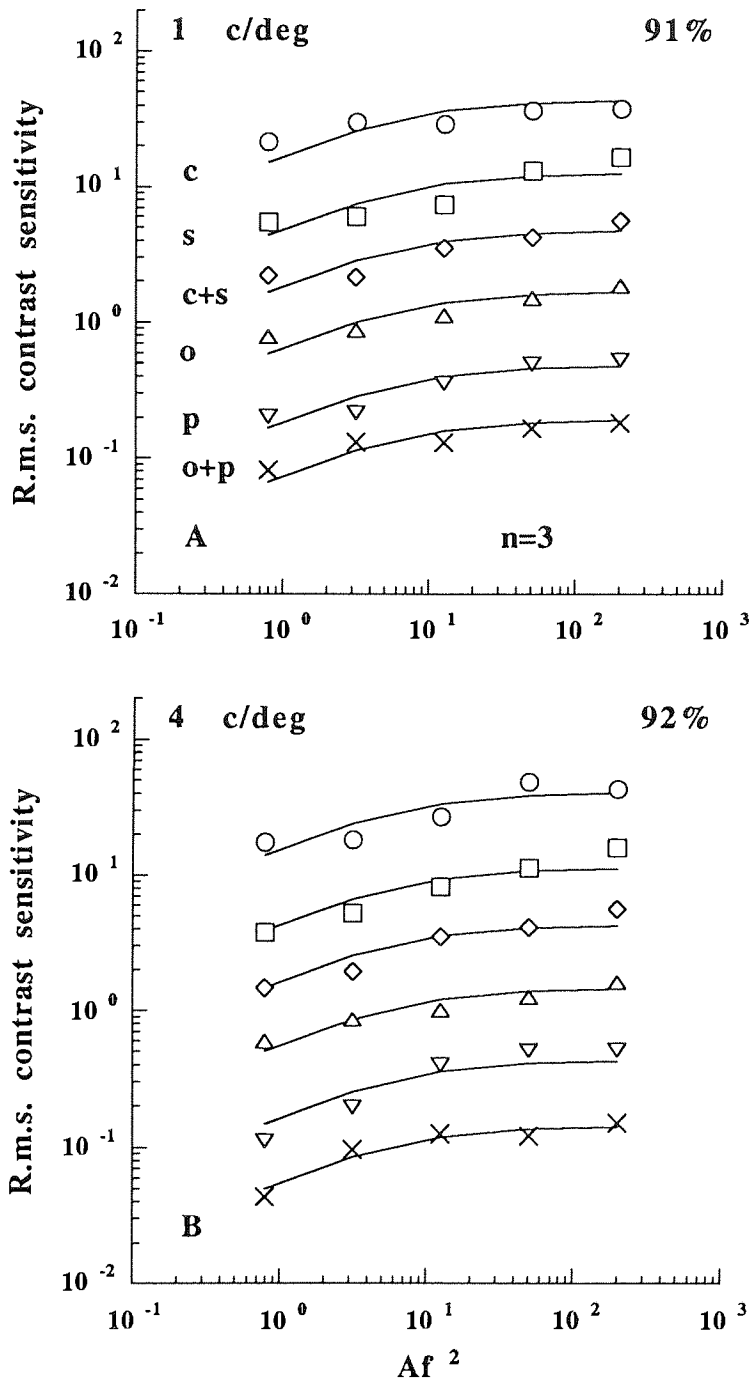


**Figure 4.11** R.m.s. contrast sensitivity as a function of the number of square cycles for sums of 3 simple gratings. The letters close to the data refer to the different types of stimuli: cosine (c), sine (s), cosine+sine (c+s), random orientation (o), random phase (p), and random orientation+phase (o+p). Subjects were OU (A), and HK (B).

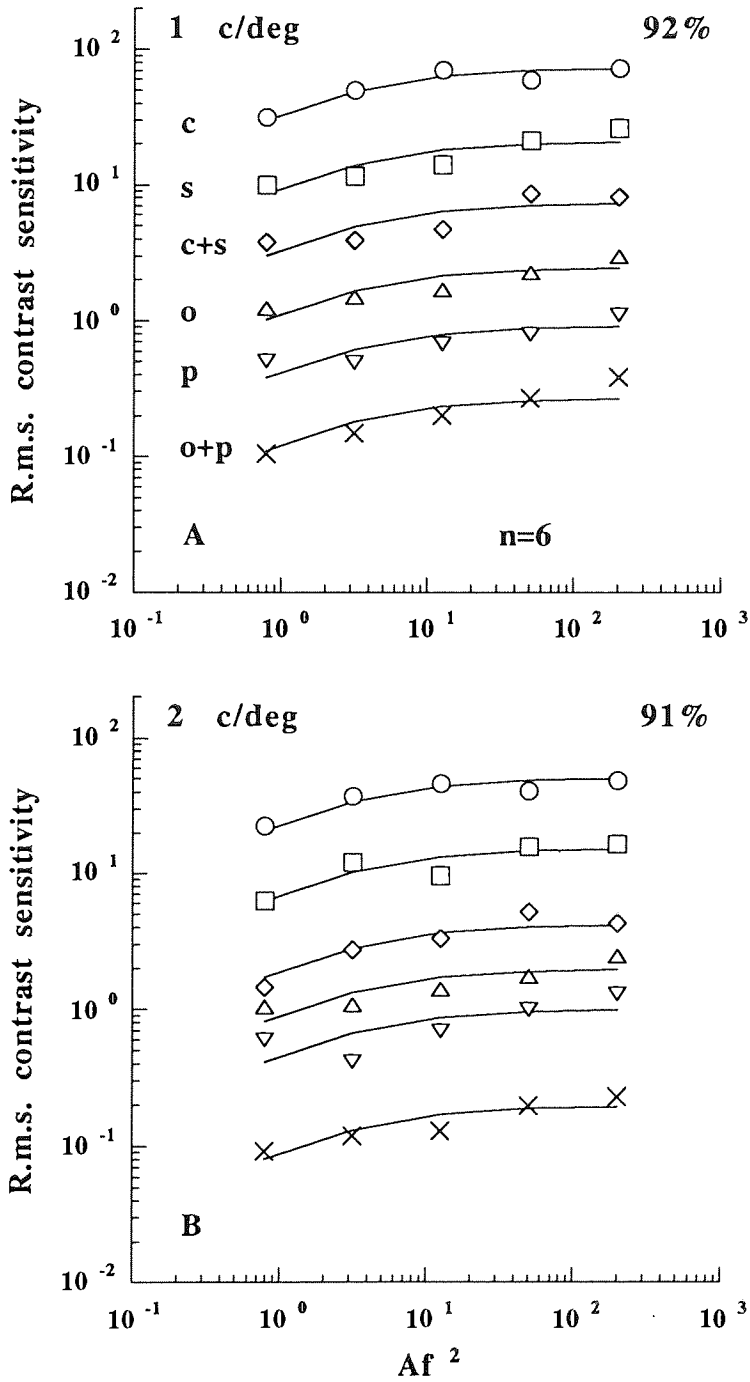


Figure 4.12 R.m.s. contrast sensitivity as a function of the number of square cycles for sums of 6 simple gratings. Symbols and subjects as in Figure 4.11.

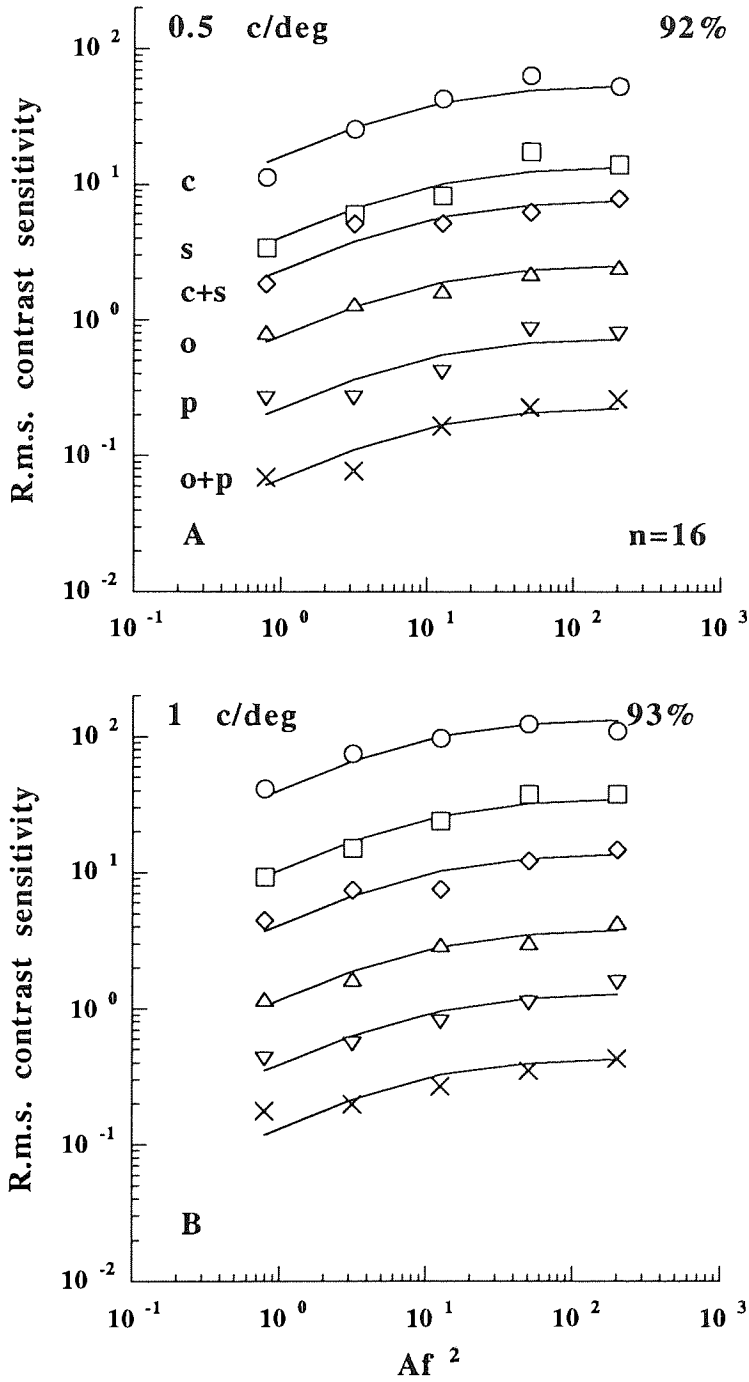
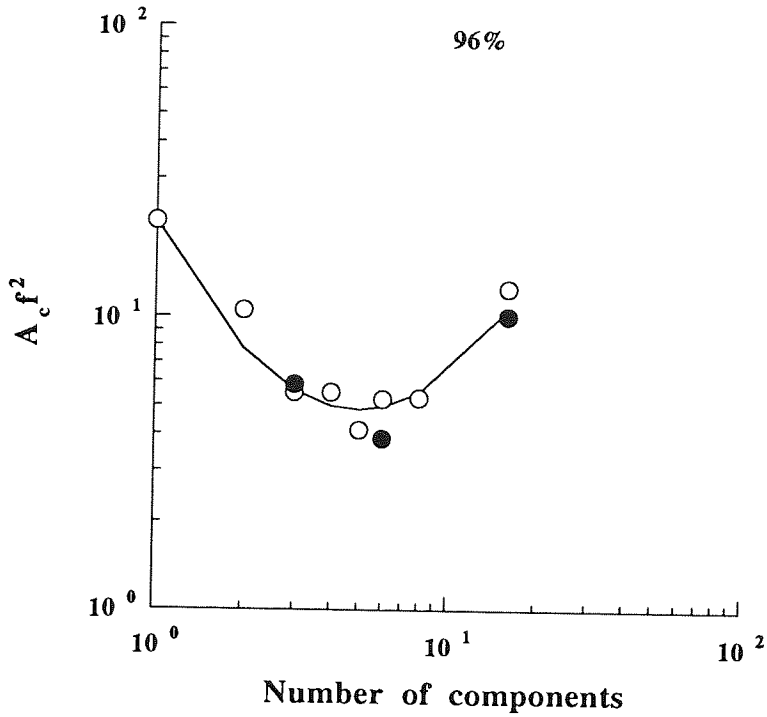


Figure 4.13 R.m.s. contrast sensitivity as a function of the number of square cycles for sums of 16 simple gratings. Symbols as in Figure 4.11. Subjects were TH (A), and OU (B).

The smooth curves of Figures 4.11 - 4.13 were obtained in the following way: in each Figure grating areas were expressed in terms of square cycles ( $Af^2$ ) and contrast sensitivities were averaged across different stimulus types and spatial frequencies at each number of square cycles. An estimate of  $A_c f^2$  was then obtained by fitting equation 3.21 described in Section 3.3 to the averaged data. Thereafter on the basis of equation 3.21 the r.m.s. contrast sensitivities measured for each stimulus type and spatial frequency were first divided by the corresponding values of the term  $(1 + A_c f^2 / Af^2)^{-0.5}$  and then geometrically averaged in order to get the estimates of  $S_{\max}$  for each stimulus type and spatial frequency.  $S_{\max}$  was allowed to vary across stimulus types and spatial frequencies because neither  $N_e$  or  $N_e f^2$  was not constant. The model described the data quite well. Goodness of fit calculated by equation 2.29 described in Section 2.6.6 was 91-93%.

As Figures 4.11 - 4.13 show the critical area and thus, the horizontal location of the spatial integration function for grating sums with a constant number of components can be regarded as independent of the stimulus type and spatial frequency.

In Figure 4.14 the critical number of square cycles ( $A_c f^2$ ) is plotted as a function of the number of components. The critical number of square cycles ( $A_c f^2$ ) marks the saturation point of spatial integration. The values of  $A_c f^2$  for sums of simple cosine gratings ( $n = 1$  to 16) with equally spaced orientations ( $180^\circ/n$ ) from the Section 4.2 have been averaged across subjects and spatial frequencies. The values of  $A_c f^2$  of the current study were obtained when equation 3.21 described in Section 3.3 was fitted to the data of Figures 4.11 - 4.13. As Figure 4.14 shows, the critical number of square cycles first decreased with increasing number of components reaching the minimum at  $n = 5$  to 6 and increased thereafter. Hence, spatial integration and the critical number of square cycles was found to depend on the number of orientation components. The critical numbers of square cycles from Section 4.2 and the current ones for 3, 6, and 16 components were found to be almost identical,



**Figure 4.14** The critical number of square cycles as a function of the number of components. Solid symbols refer to the earlier data from Section 4.2. and open symbols refer to the current data.

although earlier experiments were performed without external noise while current experiment were performed in additive spatial noise.

The normalised number of square cycles ( $A_c f^2 / Z_0$ ) was calculated by dividing all the values of  $A_c f^2$  in Figure 4.14 by the value 21.3 valid for one component, because  $g(1) = 1$  and thus  $A_c(f, 1?)f^2 = Z_0$ . According to Figure 4.14 the relationship between  $g$  and the number of components ( $n$ ) plotted in double logarithmic coordinates can be described by a second order polynomial, which goes through the origin  $(0, 0)$ . Thus,

$$\ln g(n) = a \ln(n) + b [\ln(n)]^2 \quad \text{i.e.} \quad g(n) = n^{a+b \ln(n)} . \quad (4.1)$$

According to equation 3.26 described in Section 3.3  $A_c f^2 / Z_0$  describes the dependence of  $g$  on the number of orientation components. Hence, equation 4.1 was fitted to the normalised data of Figure 4.14 by the method of least squares. The values of  $a$  and  $b$  were found to be  $-1.85$  and  $0.58$ , respectively. The solid curve was then calculated by multiplying equation 4.1 by  $Z_0$ . Goodness of fit was 96%.

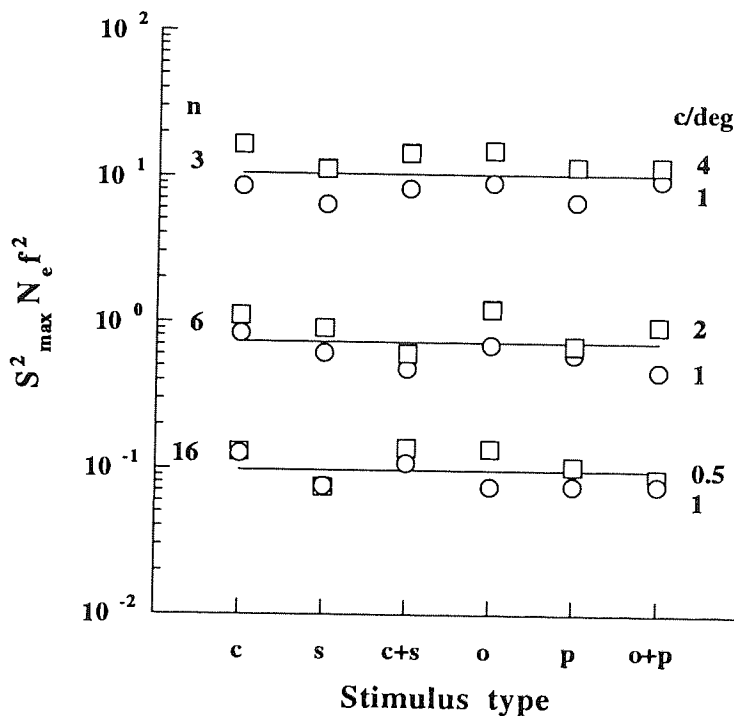


**Figure 4.15** The values of  $S_{\max}^2 N_e f^2$  as a function of the stimulus type. Subjects were TH (0.5 c/deg), OU (1 c/deg), and HK (2 and 4 c/deg).

On the basis of equation 3.24 described in Section 3.3 the estimates of maximum contrast sensitivity ( $S_{\max}$ ) squared were multiplied by  $N_e$  and  $f^2$  to eliminate the effects of varying spatial frequency and spectral density of spatial noise. In Figure 4.15  $S_{\max}^2 N_e f^2$  is plotted as a function of stimulus type. As Figure 4.15 shows, maximum sensitivity was fairly constant across the different stimulus types at each number of components.

However, maximum sensitivity was found to vary between subjects. The solid lines indicate the geometric means of values at each number of components. With few exceptions the values of  $S_{\max}^2 N_e f^2$  for subject HK at 4 and 2 c/deg were above the mean line whereas the values for subject OU at 1 c/deg fell below the mean line when the number of orientation components was 3 or 6. The difference between the values of  $S_{\max}^2 N_e f^2$  for sixteen component is not as noticeable between subjects TH at 0.5 c/deg and OU at 1 c/deg. On the basis of equation 3.24 the result of Figure 4.15 implies that the maximum efficiency of detection tends to be lower for subject OU than HK or TH.

The experimental contrast sensitivity data of Figures 4.11 - 4.13 were transformed to detection efficiencies by equation 2.25 described in Section 2.6.4 and plotted in Figures 4.16 - 4.18 as a function of the number of square cycles  $[Af^2 / g(n)]$  valid for sums of gratings with various numbers of orientation components. The values of  $g(n)$  were calculated by equation 4.1 described above for 3, 6, and 16 components. Figures 4.16 - 4.18 show that detection efficiency decreased with increasing number of square cycles irrespective of the spatial frequency or stimulus type. The smooth curves of Figures 4.16 - 4.18 were obtained as follows: in each frame of Figures 4.16 - 4.18 the efficiencies measured experimentally were averaged geometrically across all stimulus types used at each number of square cycles  $Af^2 / g(n)$  valid for sum of gratings with different orientations. On the basis of equation 3.27 described in Section 3.3 the averages were multiplied by  $\left[1 + \left(Af^2 g(n)^{-1} / Z_0\right)\right]$  and then geometrically averaged in order to get the estimate of  $\eta_{\max}$  for each frame of Figures 4.16 - 4.18. Goodness of fit calculated by equation 2.29 described in Section 2.6.6 was 91-92%.

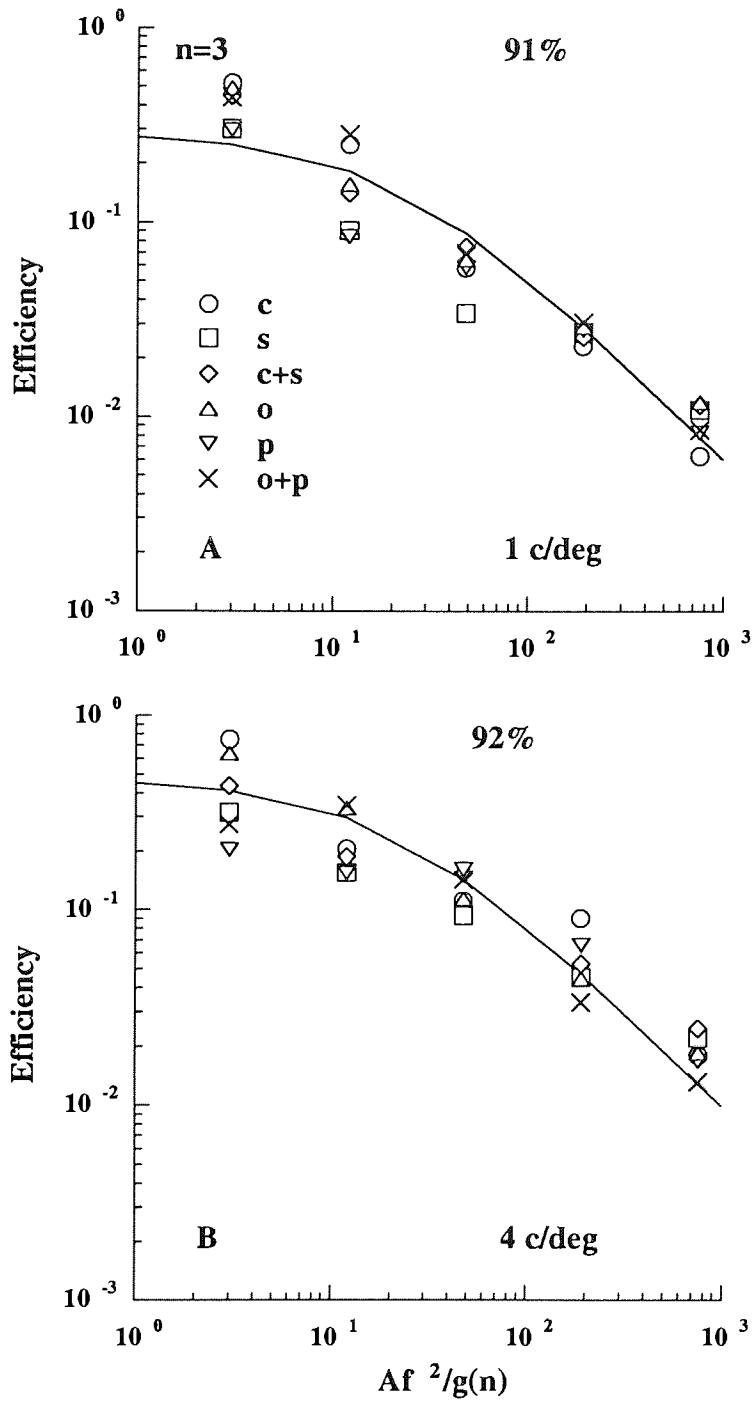


**Figure 4.16** Efficiency as a function of the number of square cycles for 3 components. Symbols as in Figure 4.11. Subjects were OU (A), and HK (B).

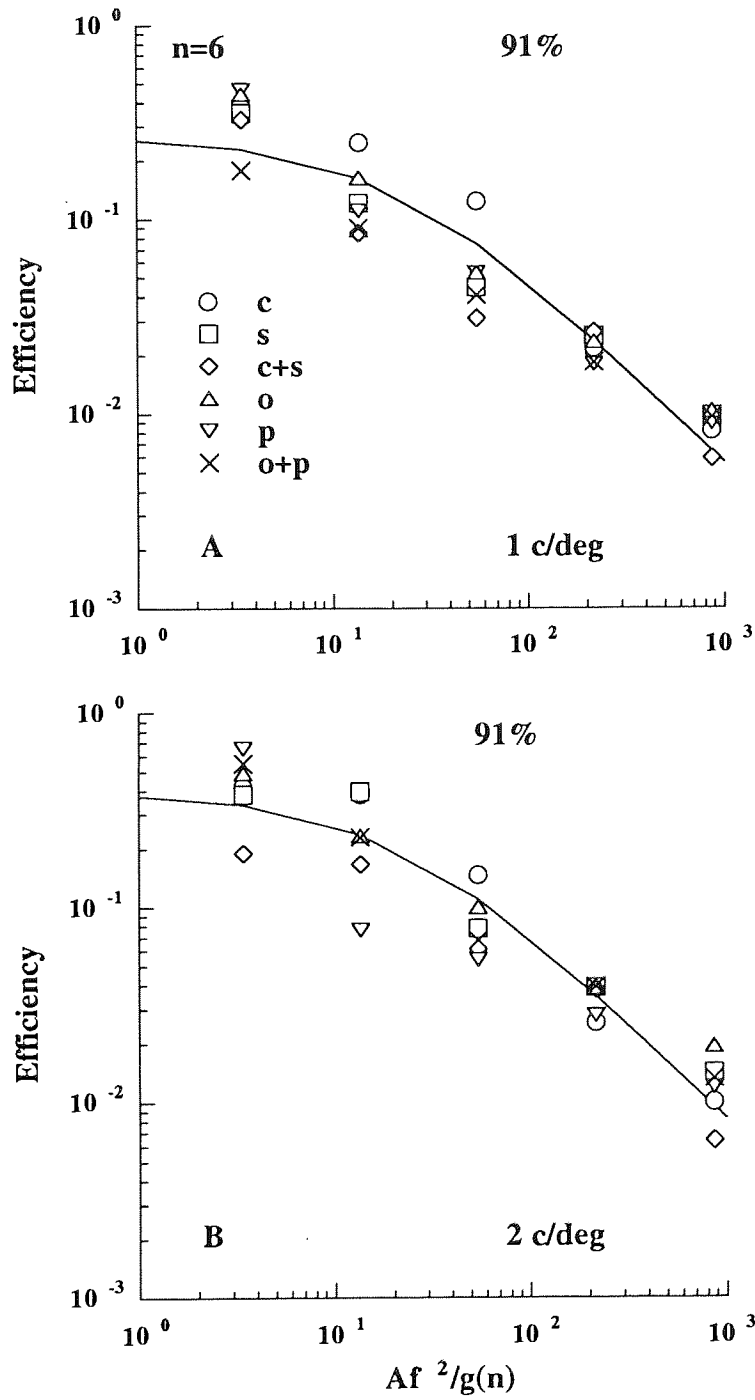


**Figure 4.17** Efficiency as a function of the number of square cycles for 6 components. Symbols as in Figure 4.11. Subjects were OU (A), and HK (B).

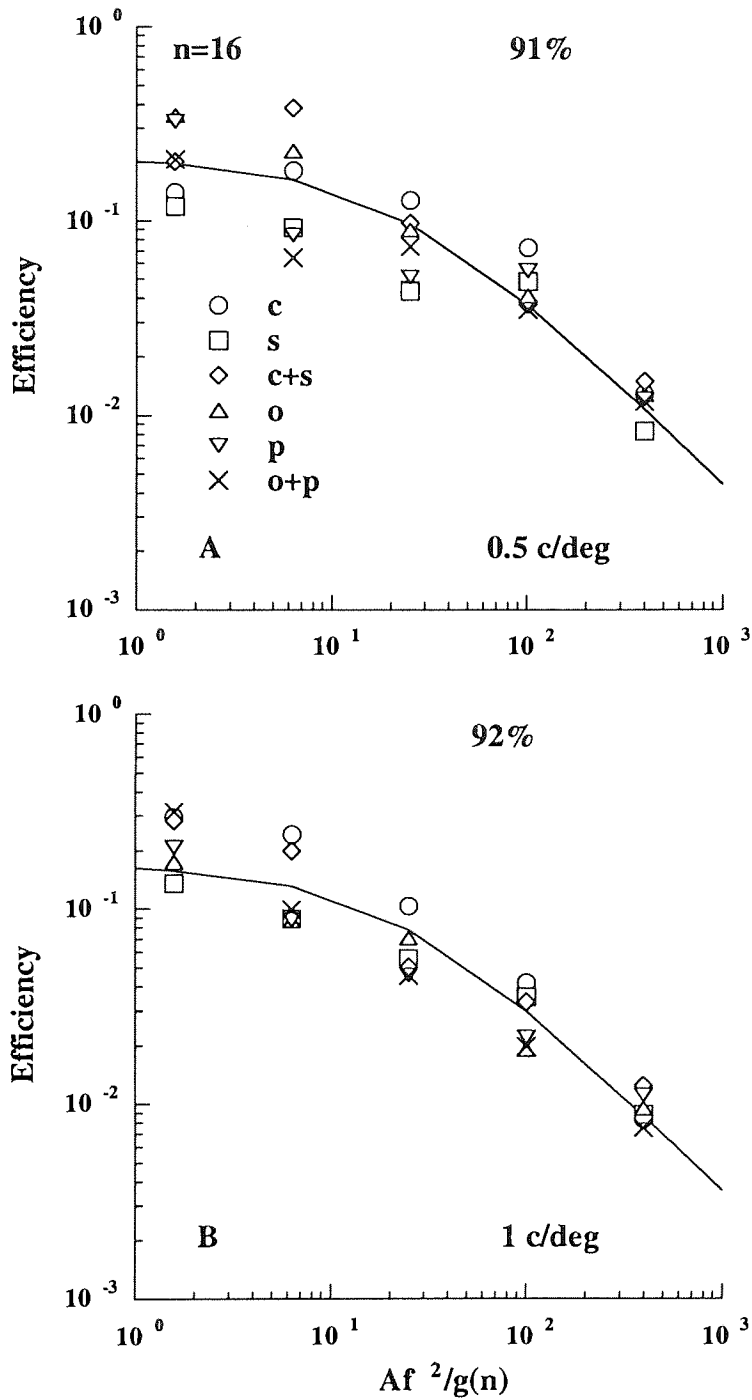


**Figure 4.18** Efficiency as a function of the number of square cycles for 16 components. Symbols as in Figure 4.11. Subjects were TH (A), and OU (B).

Scrutiny of Figures 4.16 - 4.18 at  $Af^2 / g(n) = 1$  revealed that maximum efficiency varied among the subjects. Subject OU had lower maximum efficiencies (0.29 and 0.27) than subject HK (0.47 and 0.39) for 3 and 6 components. Subject OU's maximum efficiency (0.17) is also slightly lower than that of subject TH (0.21) for 16 components although the difference is marginal.

It is interesting to know whether the spectral density of equivalent noise (i.e., external noise equivalent to internal neural noise) varies with the number of components. The spectral density of equivalent noise was calculated by equation 2.27 described in Section 2.6.5 using subject OU's contrast sensitivity data from Section 4.2 measured for cosine gratings without external noise and her current contrast sensitivity data measured in spatial noise. Geometric mean  $\pm$  standard deviation of the spectral density of equivalent noise was found to be  $7.10 \pm 1.38$ ,  $6.51 \pm 1.22$ , and  $4.82 \pm 1.23 \times 10^{-5}$  at 3, 6, and 16 orientation components. Hence, equivalent noise was not affected by the number of orientation components, in agreement with the model of human spatial vision (Rovamo et al., 1993b).

### 4.3.4 Discussion

The experiments of this section showed that r.m.s. contrast sensitivity first increased with the number of square cycles, but the increase then ceased at larger numbers of square cycles when stimuli were sums of 3, 6, or 16 simple gratings with the same Michelson contrast and spatial frequency but different orientations and/or phases embedded in external spatial noise. The finding is in agreement with earlier studies with and without noise (e.g. Savoy & McCann, 1975; Virsu & Rovamo, 1979; Rovamo et al., 1993b; Coltman & Anderson, 1960).

The contrast detection model described the data accurately. The critical number of square cycles ( $A_c f^2$ ), and thus spatial integration, were found to be similarly dependent on the number of orientation components with noise in the experiments of this section, and

without external noise in the experiments of Section 4.2. This finding gives further evidence that spatial integration is similar with and without noise. The experiments showed that spatial integration depended on the number of grating components but different stimulus configurations had no effect on the critical area.

According to equation 3.24 described in Section 3.3 the parameters which affect maximum sensitivity are the critical number of square cycles ( $A_c f^2$ ), maximum efficiency ( $\eta_{\max}$ ), spectral density of external noise ( $N_e$ ) and spatial frequency squared ( $f^2$ ). When the effects of varying spatial frequency ( $f$ ) and the spectral density of external noise ( $N_e$ ) were eliminated, maximum sensitivity was found to be fairly constant across the different stimulus types. However, maximum sensitivity varied between subjects.

Detection efficiencies decreased with increasing number of square cycles valid for sums of gratings with various numbers of orientations, in agreement with the model and earlier studies (e.g. van Meeteren & Barlow, 1981; Näsänen et al., 1994; Kukkonen et al., 1994). Kukkonen et al. (1994) found that detection efficiency for bandpass-filtered point stimuli decreased as a function of stimulus area expressed in terms of spatial spread of contrast energy. A simple decreasing power function ( $y = ax^{-b}$ ) was found to accurately describe their data. The model used in this thesis describes efficiency data as a single decreasing function of the form  $y = \frac{1}{1 + x/x_c}$ , even though a power function would also be appropriate fit for the current data. The maximum efficiency was found to vary between subjects which explains the differences in maximum sensitivities according to equation 3.24 described in Section 3.3.

The estimated spectral density of equivalent noise (i.e., external noise equivalent to internal noise) was not affected by the number of orientation components. The finding provides further information of internal noise which, according to Burgess (1990), is one of the limiting factors of human performance.

#### 4.4 *COMPLEX GRATINGS WITH TWO SPATIAL FREQUENCIES IN NOISE*

##### 4.4.1 Introduction

Gratings consisting of two or more spatial frequency components have been widely used in sinewave summation experiments which have provided some of the strongest support for the multiple channel theory in the human visual system (Sachs et al., 1971; Graham & Nachmias, 1971; Kulikowski & King-Smith, 1973; Pantle, 1973; Quick & Reichert, 1975; Mostafavi & Sakrison, 1976; Graham, Robson & Nachmias, 1978; Quick, Mullins & Reichert, 1978; Graham & Robson, 1987). The above studies have shown that a compound grating containing two or more components of far-apart spatial frequencies is only slightly more detectable in terms of Michelson contrast than its most detectable component. Furthermore, they have found that the detectability of the compound grating does not depend on the relative phase of its components.

Although sums of two spatial frequencies have evoked wide interest among vision researchers, no references in the existing literature have been found concerning spatial integration of such stimuli. Earlier integration studies have shown that contrast sensitivity first increases with grating area but then the process of spatial integration saturates (e.g. Findlay, 1969; Howell & Hess, 1978; Estevez & Cavonius, 1976; Coltman & Anderson, 1960). Stimuli were embedded in external spatial noise which makes it possible to estimate the human detection efficiency, thus providing alternative metrics for summation-square plots found, for example, in the study of Graham et al. (1978).

In this section spatial integration was investigated for sums of two vertical cosine or sine gratings with two different spatial frequency components. The ratio between spatial frequencies was 1:3 and their relative Michelson contrasts varied in the range 0 to 1. The gratings were embedded in white external spatial noise. The aim was to find out how

spatial integration depends on the relative contrasts of two spatial frequency components and how the number of square cycles is calculated for sums of gratings with two different spatial frequencies. In addition, the model was tested under an assumption that the logarithmic critical area for a grating comprising the sum of two spatial frequencies is the sum of the logarithmic critical areas of the component frequencies weighted by their relative contrasts.

### 4.4.2 Methods

#### *Apparatus*

The experiments were carried out using Apparatus 1 and Apparatus 2 described in Sections 2.1 and 2.2, respectively.

#### *Stimuli*

The stimuli consisted of circular grating fields (diameters 0.5, 1, 1.5, 2, 4, 8, or 16 cm on the screen) with an equiluminous surround limited to a circular field (diameter 20 cm) by a black cardboard. The stimuli were sums of two simple vertical gratings (0.67 and 2 c/cm on the screen) added in cosine (peaks-add) or sine (peaks-subtract) phase. The relative Michelson contrasts for the fundamental spatial frequency and its third harmonic were 1/0, 0.75/0.25, 0.5/0.5, 0.25/0.75, or 0/1. Thus, there were 5 different sums of two cosine gratings and 5 different sums of two sine gratings with the spatial frequency ratio of 1:3. The various pairs of spatial frequencies (0.5+1.5, 1.0+3.0, and 2.0+6.0 c/deg) studied were obtained by changing viewing distance.

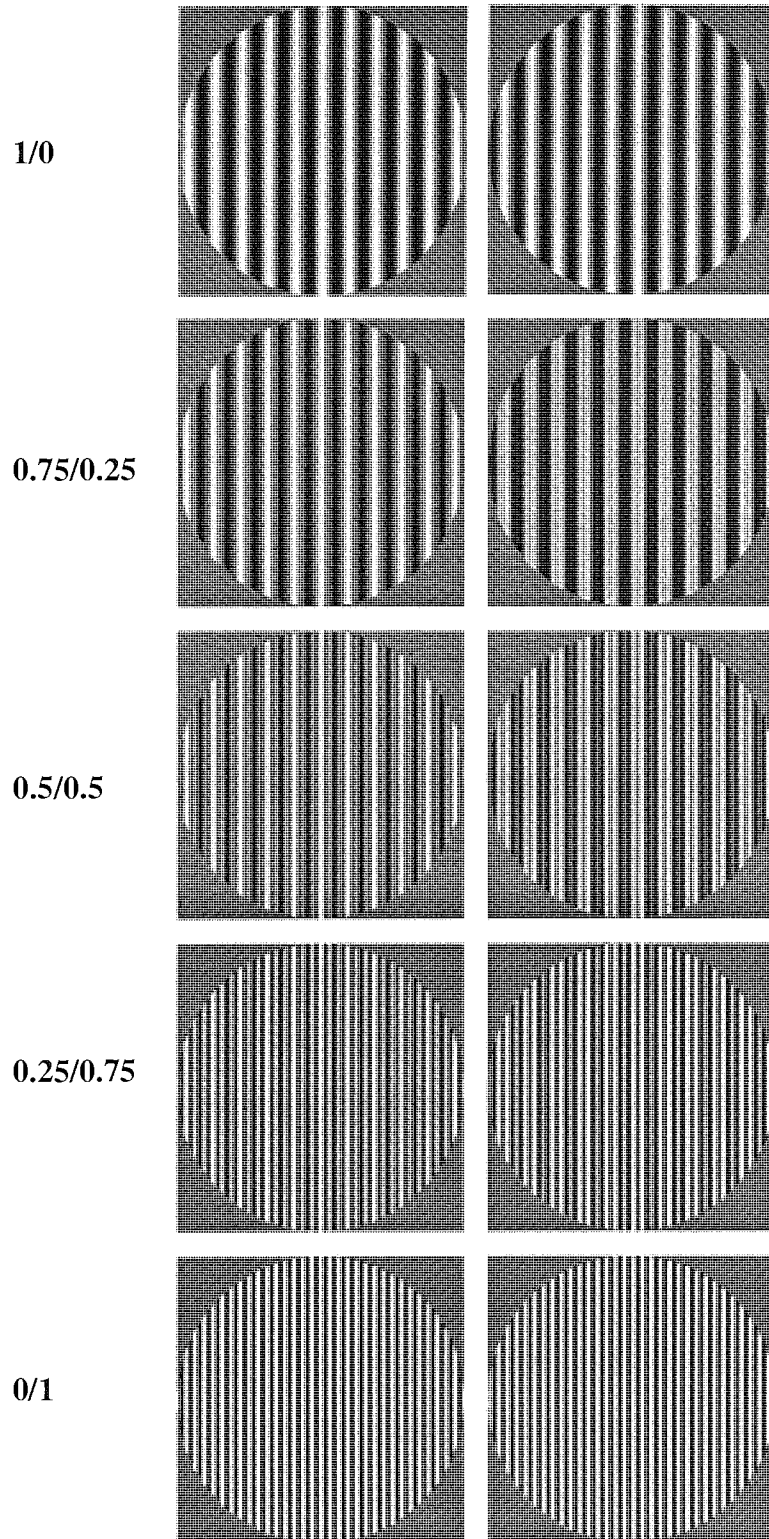


Figure 4.19 The stimuli in the experiments of Section 4.4.

The stimuli are shown without external noise in Figure 4.19 although the experiments were performed in noise. Cosine stimuli are shown on the left and sine stimuli on the right. The grating fields shown had a diameter of 16 cm on the screen. The numbers on the left refer to the relative contrasts of the fundamental and its third harmonic. Notations 1/0 and 0/1 mean that the stimulus only contains fundamental or the third harmonic. Figure 4.19 shows that the differences in luminance profile between peaks-add (cosine) and peaks-subtract (sine) were most noticeable when the contrast ratio between the fundamental and the third harmonic was 0.75/0.25 or 0.5/0.5.

The stimuli were embedded in white external spatial noise and the circular noise field had always the same diameter as the grating. Two-dimensional stationary spatial noise was produced by adding to each noise check within the noise field a random number drawn independently from a Gaussian distribution with zero mean. The distribution was truncated at  $\pm 2.5$  SD units. The r.m.s. contrast of spatial noise was varied by changing the standard deviation of the Gaussian luminance distribution. Neighbouring noise check luminances were uncorrelated. Each noise check consisted of 1x1 or 2x2 image pixels corresponding to 24 and 12 noise checks per cm, respectively. The highest spatial frequency was 2 c/cm. Check noise can be regarded as white if there are at least four noise checks per grating cycle at all spatial frequencies (Kukkonen et al., 1995). Thus, the two-dimensional spatial external noise was regarded as white because there were at least 6 checks per cycle at the spatial frequencies used in the experiments.

Noise pixel size was 0.084 cm x 0.084 cm for 0.5+1.5 and 2.0+6.0 c/deg but 0.042 cm x 0.042 cm for 1.0+3.0 c/deg. The r.m.s. contrast of external spatial noise was 0.3 at all spatial frequencies. The spectral density of external noise on the screen calculated by equation 2.11 described in Section 2.6.2 was  $1.1 \times 10^{-3} \text{ deg}^2$  at 0.5+1.5 and 2.0+6.0 c/deg but  $7.0 \times 10^{-5} \text{ deg}^2$  at 1.0+3.0 c/deg.

### *Procedure*

Contrast thresholds for gratings with noise were determined by using the forced-choice algorithm at the probability of 0.84 correct responses described in detail in Section 2.5. All data points of contrast sensitivity shown are the inverses of the geometric means of at least three threshold estimates.

Because the gratings were embedded in noise, there were 5 samples of the stimuli (grating+noise) at each stimulus contrast level. One of them was chosen randomly for each exposure. The comparison stimulus (noise only) was chosen randomly from a set of 21 different noise stimuli. A new set of comparison stimuli was generated each time stimulus configuration or noise check size on the screen changed.

Viewing was binocular with natural pupils and their diameter increased from 5 to 6 mm with viewing distances of 43 to 172 cm. The range of retinal illuminance was thus 980 - 1,400 phot.td.

The duration of grating exposure was 500 msec. Each trial consisted of two exposures separated by 600 msec and the observer indicated, which exposure contained the grating by pressing one of the two keys on a computer keyboard. Sound signal provided the feedback indicating whether the observer's response was incorrect. A chin-rest was used to stabilise the head. The only light source was the display, otherwise the room was dark. No fixation point was used. The main experiments were performed in external spatial noise. Control experiments showed that the spectral densities of noise used reduced contrast sensitivity at least by a factor of three for each subject, which guarantees that external spatial noise is the principal source of noise determining the contrast threshold.

### *Subjects*

Three experienced subjects, aged 24 - 28 years, served as observers. Subjects AS and KL were corrected astigmatic myopes (od. -2.25/-0.5 x 5 / os. -2.25/-0.5 x 5) and (od. -1.75/-0.5 x 90 / os. -1.5/-0.5 x 90), respectively, but OU was a corrected non-astigmatic myope/hyperope (od. -0.75 DS / os. +0.75 DS). Their accommodation had a range of at least 6 D. Hence, they were emmetropes at the viewing distances used in the experiments. With optimal refraction binocular Snellen acuity at 6 meters was 1.2 for AS, 1.6 for KL, 1.5 for OU.

### *R.m.s. contrast and energy threshold*

Contrast energy and r.m.s contrast were calculated by equations 2.6 and 2.7 respectively and they are described in Section 2.6.1.

### *Spectral density of external noise*

Spectral density of external noise was calculated by equation 2.11 described in Section 2.6.2.

### *Detection efficiency*

Detection efficiency was calculated by equation 2.25 described in Section 2.6.4.

4.4.3 Results

In the experiments of Figure 4.20 binocular r.m.s. contrast sensitivity as a function of area was measured for the sums of two simple vertical cosine or sine gratings comprising a fundamental spatial frequency ( $f$ ) and its third harmonic ( $3f$ ). The gratings were embedded in white additive external spatial noise. The fundamental spatial frequencies were 0.5, 1, and 2 c/deg and their third harmonics 1.5, 3, and 6 c/deg, respectively. Viewing distance was 43 cm at 0.5+1.5 c/deg, 86 cm at 1.0+3.0 c/deg, and 173 cm at 2.0+6.0 c/deg. The relative Michelson contrasts for the fundamental and its third harmonic were 1/0, 0.75/0.25, 0.5/0.5, 0.25/0.75 or 0/1.

In Figure 4.20 the ratios on the top left refer to the relative Michelson contrasts of the fundamental spatial frequency and its third harmonic, respectively. The numbers on the top right refer to the goodness of the calculated by equation 2.29 described in Section 2.6.6.

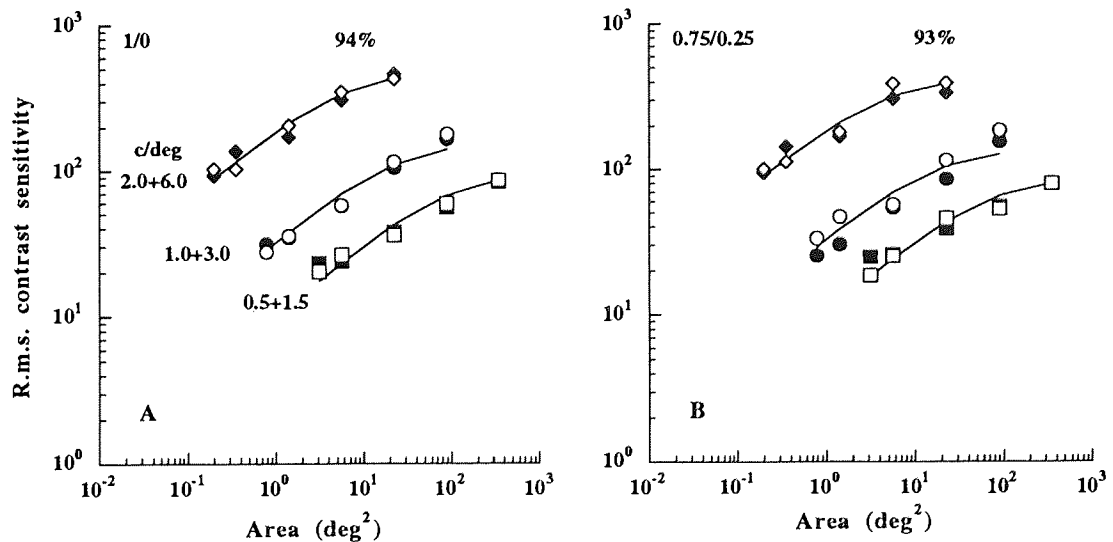


**Figure 4.20** A-B R.m.s. contrast sensitivity as a function of grating area for sums of two spatial frequency components in cosine (solid symbols) or in sine phase (open symbols). Subjects were KL (2.0+6.0 c/deg), OU (1.0+3.0 c/deg), and AS (0.5+1.5 c/deg).

## Spatial integration

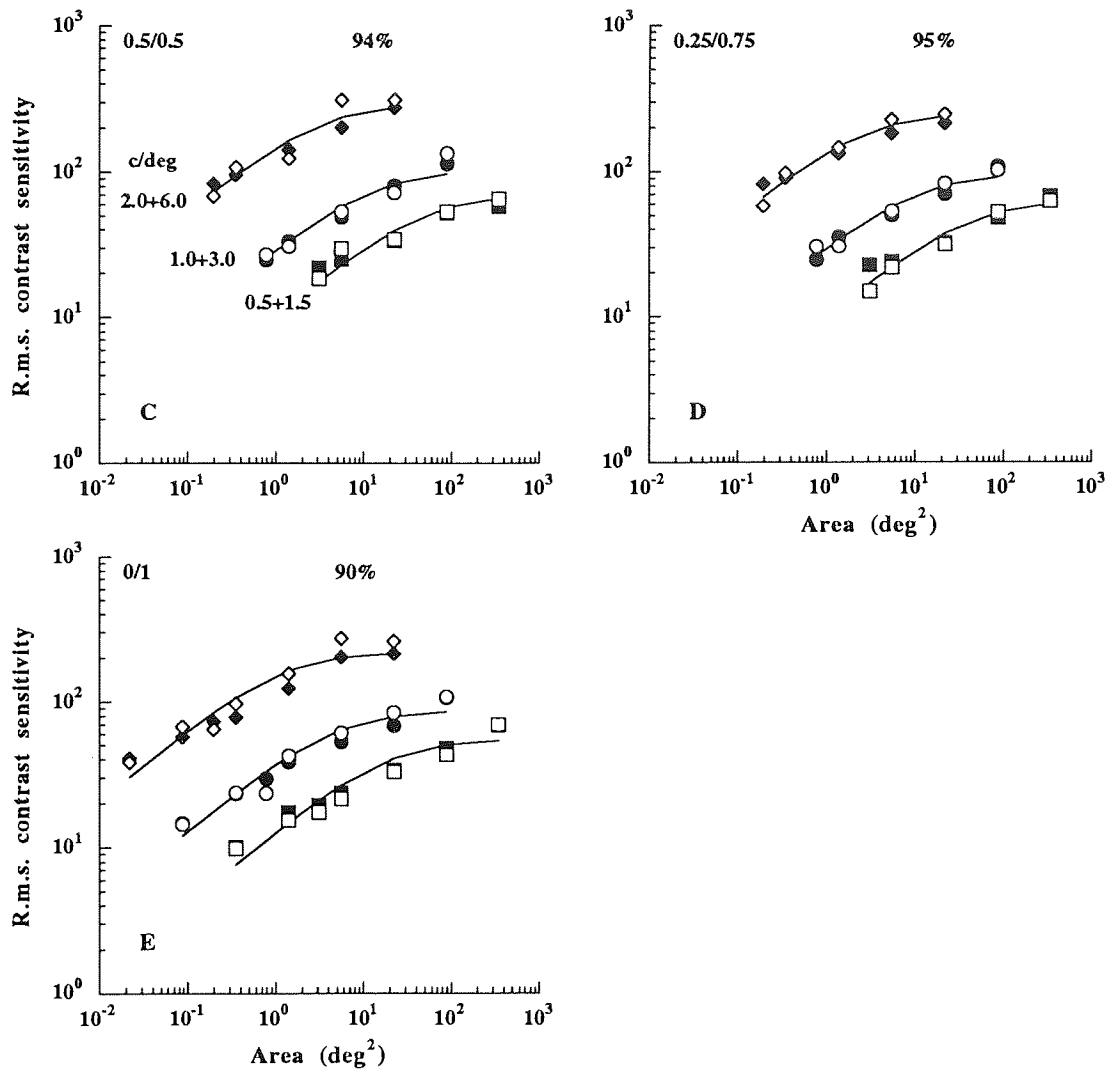


**Figure 4.20** C-E R.m.s. contrast sensitivity as a function of grating area for sums of two spatial frequency components in cosine (solid symbols) or in sine phase (open symbols). Subjects were as in Figure 4.20 A-B.

For clarity of presentation the uppermost curve and data points have been shifted upwards by a factor of four. The numbers close to the curves on the left refer to the spatial frequencies studied.

As Figure 4.20 shows, contrast sensitivity increased with grating area at all relative contrasts and spatial frequencies of the fundamental and its third harmonic. Also, contrast

sensitivity was always similar for the sums of cosine and sine gratings. However, the contrast sensitivity functions were displaced horizontally to smaller areas at higher spatial frequencies of the fundamental and its third harmonic. In addition, the close inspection of Figure 4.20 revealed that the contrast sensitivity functions were displaced horizontally to smaller areas with increasing relative contrast of the third harmonic.

In agreement with the model (Rovamo et al., 1993b) the increase of contrast sensitivity at small grating areas had a slope of 0.5 in double logarithmic coordinates, but the slope decreased approaching zero at large grating areas suggesting that contrast sensitivity increase saturates at even larger areas.

The scrutiny of Figure 4.20 revealed that the critical area ( $A_c$ ) marking the transition between increasing and constant parts of the contrast sensitivity function decreased with increasing spatial frequency of the pair ( $f, 3f$ ). Also,  $A_c$  decreased with increasing relative contrast of the third harmonic.

The smooth curves of Figure 4.20 were fitted separately to the data of each frame in the following way: first grating areas were expressed in terms of square cycles ( $Af^2$ ) and contrast sensitivities were averaged across the three spatial frequency pairs ( $f, 3f$ ) at each number of square cycles. An estimate of the critical number of square cycles ( $A_c f^2$ ) was then obtained by fitting equation 3.21 described in Section 3.3 to the averaged data. The critical areas for the individual curves in each frame were then obtained by dividing the critical number of square cycles by the corresponding fundamental spatial frequency squared. Thereafter on the basis of equation 3.21 described the r.m.s. contrast sensitivities measured for each spatial frequency pair were first divided by the corresponding values of the term  $(1 + A_c/A)^{-0.5}$  and then geometrically averaged in order to get the estimates of  $S_{max}$  for each spatial frequency pair. The goodness of the fit calculated by equation 2.29 described in Section 2.6.6 was on average 93% ranging from 90% to 95%.

In Figure 4.21 the critical area ( $A_c$ ) marking the saturation of spatial integration is plotted as a function of the relative contrast of the third harmonic spatial frequency. The

values of  $A_c$  were obtained when equation 3.21 described in Section 3.3 was fitted to the data of Figure 4.20. Figure 4.21 shows that  $A_c$  decreased with increasing relative contrast of the third harmonic at all spatial frequency pairs. In addition,  $A_c$  was found to decrease with increasing spatial frequency of the pair ( $f, 3f$ ). The solid lines were calculated by equation 3.29 described in Section 3.4 fitted to the data of Figure 4.20.  $Z_0$  was found to be 34.9. According to equation 3.29  $A_c$  decreased by a factor of 9 when the relative contrast of the third harmonic increased from zero to unity. The model described the data rather well and the goodness of fit calculated by equation 2.29 described in Section 2.6.6 was 94%.

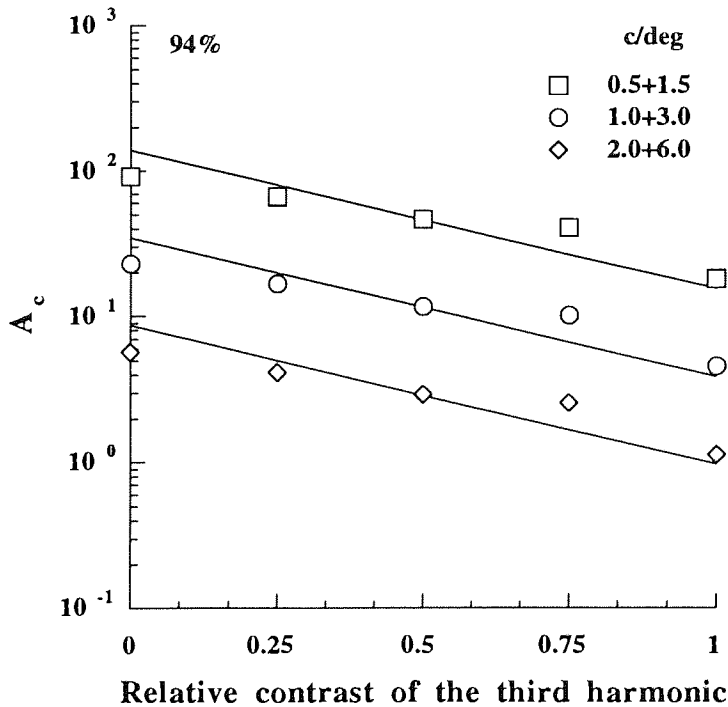


**Figure 4.21** The critical area ( $A_c$ ) as a function of the relative contrast of the third harmonic.

In Figure 4.22 the maximum sensitivity ( $S_{max}$ ) is plotted as a function of the relative contrast of the third harmonic spatial frequency. The values of  $S_{max}$  were obtained when equation 3.21 described in Section 3.3 was fitted to the data of Figure 4.20. As Figure

4.22 shows the maximum sensitivity decreased with the increasing relative contrast of the third harmonic at all spatial frequency pairs. The solid lines were calculated by equation 3.31 described in Section 3.4 fitted to the data of each spatial frequency pair separately. The values of  $S'_{\max}$  were found to be 63.2, 197, and 277 at spatial frequency pairs of 0.5+1.5, 1.0+3.0, and 2.0+6.0 c/deg, respectively. The model described the data quite well and goodness of fit calculated by equation 2.29 described in Section 2.6.6 was 93%.

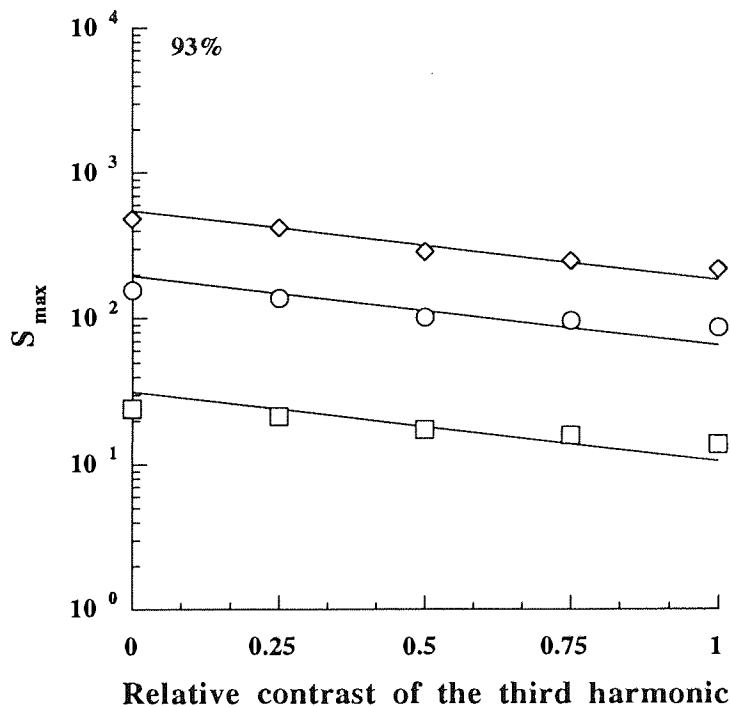


**Figure 4.22** The maximum sensitivity ( $S_{\max}$ ) as a function of the relative contrast of the third harmonic. Subjects were KL (2.0+6.0 c/deg), OU (1.0+3.0 c/deg), and AS (0.5+1.5 c/deg).

In Figure 4.23 the data from Figure 4.20 was expressed in terms of normalised r.m.s. contrast sensitivity ( $S_{n^2Af^2}$ ) and plotted as a function of the number of square cycles ( $n^2Af^2$ ) valid for simple gratings and grating sums. Figure 4.23 shows that the data from Figure 4.20 collapsed to a single contrast sensitivity function for each spatial frequency pair. The

normalised r.m.s. contrast sensitivity for a grating sum first increased with the slope of 0.5 in double logarithmic coordinates but then saturated with increasing number of square cycles. The smooth curves were calculated by equation 3.30 described in Section 3.4. The values of  $Z_0$  and  $S'_{\max}$  were obtained when equations 3.29 and 3.31 described in Section 3.4. were fitted to the data of Figures 4.21 and 4.22, respectively. The goodness of the fit calculated by equation 2.29 described in Section 2.6.6 was 91-92%.

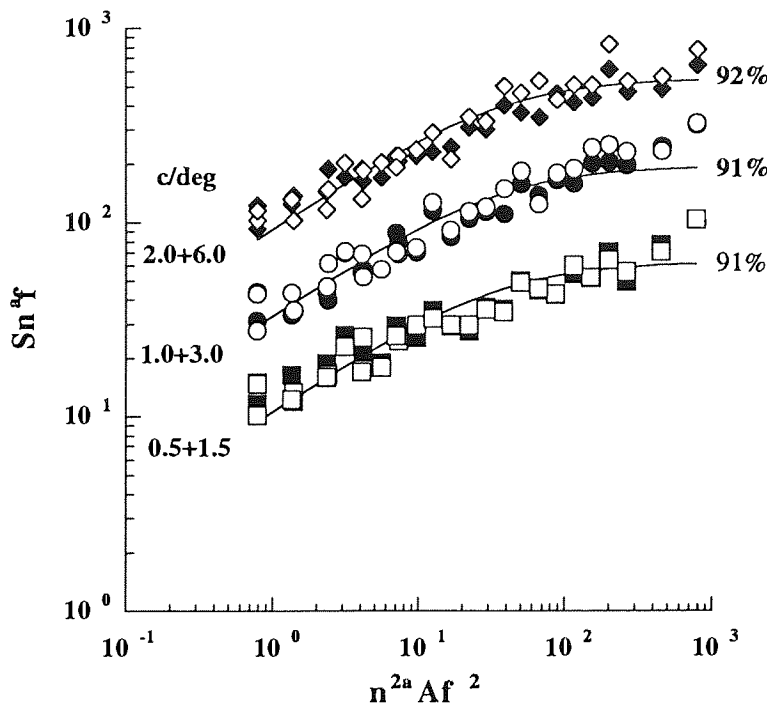


**Figure 4.23** Normalised r.m.s. contrast sensitivity ( $Sn^4f$ ) for sums of two spatial frequency components added in cosine (solid symbols) or sine (open symbols) phase as a function of square cycles for grating sums ( $n^{2a}Af^2$ ). Subjects were KL (2.0+6.0 c/deg), OU (1.0+3.0 c/deg), and AS (0.5+1.5 c/deg).

In Figure 4.24 the contrast sensitivity data from Figure 4.20 was transformed to contrast energy thresholds by equation 2.7 described in Section 2.6.1 and plotted as a function of the number of square cycles for grating sums. The contrast energy thresholds

were first constant when the number of square cycles was small but then they started to increase with increasing number of  $n^{2a}Af^2$ . The smooth curves were calculated by equation 3.33 described in Section 3.4. The goodness of the fit calculated by equation 2.29 described in Section 2.6.6 was again 91 - 92%. The estimates of contrast energy threshold for very small grating areas ( $E_0$ ) at various spatial frequency pairs were calculated by equation 3.33 under the assumption that  $A = 0$ . They were found to be 87.4, 8.98, and  $4.55 \times 10^{-3}$  at spatial frequency pairs of 0.5+1.5, 1.0+3.0, and 2.0+6.0 c/deg, respectively.

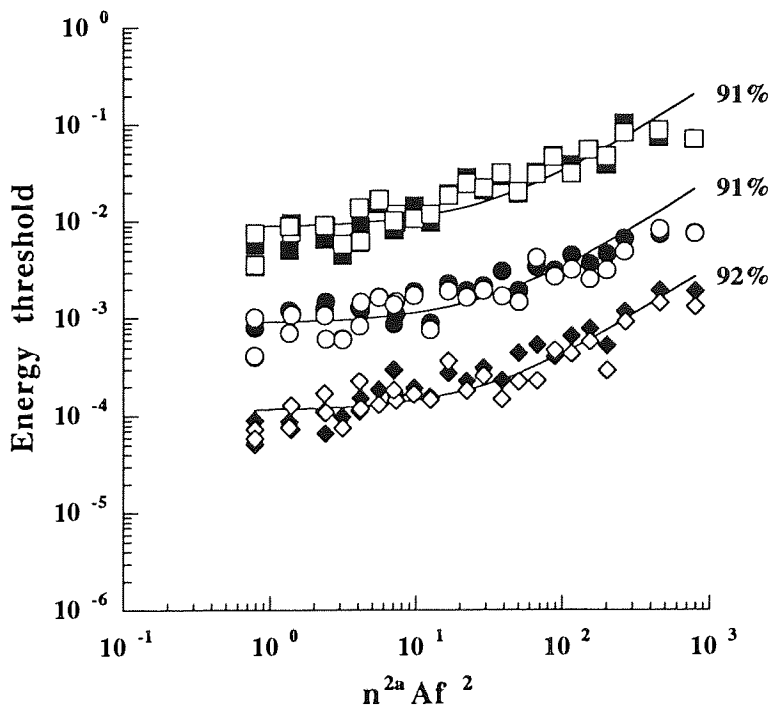


**Figure 4.24** Energy threshold as a function of the number of square cycles for grating sums. Symbols and subjects were as in Figure 4.23.

Detection efficiency calculated from the data of Figure 4.24 by equation 2.25 described in Section 2.6.4 was plotted as a function of the number of square cycles in Figure 4.25.

Efficiency remained first constant but then started to decrease with increasing  $n^{2a}Af^2$  reaching the slope of -1 at largest numbers of square cycles. The smooth curves were calculated by equation 3.34 described in Section 3.4. The goodness of fit calculated by equation 2.29 described in Section 2.6.6 was 91 - 92%. The maximum detection efficiency calculated by equation 3.34 under the assumption that  $A = 0$  was almost constant being 0.25, 0.15, and 0.30 at 0.5+1.5, 1.0+3.0, and 2.0+6.0 c/deg, respectively.

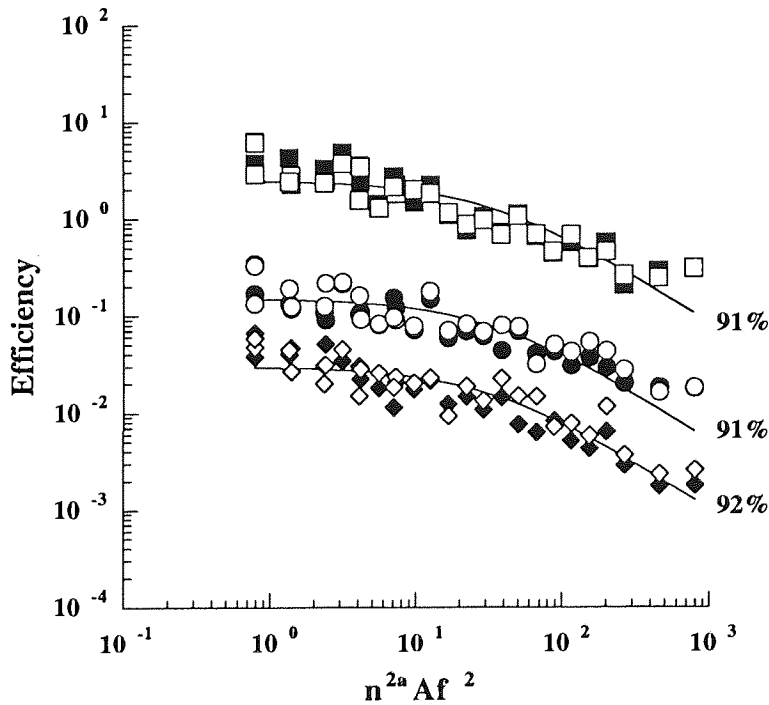


**Figure 4.25** Efficiency as a function of the number of square cycles for grating sums. Symbols and subjects as in Figure 4.23.

#### 4.4.4 Discussion

The experiments of this section showed that spatial integration in noise was similar for sums of two vertical cosine and sine gratings with various relative Michelson contrasts at 0.5+1.5, 1.0+3.0, and 2.0+6.0 c/deg. The model of contrast detection described the experimental data quite accurately under the assumption that the logarithmic critical area for a grating sum is the sum of the logarithmic critical areas for the component gratings weighted by their relative Michelson contrasts ( $a, [1-a]$ ).

The finding that contrast sensitivity first increased with grating area and then saturated with larger areas is consistent with many spatial integration studies for simple gratings (e.g. Hoekstra et al., 1974; Howell & Hess, 1978; Coltman & Anderson, 1960; Rovamo et al., 1993a) and for complex stimuli with and without noise (Kukkonen et al., 1994). The result that r.m.s. contrast sensitivity is independent of the component phase is in agreement with many previous studies concerning two spatial frequency component gratings (e.g. Sachs et al., 1971; Graham & Nachmias, 1971; Graham et al., 1978; Ross & Johnstone, 1980). Graham and Nachmias (1971) studied patterns which contained two spatial frequencies with the ratio 1:3 which were added either in cosine or sine phase. They found that the component phase had no effect on Michelson contrast threshold.

The critical area ( $A_c$ ) marking the transition between increasing and constant parts of the contrast sensitivity function decreased with increasing spatial frequency of the pair ( $f, 3f$ ), in agreement with Rovamo et al. (1993b) who reported similar findings for simple cosine gratings. The critical area decreased monotonically by a factor of 9 when the relative contrast of the third harmonic increased from zero to unity. This was as expected (Rovamo et al., 1993b) because the increase of the relative contrast of the third harmonic from zero to unity means that at the same time the relative contrast of the fundamental decreased from unity to zero (i.e., the spatial frequency of the simple grating had tripled from fundamental to the third harmonic).

Experimental contrast sensitivities were expressed in terms of normalised r.m.s. contrast sensitivity ( $S_n^a f$ , where  $n$  refers to the ratio of the lower and higher spatial frequencies, and  $a$  indicates the relative contrast of the higher spatial frequency) and plotted as a function of the number of square cycles ( $n^{2a} A f^2$ ) valid for simple gratings and grating sums. The normalised data collapsed to a single contrast sensitivity function for each spatial frequency pair, which was predicted by the model. The finding implies that the measure of square cycles is valid for simple gratings as well as grating sums.

The finding of increasing contrast energy threshold as a function of square cycles is consistent with previous results in noise (e.g. Kersten, 1984; Näsänen et al., 1993; Näsänen et al., 1994). Kersten (1984) studied spatial integration for Gaussian enveloped simple vertical sinusoidal gratings with different spatial frequencies in dynamic noise (i.e., the luminance of noise varied in time) as a function of square cycles and found that contrast energy threshold increased with square cycles up to 32 c/deg.

The detection efficiency, which is inversely proportional to contrast energy threshold, decreased with increasing number of square cycles, in agreement with van Meeteren and Barlow (1981), for example. They formed sinewave gratings by modulating the average dot density and concluded that efficiency decreased when the number of square cycles is raised.

To conclude, the model predicted spatial integration well. This suggests that the assumption of critical area for compound grating is indeed a sum of the critical areas of single components weighted by their relative contrasts. In addition, despite earlier findings (e.g. Mostafavi & Sakrison, 1976; Quick et al., 1978), spatial integration for sums of two spatial frequency components could be explained by a single channel model, i.e. a local matched filter with a limited sampling aperture (Burgess, 1990).

#### 4.5 CONCLUSIONS

Spatial integration for simple and complex gratings with and without external spatial noise was studied in this chapter. Spatial integration was found to depend similarly on the number of orientation components when stimuli were either 1 to 16 simple cosine gratings with equally spaced orientation components without external noise (Section 4.2) or 3, 6, or 16 simple gratings with different orientations and/or phases embedded in external noise (Section 4.3). The finding provided further experimental evidence that spatial integration is similar with and without noise.

However, it was stated in Section 4.2 that the dependence of the critical area ( $A_c$ ) on the number of orientation components was due to the amount of contour and detail in the stimulus. This conclusion was drawn as the sums of cosine gratings with different orientations seemed subjectively to become more complex when the number of components increased, reaching their most complex appearance at 5 to 6 components and becoming again more simple at 8 to 16 components (see Section 4.2.2). However, stimulus type had no effect on spatial integration in Section 4.3 where it was difficult to see changes in the amount of detail and contour at and about the stimulus centre as a function of the number of components (see Section 4.3.2). This was especially true when the orientations and/or phases were randomly chosen. Therefore, the dependence of the critical area on the number of components seems to be based on the global Fourier structure of the stimulus rather than the local Fourier structure.

Based on a model of contrast detection (Rovamo et al., 1993b) r.m.s. contrast sensitivity was described for simple and complex gratings in Sections 3.2 - 3.4. In Section 4.2 stimuli were 1 to 16 simple cosine gratings with equally spaced orientation components without external noise and the model described on average 96% of the experimental data (see Section 3.2). In Section 4.3 model was extended to include 3, 6, or 16 simple gratings with different orientations and/or phases embedded in external noise under the assumption

that stimulus type does not affect spatial integration. The extended model described on average 92% of the experimental data (see Section 3.3). Finally, in Section 4.4 sums of two cosine or sine gratings with two different spatial frequency components and varying Michelson contrasts between the components in external spatial noise were investigated. The model described in Section 3.4 was tested under the assumption that the logarithmic critical area for a grating sum is a sum of the logarithmic critical areas for the component frequencies weighted by their relative contrasts. Spatial integration was found to be similar for the sums of two spatial frequencies in external noise irrespective of the phases and relative Michelson contrasts of the components. The model described on average 93% of the experimental data. Overall, the model described spatial integration for simple and complex gratings very accurately.

Additionally, the measure of square cycles described in Sections 3.3 and 3.4 was found to be valid for simple as well as complex gratings. Experimental data in Sections 4.3 and 4.4 suggest that the number of square cycles determines detection efficiency for a large variety of spatial stimuli.

## 5. PARAMETER UNCERTAINTY

### 5.1 INTRODUCTION

Contrast sensitivity is usually measured as a function of a parameter such as spatial frequency (DePalma & Lowry, 1962), exposure time (Nachmias, 1968) or area (Hoekstra et al., 1974). During the experiment the stimulus to be detected is kept constant except for its contrast and is thus known to the observer.

The effect of uncertainty on visual detection has been measured by randomising stimulus parameters. When randomisation is used in an experiment, one or more stimulus parameters are uncertain to the observer, and most of the studies concerning uncertainty found that detectability of the stimulus decreased if observers were not given prior information about the stimulus. Davis (1981) studied the effect of uncertain spatial frequency by comparing human detection performance when a 4 c/deg sinusoidal grating appeared alone or mixed with three lower (1, 1.5, and 2.5 c/deg) or higher (6.5, 10, and 16 c/deg) spatial frequencies. Davis (1981) found that observers do worse at detecting the grating when they are uncertain (mixed session) about its spatial frequency than when they are certain (alone session). In a similar study, Davis and Graham (1981) investigated three primary and six secondary spatial frequencies of which three were lower and three higher than the primary spatial frequency. They found the grating to be less detectable when it was mixed with gratings of different spatial frequencies than when it was presented alone. Additionally, Cormack and Blake (1980) presented vertical sinusoidal gratings in two conditions: in the first condition observers knew the spatial frequency (1 and 4 c/deg) of the test grating and in the second condition the above spatial frequencies were randomly intermixed. They concluded that spatial frequency uncertainty degraded detection by about

15%. They also found that uncertainty of which eye was stimulated degraded detection performance for stereo-blind observers but not for normal ones.

Lowe (1967) studied temporal uncertainty in an experiment where subjects were uncertain when a brief circular light flash might occur within the given observation interval. The duration varied from 0.375 to 6 seconds. Lowe (1967) found that when the interval of temporal uncertainty increased the detectability of the signal first increased and then decreased. Uncertainty in the brightness domain has been studied by Lasley and Cohn (1981). They found that thresholds for bright light-emitting diodes increased when the observer had to judge whether one of eight stimuli had its luminance increased incrementally compared to the threshold for only one stimulus.

Greenhouse and Cohn (1978) asked their observers to fixate superimposed green and red light-emitting diodes, which appeared yellow. A chromatic shift of the LED could occur either toward red or green. If observers were uncertain of the direction of the chromatic shift, the detectability of the signal reduced by about 25%.

Knowledge of the direction of a moving target has also been found to enhance detectability. Sekuler and Ball (1977) used random bright dot patterns in their experiment and asked their observers to indicate the interval which contained the moving target. In one condition the direction of motion was always upwards and in another condition dots moved randomly upwards or rightwards. They found that the detectability was better in the condition where observers had prior knowledge about the direction of the movement. Ball and Sekuler (1981) have also showed that human performance gets better if a cue indicating the direction of the target motion appeared before the moving target.

Lindblom and Westheimer (1992) studied the effect of spatial uncertainty on line orientation thresholds. The test line, whose orientation changed randomly, appeared either in isolation or was embedded within a pattern consisting of an array of 36, 49, or 81 vertically oriented lines. the observers' task was to signal the direction of the tilt of the test, line and they knew that the test line could appear either only in the centre of the matrix or

in one of the central 4, 9, or 25 positions of the matrix. Lindblom and Westheimer (1992) found that the orientation thresholds increased with the number of possible locations of the test line.

In Section 5.2. the effect of spatial location and orientation uncertainty on r.m.s. contrast sensitivity with and without external spatial noise in peripheral and foveal vision is investigated, whereas Section 5.3. concentrates on the effect of randomised orientation and/or phase on spatial integration for simple and compound gratings..

## **5.2    *UNCERTAINTY OF SPATIAL LOCATION***

### **5.2.1    Introduction**

According to the literature, the uncertainty of spatial location may improve or reduce stimulus detectability, or even leave it unchanged in peripheral vision. Mertens (1956) measured the probability of seeing a peripheral test spot when its location was known to the observer or when it was at any of four possible orthogonal (i.e., spatially separate) locations, and found that detectability was better when the observer was uncertain of spatial location. Howarth and Lowe (1966) used a peripheral circular test flash whose location, size, and time of occurrence were either known or uncertain and found a small but significant decrease in threshold in the uncertain condition. However, Pelli (1981) reported an increase in the contrast threshold for a thin vertical bar with a brief exposure when the signal could appear at any of 9700 possible orthogonal locations in space and time. On the other hand, Schuckman (1963) found no significant difference in detectability between a group of observers who knew about the location of a test spot and another who knew that the stimulus appeared randomly in a location on the left or right side of the fixation point.

Grindley and Townsend (1968) asked their subjects to state (i) stimulus location and orientation of a letter T with four possible locations and orientations, (ii) stimulus location and orientation of a bar with six possible locations and vertical or horizontal orientation, and (iii) stimulus location and whether it was a luminance increment or decrement for a test spot with six possible locations. They found no difference in performance irrespective of whether stimulus parameters were certain or uncertain to the observer. According to Shiffrin, McKay, and Shaffer (1976) the detection of a briefly presented dot is the same irrespective of whether observers know the stimulus location or the stimulus can appear randomly at any of 49 possible locations. The result is the same for a letter presented briefly at any of 9 possible locations (Shiffrin et al., 1976).

According to the literature, the uncertainty of spatial location always reduces stimulus detectability in foveal vision. Cohn and Lasley (1974) used four possible orthogonal locations where a circular light-emitting diode could appear and found that observers' ability to detect a luminance increment is reduced when spatial location is uncertain. A similar result was obtained by Cohn and Wardlaw (1985) when using a circular light-emitting diode and 140 spatially orthogonal locations. Davis, Kramer and Graham (1983) measured contrast sensitivity for sinusoidal gratings with three possible non-overlapping (i.e., orthogonal) spatial locations, and found that detectability decreases when stimulus location is randomised and auditory cues are not given to indicate in which location the stimulus will appear.

All the experiments described above were performed without external spatial noise. However, Lappin and Uttal (1976) found that stimulus detectability in foveal vision decreases with increasing number of possible positions when four dots masked by noise and arranged along a straight vertical, horizontal or oblique line appear at one of 2, 4, or 8 alternative orientations. Burgess and Ghandeharian (1984b) showed that foveal detectability decreases when the number of spatially orthogonal locations increases from 2

to 1800 by asking their observers to identify the spatial location of a disk, square and sine-wave signal embedded in noise.

The present study consists of three experiments designed to cover evident gaps in the existing literature. Firstly, the effect of location uncertainty on contrast sensitivity in peripheral vision was studied when a stimulus was embedded in external spatial noise, because to my knowledge, there are no previous location uncertainty experiments of peripheral vision performed in external spatial noise. Secondly, the effect of location uncertainty on contrast sensitivity was studied in foveal vision when a stimulus was presented with and without spatial noise in a search task with free eye movements. This was done in order to see whether the effect of location randomisation could be compensated for by eye movements. Thirdly, it was studied whether the effect of randomised aperture orientation on contrast sensitivity in foveal vision is the same when a stimulus was presented with and without external spatial noise.

### 5.2.1 Methods

#### *Apparatus*

The experiments were carried out by using Apparatus 1 described in Section 2.1.

#### *Stimuli*

In the experiments of Figures 5.4 and 5.5 the diameter of the sharp-edged circular vertical cosine grating was 0.7 cm within the rectangular noise field, which was 0.7 cm in width and 9.3 cm in height. In the non-randomised condition the grating appeared in the centre of the noise field located at the eccentricity of  $10^\circ$  in the left visual field. In the randomised condition the grating appeared in a random location within the noise field. The

gratings with randomised location were not spatially orthogonal, because they would overlap if presented simultaneously. Spatial frequency was 1.4 c/cm on the screen. The r.m.s. contrast of noise was 0.25 and the size of noise checks was 0.042 cm x 0.042 cm. The spectral density of external spatial noise calculated by equation 2.11 described in Section 2.6.2 was  $1.10 \times 10^{-4} \text{ deg}^2$ . The stimuli are shown in Figure 5.1. The non-randomised condition is shown on the left and the randomised condition on the right.

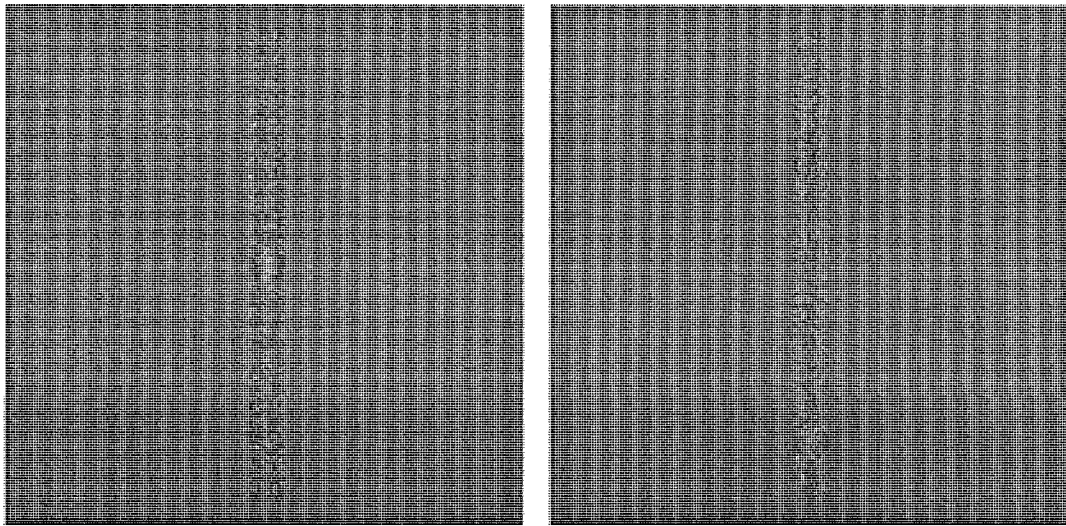


**Figure 5.1** The stimuli of the experiments in Figures 5.4 and 5.5.

In the experiments of Figures 5.6 - 5.8 the diameter of the sharp-edged circular vertical cosine grating was 0.7 cm within the circular noise field of 11.3 cm. In the non-randomised condition the grating appeared in the centre of the screen. In the randomised condition the grating appeared in a random location of the square-shaped field of 2.6 x 2.6, 5.2 x 5.2, or 7.8 cm x 7.8 cm. The centre of the square-shaped field was the same as that of the circular noise field (11.3 cm). The square-shaped field had no visible borders as it

only indicated the possible randomisation range of stimulus locations in degrees. The gratings with randomised location were not spatially orthogonal, because they would overlap if presented simultaneously. Spatial frequency was again 1.4 c/cm on the screen. The r.m.s. contrast of noise was either 0.29 or 0 and the size of noise checks was again 0.042 cm x 0.042 cm. The spectral density of external spatial noise calculated by equation 2.11 described in Section 2.6.2 was  $5.93 \times 10^{-4} \text{ deg}^2$  or  $0 \text{ cm}^2$  in the visual field. The examples of non-randomised and randomised conditions are shown in Figure 5.2. The non-randomised condition without external spatial noise is shown on the left and the randomised condition with noise on the right.

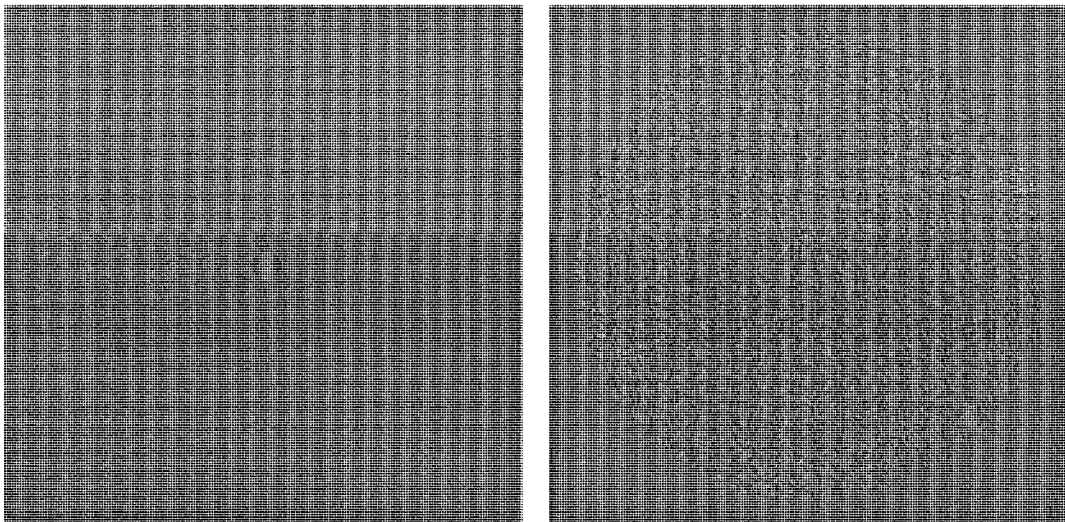


**Figure 5.2** Examples of the stimuli used in the experiments of Figures 5.6 - 5.8.

In the experiments of Figures 5.9 - 5.11 the vertical cosine grating had an aperture whose dimensions were 11.3 x 1.4 cm on the screen. The grating appeared within a circular noise field of 16 cm. Spatial frequency was 1 c/cm on the screen and three different spatial frequencies (0.5, 2, and 8 c/deg) used were obtained by changing the viewing

distance. In the non-randomised condition the aperture orientation was vertical at 0.5 and 2 c/deg, but horizontal at 8 c/deg. In the randomised condition the grating orientation remained always vertical but the aperture orientation were randomised within  $\pm 5.65^\circ$ ,  $\pm 11.3^\circ$ ,  $\pm 22.5^\circ$ ,  $\pm 45^\circ$  or  $\pm 90^\circ$  about the vertical or horizontal. When external noise was used, the r.m.s. contrast of noise was 0.3. The size of noise checks was 0.042 cm x 0.042 cm at 0.5 and 2 c/deg but 0.084 cm x 0.084 cm at 8 c/deg. The corresponding spectral densities of external spatial noise calculated by equation 2.11 described in Section 2.6.2 were 635, 39.7, and  $9.92 \times 10^{-6} \text{ deg}^2$  at 0.5, 2, and 8 c/deg, respectively. The examples of non-randomised and randomised condition are shown in Figure 5.3. The non-randomised condition without external spatial noise is shown on the left where the aperture orientation is vertical (0.5 and 2 c/deg). The randomised condition where the noise check size was 0.042 cm x 0.042 cm is shown on the right.

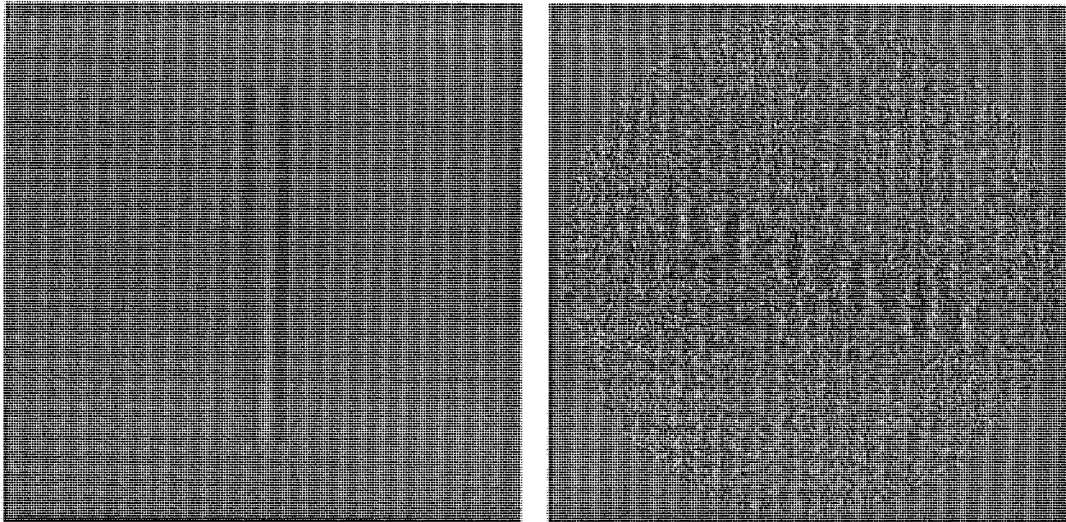


**Figure 5.3** Examples of the stimuli used in the experiments of Figures 5.9 - 5.11.

The stimuli had an equiluminous surround which was limited to a 20 cm circular field by a black cardboard. Each noise check consisted of 1x1 or 2x2 image pixels corresponding 24 and 12 noise checks per cm, respectively. The highest spatial frequency used was 1.4 c/cm and hence, the width of one cycle was 0.71 cm on the screen. Pixel noise can be regarded as white, if there are at least four noise checks per grating cycle at all spatial frequencies (Kukkonen et al., 1995). Thus, the two-dimensional external noise used was regarded as white, because there were at least 9 checks per cycle at the spatial frequencies used in the experiments.

### *Procedure*

The contrast thresholds (See Section 2.5.1) with and without noise were determined at the probability of 0.84 correct responses using a forced-choice algorithm described in detail in Section 2.4. All data points shown are based on geometric means of at least three threshold estimates.

When gratings were embedded in noise and/or when the grating positions were randomised, there were 5 samples of the stimuli at each contrast level. One of them was chosen randomly for each exposure. For gratings with noise the comparison stimulus was chosen randomly from a set of 21 different noise stimuli. A new set of comparison stimuli was generated each time the noise field configuration or noise check size on the screen was changed.

Viewing was binocular with natural pupils. Their diameter increased from 4 to 5 mm with viewing distances of 28.6 - 458 cm. The range of retinal illuminance was thus 630 - 980 phot.td. The spatial frequencies used were obtained by changing the viewing distance and/or spatial frequency on the screen. The experiments were performed in a dark room; the only light source was the display. A chin-rest was used to stabilise the head.

In the experiments of Figures 5.4 and 5.5 the duration of grating exposure was 33, 133, or 533 msec. Each trial consisted of two exposures, separated by 600 msec. One of the exposures contained the stimulus. The observer indicated which exposure contained the stimulus by pressing one of the two keys on a computer keyboard. Between two exposures the observer saw only the equiluminous field. A new trial began 250 msec after the observer's response. Sound signals provided the feedback indicating whether the observer's response was correct or incorrect. A fixation point was placed 10 cm to the right of the centre of a narrow vertically oriented noise field. No cue of the next location was given before exposure, but the subject knew whether the grating location was constant or randomised. The experiments were performed in external spatial noise.

In the experiments of Figures 5.6 - 5.8 the observer had an unlimited viewing time to indicate whether or not the exposure contained the grating by using a single interval yes-no procedure. No fixation point was used, because observers were expected to search for the grating with random location on the screen. No cue of the next location was given before exposure, but the subject knew whether the grating location was constant or randomised and what was the size of the square-shaped field used. The experiments were performed with and without external noise.

In the experiments of Figures 5.9 - 5.11 the observer was asked to look at the centre of the screen. No fixation point was used. Exposure duration was 500 msec. The experiments were performed with and without external noise. Other details were as in the experiments of Figures 5.4 and 5.5.

### *Subjects*

Five experienced subjects, aged 25 - 33 years, served as observers. Subject OL was a corrected non-astigmatic myope (od. -1.25 DS / os. -1.25 DS), JM was a corrected astigmatic myope (od. -1.5 DS / os. -0.5/-0.5 x 180), TH was a corrected astigmatic

myope (od. -1.75 DS / os. -1.5/-0.25 x 155), KT was a corrected non-astigmatic myope (od. -6.0 DS / os. -4.0 DS) and OU was a corrected non-astigmatic myope/hyperope (od. -0.75 DS / os. +0.75 DS). Their corrected binocular Snellen acuity at 6 meters was 1.7 for OL and JM, 1.6 for TH, 1.5 for KT, and OU. Their accommodation had a range of at least 6 D. Hence, they were emmetropes at the viewing distances used in the experiments.

*R.m.s. contrast*

R.m.s. contrast was calculated by equation 2.7 described in Section 2.6.1.

*Spectral density of external noise*

Spectral density of external noise was calculated by equation 2.11 described in Section 2.6.2.

*Signal-to-noise ratio*

Signal-to-noise ratio was calculated by equation 2.19 described in Section 2.6.3.

*Spectral density of equivalent noise*

Spectral density of equivalent noise was calculated by equation 2.27 described in Section 2.6.5.

### 5.2.3 Results

In the experiments of Figure 5.4 binocular r.m.s. contrast sensitivity was measured as a function of exposure duration for a vertical cosine grating embedded in external noise at the eccentricity of  $10^\circ$  in the left visual field. Spatial frequency was 1.4 c/deg and the diameter of the sharp-edged circular grating field was 0.71 deg. The viewing distance was 57 cm. The rectangular noise field (width 0.70 and height 9.3 deg) had an equiluminous circular surround (diameter 20 deg in the visual field) limited by a black cardboard. In the non-randomised condition the grating appeared in the centre of the noise field located at the eccentricity of  $10^\circ$ . In the randomised condition the grating appeared in a random location within the noise field.

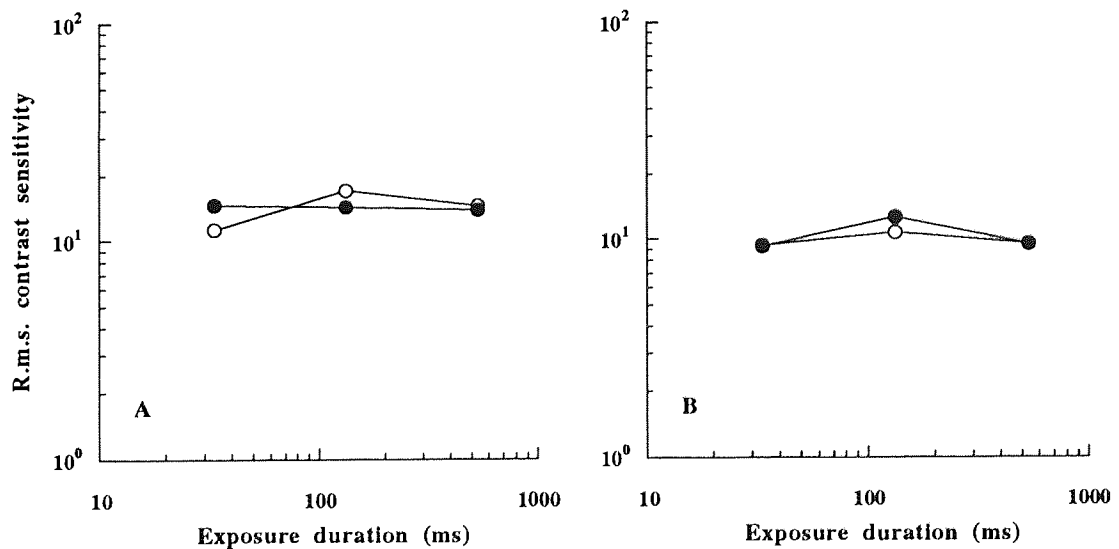


**Figure 5.4** R.m.s. contrast sensitivity for non-randomised (open symbols) and randomised (solid symbols) gratings in noise as a function of exposure duration in spatial location uncertainty experiment in peripheral vision. Subjects were TH (A), and OU (B).

As Figure 5.4 shows, r.m.s. contrast sensitivity was constant irrespective of exposure time and the same in the randomised and non-randomised conditions. The independence of contrast sensitivity of exposure duration in the non-randomised condition with external spatial noise is in agreement with the foveal result of Rovamo et al. (1993a). This is as expected, because according to Rovamo et al. (1992) r.m.s. contrast sensitivity in noise is similar at all eccentricities as long as it is lower than contrast sensitivity without noise, and the control experiments showed that external spatial noise reduced contrast sensitivity at least by a factor of three.

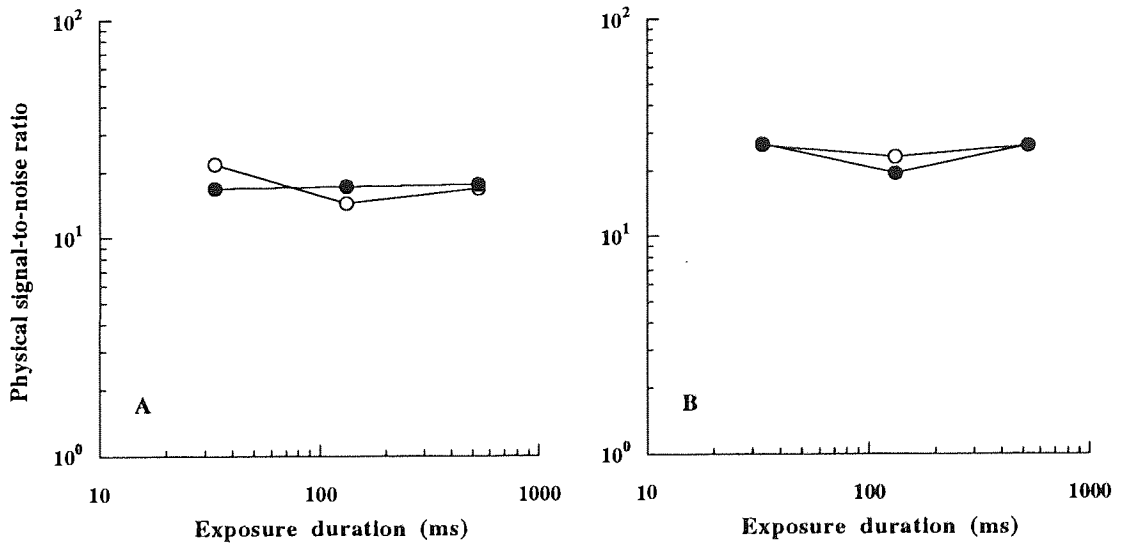


**Figure 5.5** Physical signal-to-noise ratio for non-randomised and randomised gratings as a function of exposure duration in spatial location uncertainty experiment in peripheral vision. Subjects and symbols as in Figure 5.4.

In Figure 5.5 physical signal-to-noise ratio, calculated by equation 2.19 and described in Section 2.6.3, was plotted as a function of exposure time. Physical signal-to-noise ratio at threshold was constant irrespective of exposure time and the same both in the randomised and non-randomised conditions, because contrast sensitivity was independent of exposure duration and similar in the non-randomised and randomised conditions.

Scrutiny of Figures 5.4 and 5.5 reveals however, that the data of r.m.s. contrast sensitivity and physical signal-to-noise ratio are like mirror images of each other, i.e., when one increases the other decreases and vice versa.

In the experiments of Figure 5.6 binocular r.m.s. contrast sensitivity of foveal vision was measured with and without spatial noise as a function of the randomisation range of stimulus location in a search task with free eye movements. The stimulus was a vertical grating within a sharp-edged circular aperture (diameter 1.4 deg) embedded in a circular noise field (diameter 22.6 deg) with an equiluminous surround (diameter 38.5 deg; calculated using trigonometry, because tangent plane is not accurate enough for large diameters viewed from a short distance). Spatial frequency was 0.7 c/deg and the viewing distance 28.6 cm. In the non-randomised condition the grating appeared in the centre of the screen. In the randomised condition the grating stimulus appeared in a random location within a square-shaped field of 5.2 x 5.2, 10.4 x 10.4, or 15.6 deg x 15.6 deg.

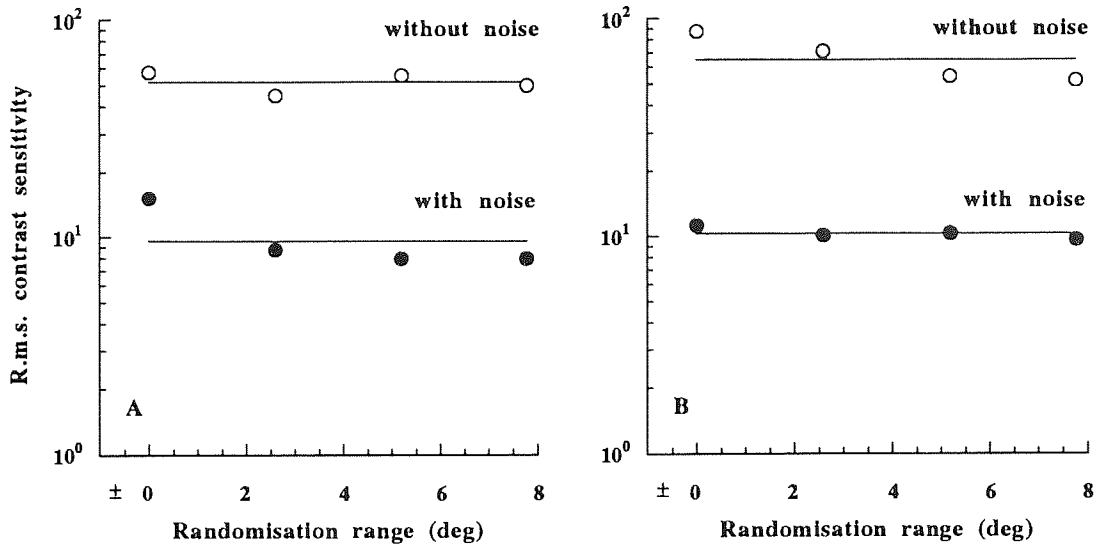


**Figure 5.6** R.m.s. contrast sensitivity for randomised gratings with (solid symbols) and without (open symbols) noise as a function of randomisation range of spatial location in foveal vision. Subjects were KT (A), and OU (B).

The solid lines refer to the mean sensitivities with and without noise in each condition.

Figure 5.6 shows that contrast sensitivity was higher for gratings without spatial noise than in noise, and external spatial noise reduced the sensitivity by a factor of  $5.9 \pm 0.45$  (mean  $\pm$ SEM). The reduction was independent of the randomisation range, because the r.m.s. contrast sensitivity was practically constant across the randomisation range both with and without spatial noise.

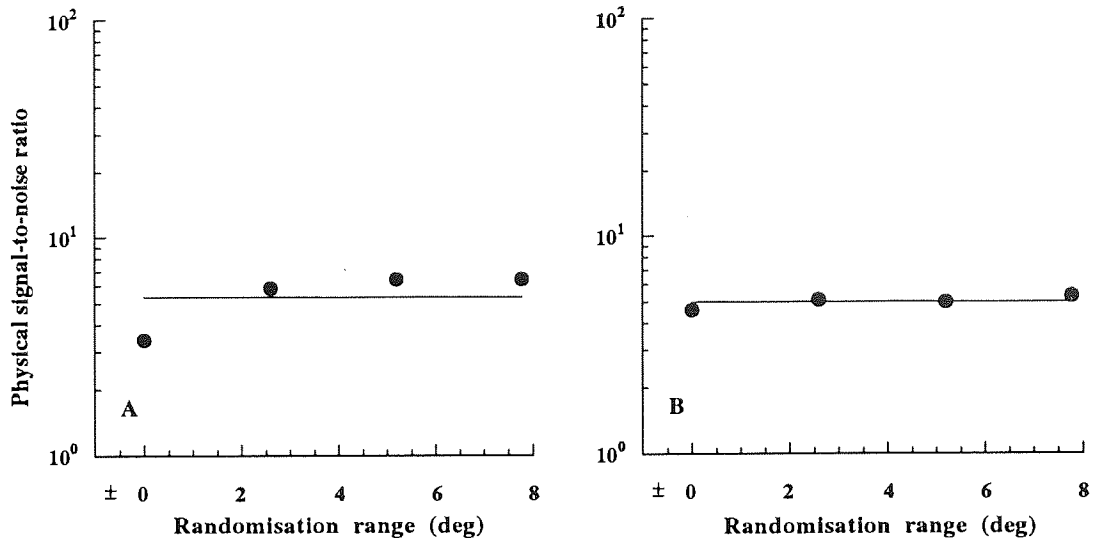


**Figure 5.7** Physical signal-to-noise ratio as a function of randomisation range of spatial location in foveal vision. Subjects as in Figure 5.6.

The physical signal-to-noise ratio at threshold, calculated by equation 2.19 and described in Section 2.6.3, is plotted as a function of the randomisation range of grating location in Figure 5.7. The solid line shows the averaged signal-to-noise ratio across the randomisation range. The ratio was fairly constant for both observers irrespective of randomisation range.

In Figure 5.8 the spectral density of external spatial noise equivalent to internal neural noise, calculated by equation 2.27 and described in Section 2.6.5, is plotted as a function of the randomisation range of spatial location. The solid line refer to the averaged spectral density of equivalent noise across the randomisation range. The spectral density of external noise equivalent to internal noise was fairly constant across the range of randomisation and thus similar in the non-randomised and randomised conditions, because contrast sensitivity as a function of randomisation range was fairly similar with and without spatial noise.

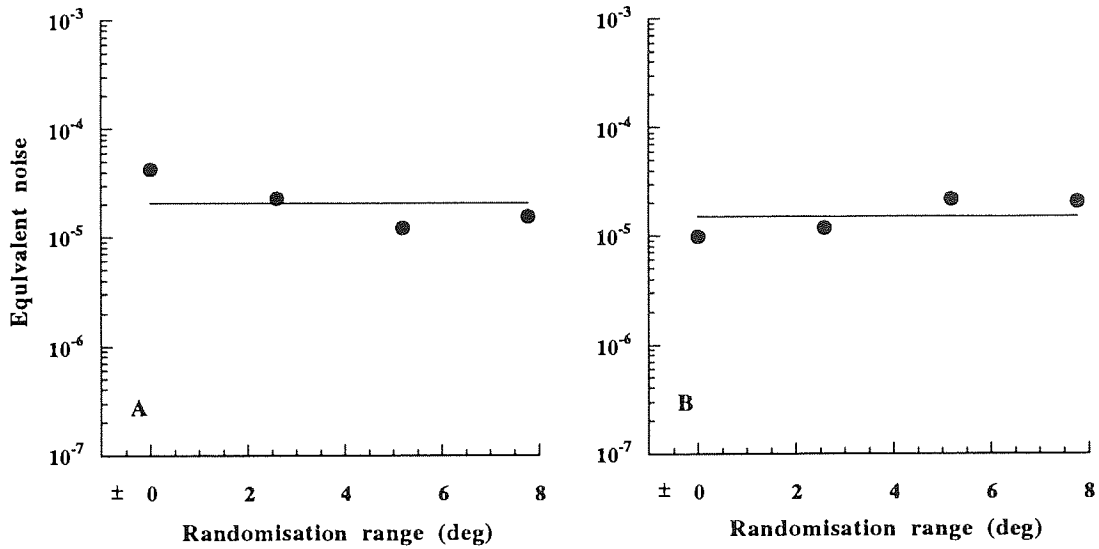


**Figure 5.8** Equivalent noise as a function of randomisation range of spatial location in foveal vision. Subjects as in Figure 5.6.

In the experiments of Figure 5.9 binocular r.m.s. contrast sensitivity for vertical gratings without and with external spatial noise was measured as a function of the randomisation range of aperture orientation. The horizontal and vertical aperture dimensions were  $22.6 \times 2.8$ ,  $5.65 \times 0.7$ , and  $0.175 \text{ deg} \times 1.41 \text{ deg}$  at spatial frequencies of 0.5, 2, and 8 c/deg, respectively. The aperture dimensions and spatial frequencies used in the experiment were obtained by changing the viewing distance, which was 28.6, 114, and 458 cm at 0.5, 2, and 8 c/deg respectively. In the non-randomised conditions the aperture orientation was vertical at 0.5 and 2 c/deg, but horizontal at 8 c/deg. In the randomised conditions the grating orientation always remained vertical but the aperture orientations were randomised within  $\pm 5.65^\circ$ ,  $\pm 11.3^\circ$ ,  $\pm 22.5^\circ$ ,  $\pm 45^\circ$  or  $\pm 90^\circ$  about the vertical or horizontal. The solid lines refer to contrast sensitivities in the non-randomised condition.

As Figure 5.9 shows r.m.s. contrast sensitivity was always lower for gratings with noise than without. The mean  $\pm$ SEM of reduction due to external spatial noise was  $6.2 \pm 0.17$ ,  $5.0 \pm 0.24$  and  $3.2 \pm 0.17$  at 0.5, 2, 8 c/deg, respectively. Sensitivity decreased similarly as a function of the increasing randomisation range of aperture orientation with and without external spatial noise. The decrease found at small randomisation ranges of aperture orientation decelerated (0.5 and 2 c/deg) and even ceased (8 c/deg) at large ranges. In spite of this, subjects reported that it became increasingly harder and more time-consuming to detect a stimulus. However, the effect of randomisation decreased with increasing spatial frequency. Contrast sensitivity for a completely randomised aperture orientation decreased to 43.7, 54.8 and 71.1% of the non-randomised sensitivity at 0.5, 2, and 8 c/deg, respectively.

The control experiments showed that r.m.s. contrast sensitivity decreased similarly irrespective of whether aperture or grating orientation was randomised about the vertical or horizontal. Thus, the data at 8 c/deg, where the aperture orientation was randomised about the horizontal, is directly comparable with the data at 0.5 and 2 c/deg where aperture orientation was randomised about the vertical. The solid curves of Figure 5.9 were obtained as follows: because the decrease of contrast sensitivity with increasing randomisation range of aperture orientation was similar with and without spatial noise, first the geometric average was calculated of the sensitivities measured for gratings with and without noise at each aperture orientation in order to get an average contrast sensitivity function across the range of aperture orientations for each spatial frequency.

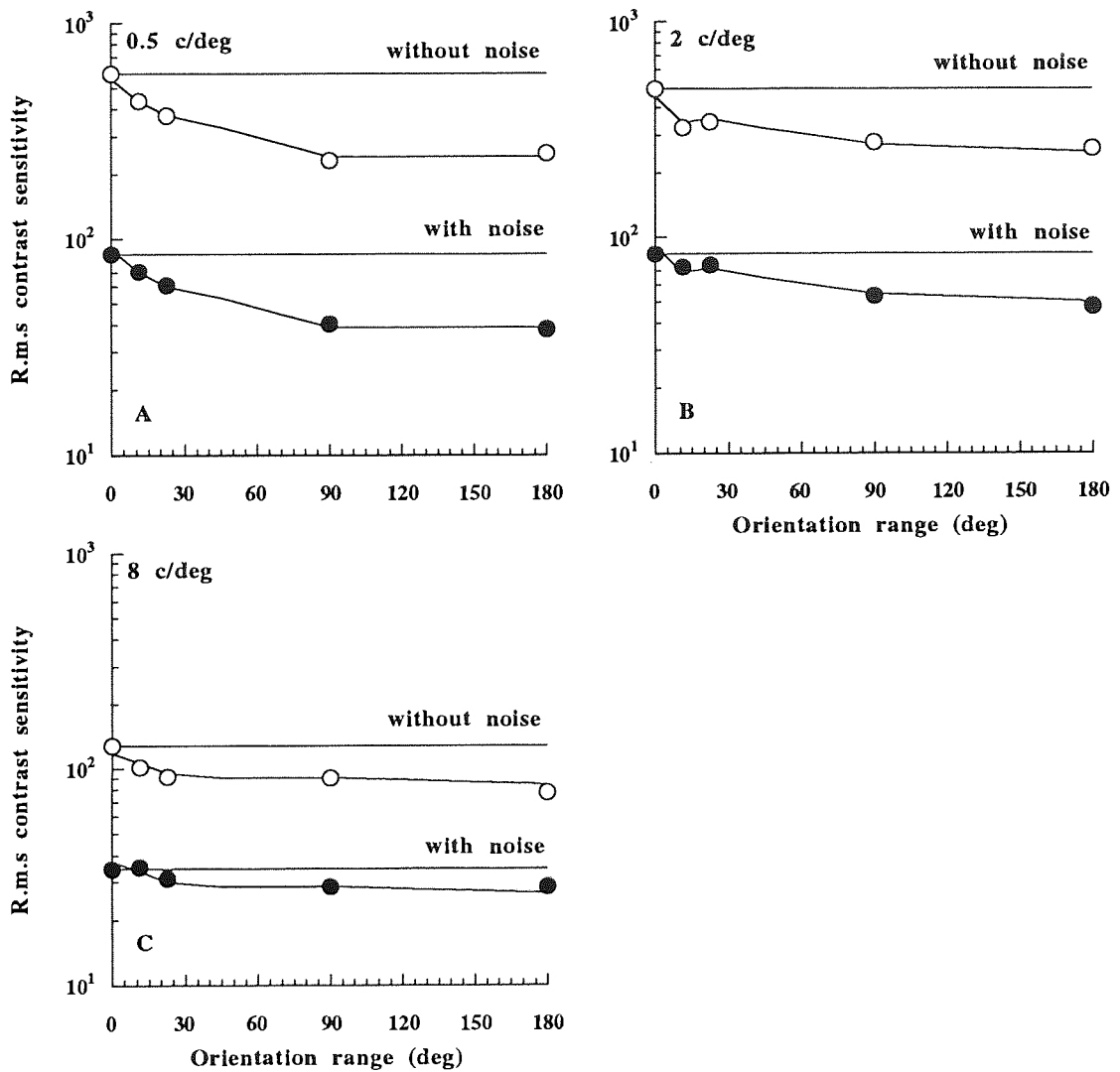


**Figure 5.9** R.m.s. contrast sensitivity with (solid symbols) and without (open symbols) noise as a function of randomisation range of aperture orientation at 0.5, 2, and 8 c/deg. Subjects were OL (A), OU (B), and JM (C).

Then three geometric means of r.m.s. contrast sensitivities were calculated across the orientation range at each spatial frequency: two for the experimental data and one for the average contrast sensitivity function. Their ratios provided two constants for each spatial

frequency. The average contrast sensitivity functions were then multiplied by the constants to produce two solid curves for each spatial frequency.

In Figure 5.10 the physical signal-to-noise ratio, calculated by equation 2.19 and described in Section 2.6.3, is plotted as function of the randomisation range of aperture orientation for gratings with spatial noise. The solid lines refer to the signal-to-noise ratio in the non-randomised condition. The signal-to-noise ratio was found to increase with randomisation range, because in Figure 5.9 more contrast energy was needed to detect the stimulus when the randomisation range of aperture orientation increased. However, the increase of signal-to-noise ratio decelerated (0.5 and 2 c/deg) or even saturated (8 c/deg) at large randomisation ranges. As in Figure 5.9 the effect of randomisation decreased with increasing spatial frequency. For a completely randomised aperture orientation the physical signal-to-noise ratio increased to 2.23, 1.76 and 1.20 times the non-randomised value at 0.5, 2, and 8 c/deg, respectively.

In Figure 5.11 the spectral density of external noise equivalent to internal neural noise is plotted against the randomisation range of aperture orientation. The spectral density of external noise equivalent to internal noise was calculated by equation 2.27 described in Section 2.6.5. The solid lines refer to averaged spectral densities of equivalent noise across the randomisation range at each spatial frequency. At each spatial frequency the spectral density was constant across the randomisation range of aperture orientation. The mean  $\pm$ SEM for the spectral density of external noise equivalent to internal noise was  $170 \pm 9.2$ ,  $17 \pm 1.3$ , and  $11 \pm 1.2 \times 10^{-7} \text{ deg}^2$  at 0.5, 2, and 8 c/deg, respectively.

## Parameter uncertainty

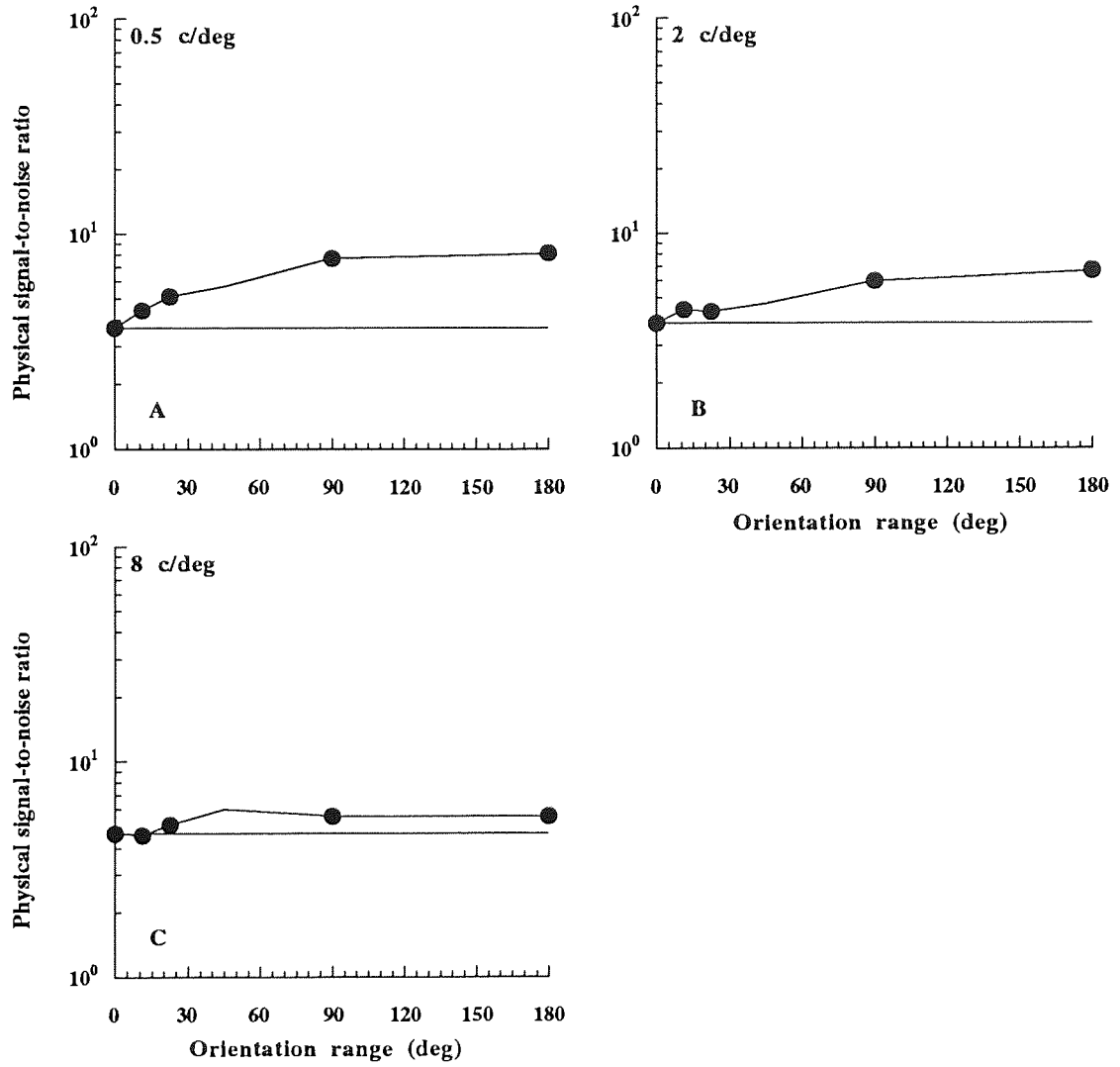
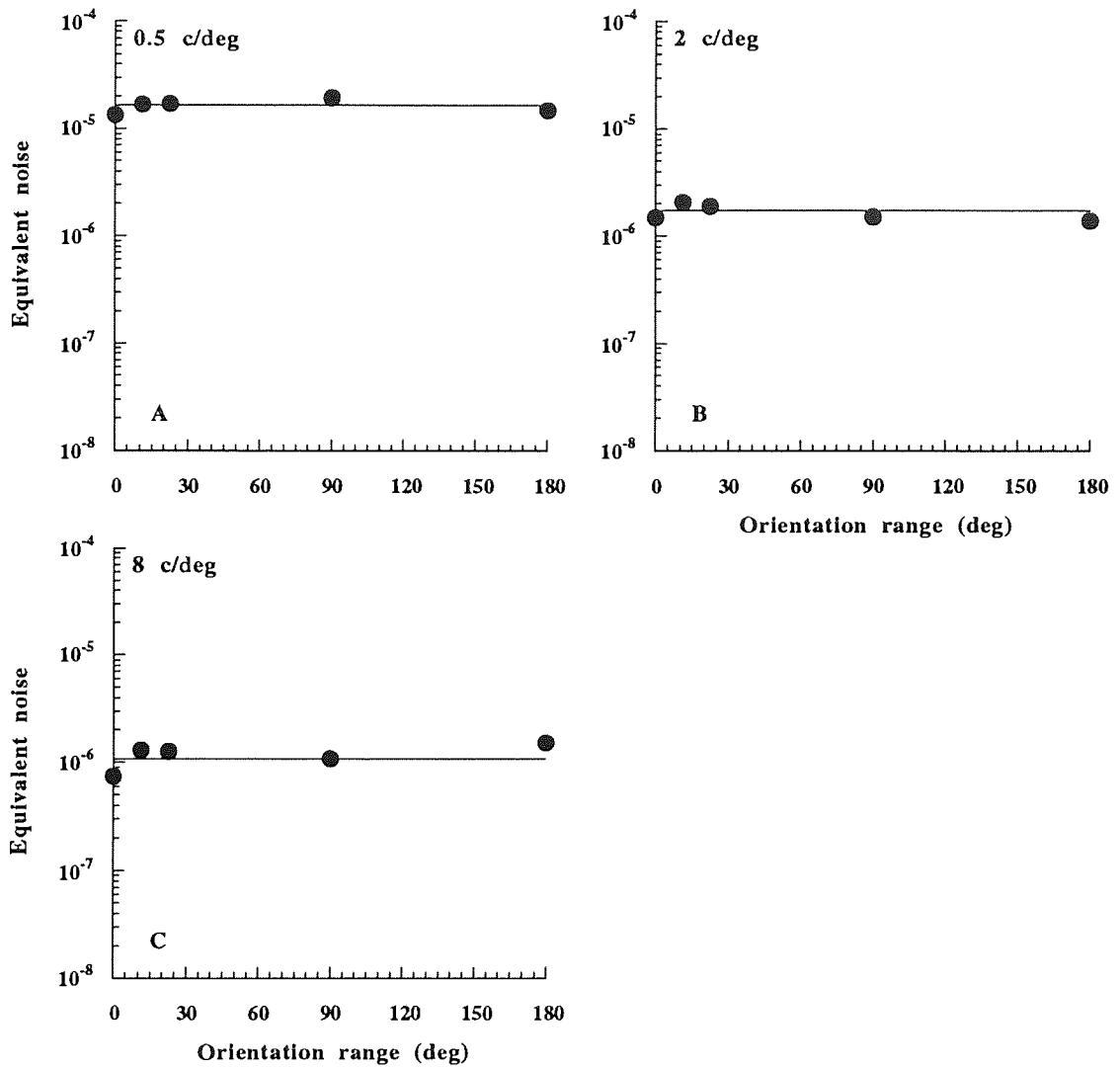


Figure 5.10 Physical signal-to-noise ratio as a function of randomisation range of aperture orientation at 0.5, 2, and 8 c/deg. Subjects as in Figure 5.9.

## Parameter uncertainty



**Figure 5.11** Equivalent noise as a function of randomisation range of aperture orientation at 0.5, 2, and 8 c/deg. Subjects as in Figure 5.9.

#### 5.2.4 Discussion

The experiments of this section showed that the uncertainty of stimulus location had no effect on r.m.s contrast sensitivity or physical signal-to-noise ratio at threshold when measured as a function of exposure time in peripheral vision for a circular cosine grating embedded in external spatial noise. Also, when r.m.s. contrast sensitivity with and without spatial noise was measured by using a single interval yes/no procedure and allowing free eye movements during the search for a grating with unlimited exposure, the location uncertainty in foveal vision had no effect on contrast sensitivity, physical signal-to-noise ratio at threshold, or spectral density of external spatial noise equivalent to internal neural noise in the human brain. On the other hand, r.m.s. contrast sensitivity for vertical gratings decreased as a function of the randomisation range of aperture orientation similarly with and without spatial noise up to  $90^\circ$  and saturated thereafter. The effect of randomisation decreased with increasing spatial frequency: for a completely randomised aperture orientation ( $180^\circ$ ) sensitivity decreased to 43.7, 54.8 and 71.1% of the non-randomised sensitivity at 0.5, 2, and 8 c/deg, respectively. The corresponding physical signal-to-noise ratios were 2.23, 1.76 and 1.20 times the non-randomised values at 0.5, 2, and 8 c/deg, respectively. The spectral density of external noise equivalent to internal neural noise was independent of randomisation range but decreased with increasing spatial frequency, being 170, 17 and  $11 \times 10^{-7}$  deg<sup>2</sup> at 0.5, 2, and 8 c/deg, respectively.

The finding that location uncertainty had no effect on r.m.s. contrast sensitivity of peripheral vision in external spatial noise is in agreement with previous studies performed without external spatial noise in peripheral vision (Schuckman, 1963; Grindley & Townsend, 1968; Shiffrin et al., 1976; Shiffrin & Gardner, 1972). To my knowledge, there are no previous location uncertainty experiments of peripheral vision performed in external spatial noise. However, studies which have been done without external noise have, in fact, been performed in internal spatiotemporal neural noise. When the added

external noise is clearly stronger than internal neural noise, as in the experiments of this section, external noise becomes the dominant source of noise in the visual system. Hence, the results obtained in spatial noise are comparable with results obtained without external noise.

An explanation for the finding that location uncertainty had no effect on detectability in peripheral vision is provided by the fact that the accuracy of positional information is inherently poor in peripheral vision (Bourbon, 1902; Westheimer, 1982; Levi, Klein & Yap, 1987; Hess & Field, 1993). In agreement, Grindley and Townsend (1968) found that orientation randomisation does not have any effect in peripheral vision. However, in disagreement with this explanation Mertens (1956) found that probability of observation was higher when the observer was uncertain at which of four possible spatial locations a peripheral test flash could appear. Also, Howarth and Lowe (1966) found a decrease in threshold when observers did not know the location, size, and time of occurrence of a peripheral test flash. On the other hand, Pelli (1981) found an increase in detection threshold when a thin vertical bar with a brief exposure could appear at any one of 9700 possible orthogonal locations in space and time (97 locations and 100 possible times, where and when the 20 msec stimulus could appear). An explanation for this finding could be the accuracy of temporal resolution reflected in the high flicker frequency of peripheral vision (Hartmann, Lachenmayr & Brettel, 1979; Rovamo & Raninen, 1984).

The result that the uncertainty of stimulus location in foveal vision had no effect on r.m.s. contrast sensitivity when subjects had an unlimited viewing time to search for a small circular cosine grating with and without spatial noise means that it is possible to find foveal tasks which do not suffer from position uncertainty. Similarly, uncertainty about stimulus contrast has no effect on detectability in the fovea (Davis et al., 1983). However, the randomisation of spatial location makes detection thresholds higher in the fovea (Cohn & Lasley, 1974; Cohn & Wardlaw, 1985; Davis et al., 1983; Lappin & Uttal, 1976) when eye movements are not allowed. In addition, when Burgess and Ghandeharian (1984b)

## Parameter uncertainty

used the M-alternative forced-choice method for orthogonal spatial locations asking the observers to identify the spatial location of a stimulus, they found that detection threshold in spatial noise increases with the number of possible locations. An explanation for the difference between the finding of these experiments and the result of Burgess and Ghandeharian (1984b) could be provided by the fact that a single-interval yes/no procedure was used in the experiments of this section and only detection in a search task was required across non-orthogonal locations.

Although r.m.s. contrast sensitivity was independent of the randomisation range, subjects reported that it became increasingly harder and more time-consuming to detect a stimulus at larger randomisation ranges. This is in agreement with the results of Posner, Nissen and Ogden (1978) who found that reaction times are shorter when a small square appears at an expected location as opposed to an unexpected one.

The result that foveal r.m.s. contrast sensitivity for vertical gratings decreased as a function of randomisation range of aperture orientation is in agreement with Lappin and Uttal (1976), who found that stimulus detectability in foveal vision decreases with increasing number of possible positions when four dots masked by noise and arranged along a straight vertical, horizontal or oblique line appear at one of 2, 4, or 8 alternative orientations.

The result that contrast sensitivity with and without noise decreased similarly as a function of the randomisation range of aperture orientation at 0.5, 2 and 8 c/deg implies that the effect of uncertainty on detectability is similar in internal spatiotemporal neural noise and external spatial noise. This finding is in agreement with earlier foveal experiments concerning location uncertainty, performed with (Lappin & Uttal, 1976) and without (Cohn & Lasley, 1974; Cohn & Wardlaw, 1985; Davis et al., 1983) external noise. The current finding, together with previous results, thus suggests that the internal neural noise is added to the signal before detection occurs in the human brain, in agreement with the model of human contrast detection (Rovamo et al., 1993b; Rovamo et al., 1994a).

## Parameter uncertainty

According to the model visual stimuli are detected by a local matched filter. Thus, one possible explanation for a reduction in contrast sensitivity could be that parameter randomisation, which exceeds intrinsic uncertainty and cannot be compensated for by eye movements, results in a noisy local matched filter. On this basis, it is possible to speculate that parameter randomisation might leave contrast sensitivity unchanged in pathological conditions which disturb the creation of matched filters used for detection.

The finding that the effect of randomisation decreased with increasing spatial frequency can be explained by the fact that involuntary fixational eye movements (Carpenter, 1988) already randomise position, and therefore the added orientation uncertainty had a smaller effect on performance at higher spatial frequencies. The finding is in agreement with Pelli (1984), who concluded that if human visual system is intrinsically uncertain, then experimentally added uncertainty would have little if any effect on performance.

The physical signal-to-noise ratio was found to increase with increasing randomisation range of aperture orientation, which means that human observers need more contrast energy to detect a stimulus, i.e. detectability decreases as the randomisation range increases. On the other hand, when the location of a circular grating was randomised in peripheral vision or in the foveal search task, randomisation had no effect on the physical signal-to-noise ratio or r.m.s. contrast sensitivity.

The finding that the spectral density of external spatial noise equivalent to internal spatiotemporal neural noise remained constant with increasing randomisation range of spatial location or aperture orientation implies that spatial uncertainty does not increase the amount of internal neural noise in the human visual system. However, the spectral density of external spatial noise equivalent to internal neural noise decreased with increasing spatial frequency from 0.5 to 8 c/deg, reflecting the dependence of the modulation transfer function of the human visual system on spatial frequency (Mustonen, Rovamo & Näsänen, 1993). The finding is in agreement with Luntinen et al. (1995) who found that the spectral density of external spatial noise equivalent to internal neural noise decreases with

increasing spatial frequency up to 8 c/deg. In a clinical context equivalent noise makes it possible to determine the modulation transfer function of the human visual system, i.e. ocular optics (Rovamo et al., 1994b) and neural visual pathways (Rovamo et al., 1995) by measuring contrast sensitivity with and without external noise.

The foveal finding that the aperture orientation randomisation reduced detectability whereas location randomisation did not can be explained by the fact that in the aperture orientation randomisation condition central fixation was used whereas in the location randomisation condition free eye movements and unlimited exposure time was allowed in a search task. Free eye movements made it possible to compensate for the effect of location randomisation whereas the aperture orientation randomisation could not be compensated for.

### **5.3 UNCERTAINTY OF ORIENTATION AND/OR PHASE**

#### **5.3.1 Introduction**

Lappin and Uttal (1976) studied both location and orientation uncertainty. Their targets were composed of dots arranged along a straight line and masked by noise. The targets appeared in one of 2, 4, or 8 alternative positions. The observers' task was to specify which of two presentations contained the target line and stimulus detectability was found to decrease with increasing number of possible positions.

Howard and Richardson (1988) studied the effect of phase uncertainty on simple sinusoidal gratings, asking their observers to detect signals with constant and randomly varied phases. They found that detection performance was better when the signal phase was kept constant across trials. Kersten (1983) studied the ability to use phase information in the detection of Gaussian windowed sinusoidal gratings in the presence and absence of

external noise. He concluded that prior knowledge benefited the detection of a low-spatial frequency (0.5 c/deg) grating in stationary noise. If the spatial frequency was raised to 2 c/deg prior knowledge improved the performance in noise but not so much as for a 0.5 c/deg signal. When the 0.5 c/deg grating was shown without noise, or when it was drifting at 6 Hz in temporal noise, no benefit of prior knowledge was found. Burgess and Ghandeharian (1984a) tested whether human observers act as phase-sensitive detectors by using a 4.6 c/deg vertical sinusoidal grating embedded in stationary noise with and without prior knowledge of phase. Observers were provided information about absolute phase of the stimulus only in test blocks with phase information, but equivalent information about the spatial frequency and spatial extent of the stimulus were given under both testing conditions. They found that humans can perform phase-sensitive detection when sufficient prior knowledge of phase is available.

In the present study the effect of parameter randomisation on spatial integration of simple and compound gratings was measured because no references in the literature have been found concerning orientation and/or phase randomisation of compound gratings. It is unknown whether parameter randomisation affects the sampling aperture (Burgess, 1990) from which the contrast energy is sampled and summed. If the orientation or the phase of a simple grating is randomised it produces a change in the orientation or location of bars leaving the one-dimensional luminance distribution undisrupted, whereas in a compound grating the randomisation changes the internal structure of the grating by breaking down the original relations between components and thus creating a completely new grating with a different appearance. Spatial integration for simple and compound gratings could therefore be affected differently by parameter randomisation.

It has been suggested (Kersten, 1983; Burgess & Ghandeharian, 1984a; Howard & Richardson, 1988) that human observers change the observer strategy from cross-correlation (e.g. a matched filter) to auto-correlation detection when parameter uncertainty is introduced to the task. These two detectors are equally good at collecting signal energy

but the auto-correlation detector is not as good at rejecting noise. The previous studies were extended and the effect of parameter randomisation on spatial integration for simple and compound gratings was modelled in Section 3.5. According to the model r.m.s. contrast sensitivity reduces by a factor of  $\sqrt{2}$  when the orientation and/or phase of the stimulus is randomised. To test the applicability of the model the stimuli were sums of simple gratings ( $n = 1, 4, \text{ or } 16$ ) with the same contrast and spatial frequency (0.5, 2 or 8 c/deg) but different orientation and/or phase. In the non-randomised condition the stimuli consisted of equally spaced orientation components ( $180^\circ/n$ ) added in cosine phase. In the randomised conditions the orientation, phase or both were randomly chosen and changed in every exposure.

### 5.3.2 Methods

#### *Apparatus*

The experiments were carried out using Apparatus 1 described in Sections 2.1.

#### *Stimuli*

The stimuli consisted of sharp-edged circular grating fields (diameters 1, 2, 4, 8, and 16 cm) with an equiluminous surround which was limited to a 20 cm circular field by a black cardboard. Stimuli were sums of various numbers of simple gratings ( $n = 1, 4, \text{ or } 16$ ) with different orientations and/or phases. In the non-randomised conditions the stimuli consisted of equally spaced orientations components ( $180^\circ/n$ ) added in cosine phase. All gratings of a sum had the same Michelson contrast and spatial frequency (1 c/cm). One of the grating components was always vertical. Thus, for example, when  $n = 1$ , the stimulus was a simple vertical cosine grating and when  $n = 4$ , there were a vertical and a horizontal

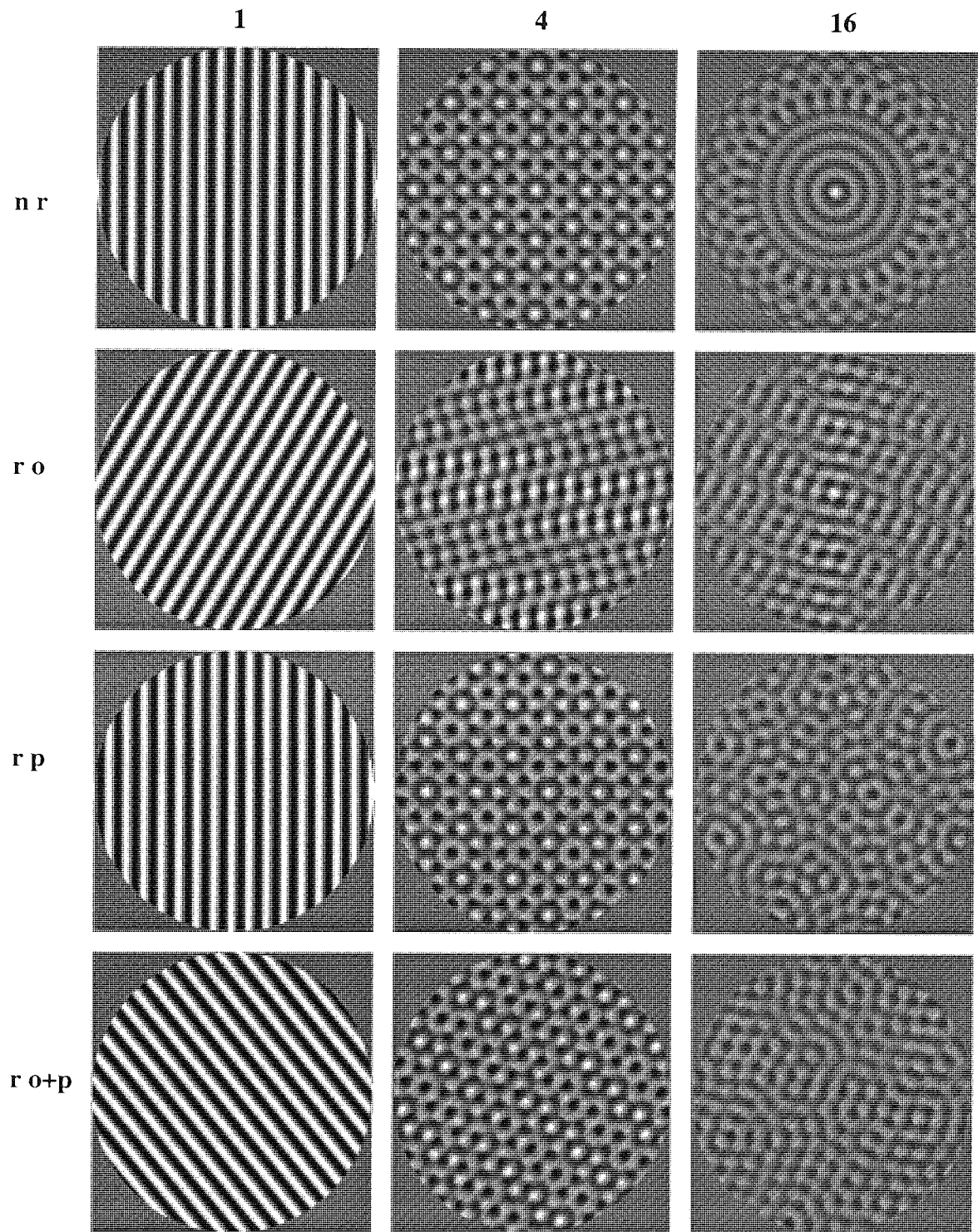


Figure 5.12 The stimuli used in the experiments of Section 5.3.

component and two oblique components i.e. the orientation difference was  $45^\circ$  between each of the components.

Three different conditions of parameter randomisation were used. In the randomised orientation condition the stimuli consisted of various numbers of simple cosine gratings ( $n = 1, 4, \text{ or } 16$ ) with completely random orientations ranging from  $0^\circ$  to  $180^\circ$ . In the randomised phase condition the stimuli consisted of equally spaced orientation components with randomly chosen phases between  $0^\circ$  to  $360^\circ$ . In the randomised orientation+phase condition the stimuli consisted of sums of simple gratings with randomly chosen orientations and phases. As orientation and/or phase could be anything within the range of randomisation the configuration of the stimulus thus changed in every exposure.

The stimuli are shown in Figure 5.12. The numbers on the top refer to the number of components. The abbreviations on the left refer to the different stimuli used in the experiment: the top row shows the non-randomised stimuli ( $n r$ ), the second row from the top the randomised orientation stimuli ( $r o$ ), the third row from the top the randomised phase stimuli ( $r p$ ), and the bottom row the randomised orientation+phase stimuli ( $r o+p$ ).

### *Procedure*

Contrast thresholds which are the inverses of contrast sensitivity were determined by using the forced-choice algorithm at the probability of 0.84 correct responses described by in detail in Section 2.5. All data points shown are based on geometric means of at least three threshold estimates.

When the orientations and/or phases of grating components were randomised, there were 5 samples of the compound grating stimuli at each contrast level. One of them was chosen randomly for each exposure.

## Parameter uncertainty

The stimuli were viewed binocularly with natural pupils. Their diameters increased with viewing distance from 4 to 5 mm. The range of retinal illuminance was thus 630 - 980 phot. td.

The exposure duration was 500 msec. Each trial consisted of two exposures which were separated by about 600 msec. The observer indicated, which exposure contained the stimulus by pressing one of the two keys on a computer keyboard. Between two exposures the observer saw only the equiluminous field. A new trial began 250 msec after the observer's response. A sound signal provided the feedback indicating whether the observer's response was incorrect. The experiments were performed in a dark room and the only light source was the display. The subject's head was stabilised using a chin rest. Fixation was binocular and directed to the centre of the stimulus field. No fixation point was used and free eye movements were allowed within the central region of the stimulus field.

### *Subjects*

Six experienced subjects, aged 21 - 30 years, served as observers. Subject KT was a corrected non-astigmatic myope (od. -6.0 DS / os. -4.0 DS), OU was a corrected non-astigmatic myope/hyperope (od. -0.75 DS / os. +0.75 DS), JM was a corrected astigmatic myope (od. -1.5 DS / os. -0.5 / -0.5 x 180), PR was a corrected astigmatic myope (od. -1.75 / -0.75 x 65 / os. -2.25 / -0.5 x 90), HN was an uncorrected hyperope (od. +0.25 DS / os. +0.5 DS), and MK was an uncorrected myope (od. -0.5 DS / os.  $\pm 0$  DS). Binocular Snellen acuity at 6 m was 1.5 for KT and OU, 1.7 for JM, 1.3 for PR, 2.0 for HN, and 1.6 for MK.

*R.m.s. contrast and energy threshold for non-randomised gratings*

Contrast energy and r.m.s contrast were calculated by equations 2.6 and 2.7 respectively and they were described in Section 2.6.1.

*R.m.s. contrast and energy threshold for randomised gratings*

When the components in the sums of simple gratings were randomised the effect of randomisation on local contrast had to be taken into account. For each grating area, number of components and type of randomisation 100 randomised compound gratings were generated and their mean contrast energy ( $E_{ave}$ ) was calculated. The standard deviation was maximally 13.5% among generated compound gratings for different conditions. Therefore, the mean contrast energy is an accurate estimate for contrast energy of randomised compound gratings. In these samples the local contrast  $\left( c(x,y) = \frac{L(x,y) - L_0}{L_0} \right)$  was equal to unity at the centre of rotation.

R.m.s. contrast was then calculated as

$$c_{r.m.s.} = c_0 \sqrt{\frac{E_{ave}}{A}}, \quad (5.1)$$

where  $c_0$  is the local contrast of the compound grating at the centre of rotation,  $E_{ave}$  is the mean contrast energy, and  $A$  is grating area in degrees.

### 5.3.3 Results

In the experiments of Figures 5.13 - 5.21 r.m.s. contrast sensitivity was measured as a function of the number of square cycles ( $Af^2$ ) for non-randomised and randomised sums of one (Figures 5.13 - 5.15), four (Figures 5.16 - 5.18) and sixteen (Figures 5.19 - 5.21) simple gratings with the same Michelson contrast and spatial frequency (1 c/cm on the screen).

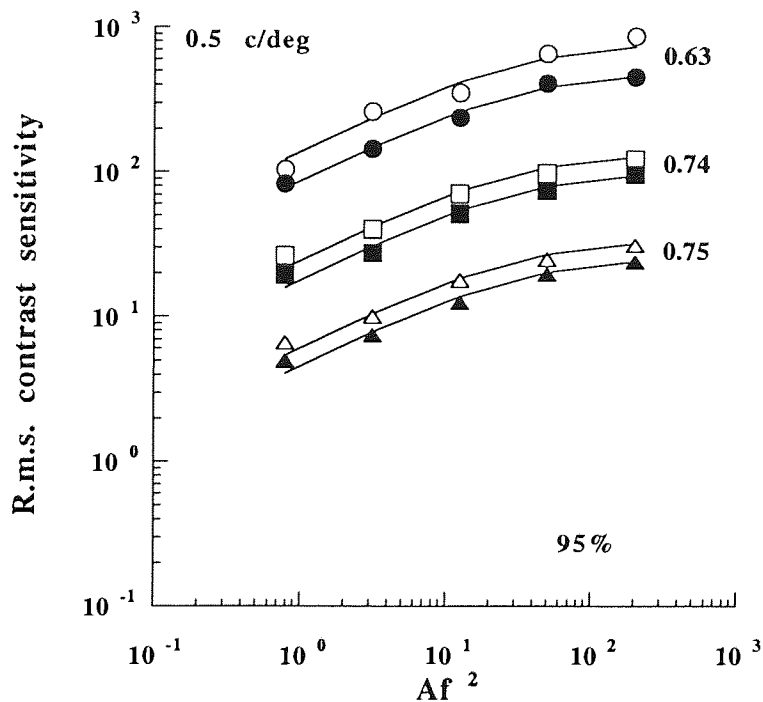


**Figure 5.13** R.m.s. contrast sensitivity as a function of square cycles for non-randomised (open symbols) and randomised (solid symbols) 1 component gratings at 0.5 c/deg in orientation and/or phase uncertainty experiments. Circles refer to orientation gratings, squares to phase gratings, and triangles to orientation+phase gratings. Subjects were KT (circles), and PR (squares and triangles).

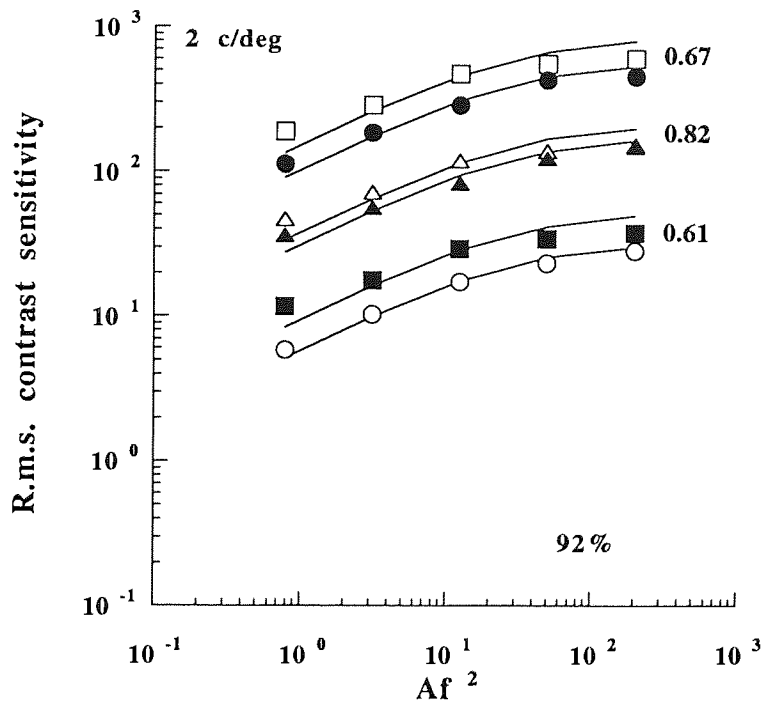


**Figure 5.14** R.m.s. contrast sensitivity as a function of square cycles for non-randomised and randomised 1 component gratings at 2 c/deg in orientation and/or phase uncertainty experiments. Symbols as in Figure 5.13. Subject was OU.

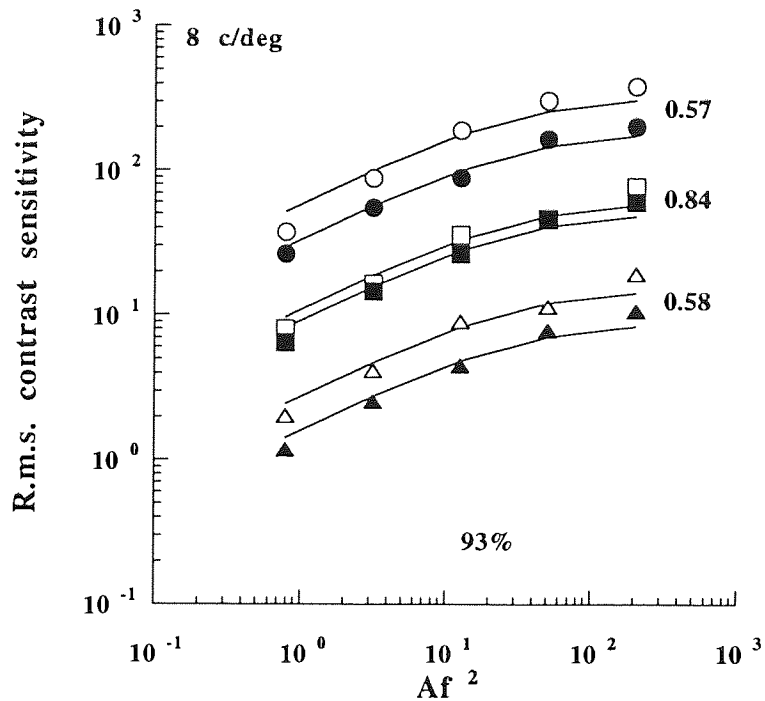


**Figure 5.15** R.m.s. contrast sensitivity as a function of square cycles for non-randomised and randomised 1 component gratings at 8 c/deg in orientation and/or phase uncertainty experiments. Symbols as in Figure 5.13. Subjects were JM (circles), MK (squares), and OU (triangles).

The number of square cycles was calculated by multiplying grating area ( $A$ ) by spatial frequency ( $f$ ) squared. In the non-randomised conditions the stimuli consisted of equally spaced orientation components ( $180^\circ/n$ , where  $n = 1, 4, \text{ or } 16$ ) added in cosine phase. In the randomised conditions the orientations and/or phases were randomly chosen from the ranges of  $0\text{-}180^\circ$  and  $0\text{-}360^\circ$ , respectively. Three different spatial frequencies studied ( $0.5, 2, \text{ and } 8 \text{ c/deg}$ ) were obtained by changing the viewing distance.

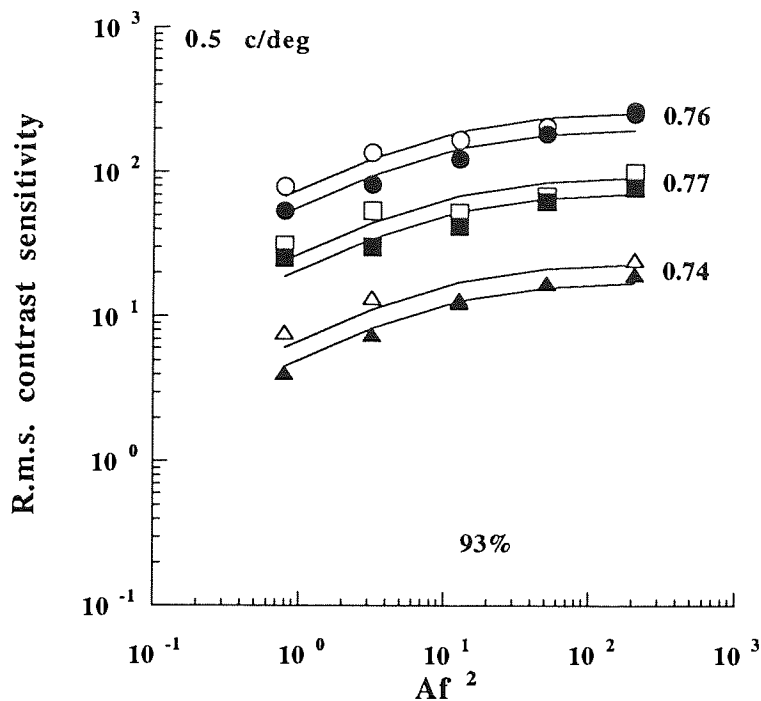


**Figure 5.16** R.m.s. contrast sensitivity as a function of square cycles for non-randomised and randomised 4 component gratings at 0.5 c/deg in orientation and/or phase uncertainty experiments. Symbols as in Figure 5.13. Subjects were HN (circles), and PR (squares and triangles).

As Figures 5.13 - 5.21 show r.m.s. contrast sensitivity first increased with the number of square cycles and then saturated with larger numbers of square cycles. For each number of components spatial integration was found to be similar for non-randomised and randomised gratings irrespective of randomisation type and spatial frequency, because the increase of contrast sensitivity in terms of  $Af^2$  was parallel at non-randomised and randomised conditions. However, scrutiny of Figures 5.13 - 5.21 revealed that spatial integration was more effective, i.e. the increase of contrast sensitivity was larger and continued to the greater number of square cycles, when the number of orientation components was 1 than 4 or 16.

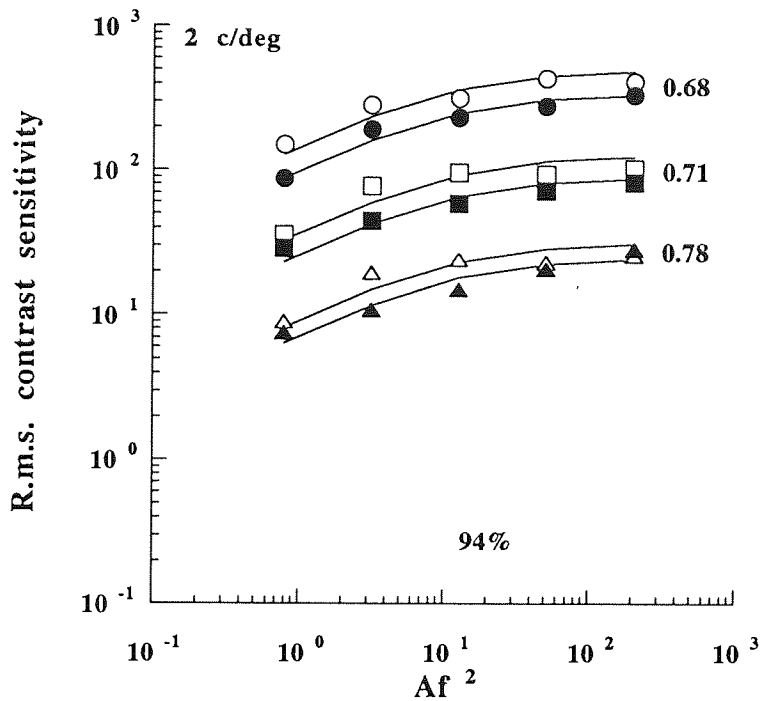


**Figure 5.17** R.m.s. contrast sensitivity as a function of square cycles for non-randomised and randomised 4 component gratings at 2 c/deg in orientation and/or phase uncertainty experiments. Symbols as in Figure 5.13. Subject was OU.

The smooth curves of Figures 5.13 - 5.21 were obtained in the following way: grating areas were first expressed in terms of square cycles ( $Af^2$ ) and contrast sensitivities were averaged separately for each number of components across different stimulus types and spatial frequencies at each number of square cycles. The critical numbers of square cycles ( $A_c f^2$ ) were then obtained by fitting equation 3.21 described in Section 3.3 to the averaged data of each number of components.

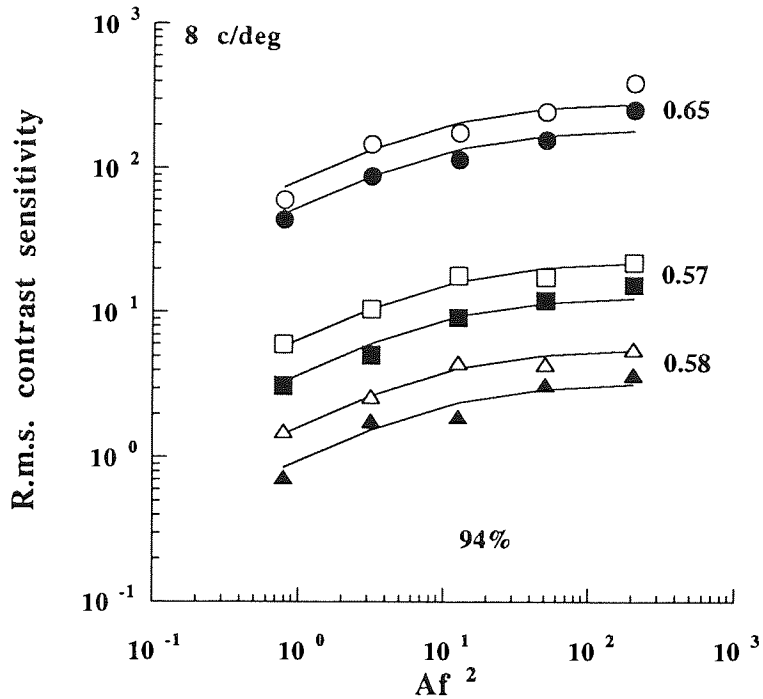


**Figure 5.18** R.m.s. contrast sensitivity as a function of square cycles for non-randomised and randomised 4 component gratings at 8 c/deg in orientation and/or phase uncertainty experiments. Symbols as in Figure 5.13. Subjects were HN (circles), and MK (squares and triangles).

Thereafter on the basis of equation 3.21 the experimental r.m.s. contrast sensitivities for each stimulus type, spatial frequency, and number of components were first divided by the corresponding values of the term  $(1 + A_c/A)^{-0.5}$  and then geometrically averaged in order to get the estimates of maximum sensitivity ( $S_{max}$ ) for each stimulus type, spatial frequency, and number of components. The model described the data fairly well and the goodness of fit calculated by equation 2.29 described in Section 2.6.6 varied from 92% to 97%.

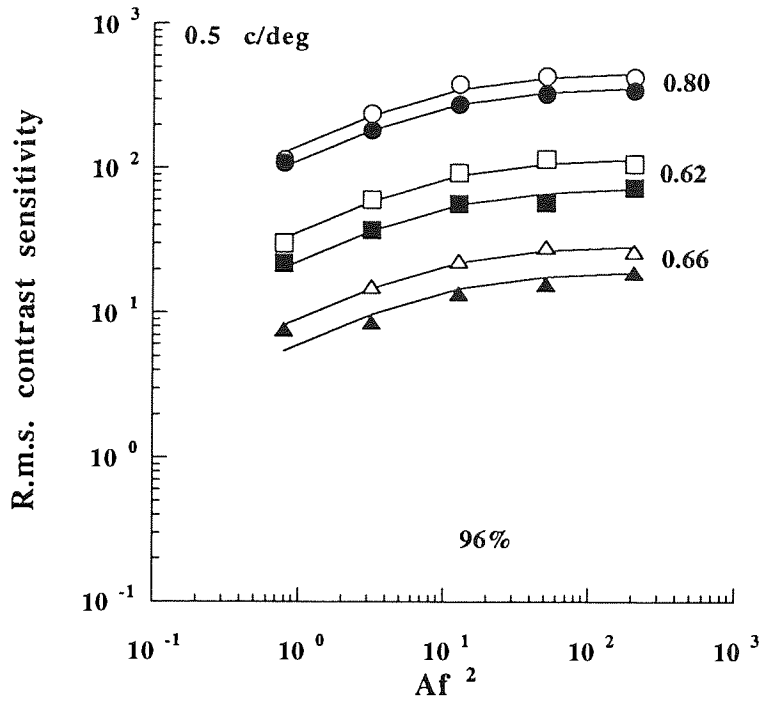


**Figure 5.19** R.m.s. contrast sensitivity as a function of square cycles for non-randomised and randomised 16 component gratings at 0.5 c/deg in orientation and/or phase uncertainty experiments. Symbols as in Figure 5.13. Subjects were KT (circles), and PR (squares and triangles).

Sensitivity was found to be lower for randomised than non-randomised gratings for all numbers of components, types of randomisation and spatial frequencies. According to the model described in Section 3.5 r.m.s. contrast sensitivity should decrease by a factor of  $\sqrt{2}$  when orientation and/or phase parameters are uncertain to the observer.

Thus, when contrast sensitivities measured in the randomised conditions were divided by corresponding sensitivities in the non-randomised conditions the ratio should be 0.71. The ratios were found to be on average 0.69 (SD± 0.10), 0.70 (SD± 0.08), and 0.70 (SD± 0.06) for the sums of one, four, and sixteen grating components, respectively. The model thus described the decrease of r.m.s. contrast sensitivity for randomised gratings very accurately.

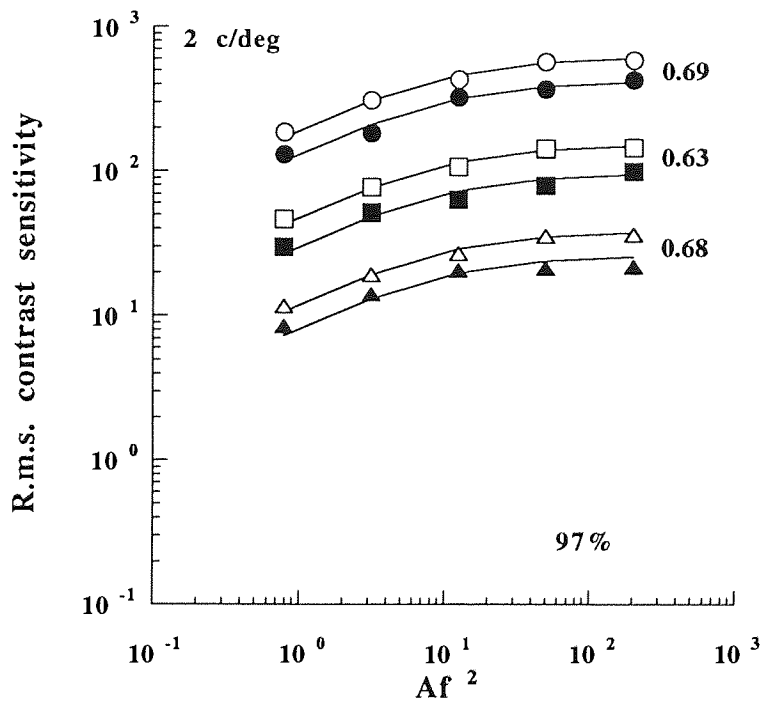
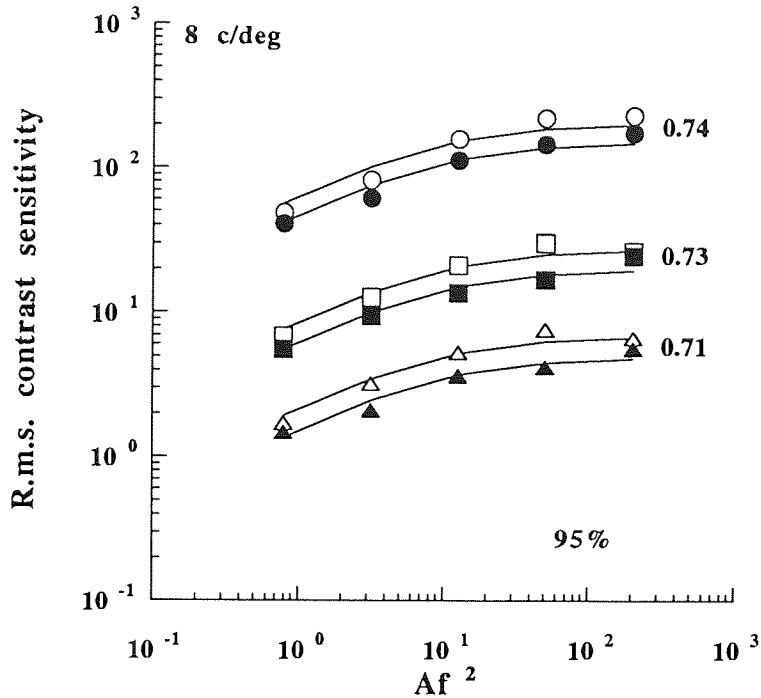


Figure 5.20 R.m.s. contrast sensitivity as a function of square cycles for non-randomised and randomised 16 component gratings at 2 c/deg in orientation and/or phase uncertainty experiments. Symbols as in Figure 5.13. Subject was OU.



**Figure 5.21** R.m.s. contrast sensitivity as a function of square cycles for non-randomised and randomised 16 component gratings at 8 c/deg in orientation and/or phase uncertainty experiments. Symbols as in Figure 5.13. Subjects were JM (circles), and MK (squares and triangles).

### 5.3.4 Discussion

The experiments of this section showed that spatial integration for sums of simple gratings ( $n = 1, 4, \text{ or } 16$ ) with the same contrast and spatial frequency (0.5, 2, or 8 c/deg) but different orientation and/or phase first increased with the number of square cycles ( $A_c f^2$ ) and later saturated with larger number of  $A_c f^2$ , in agreement with many previous studies (e.g. Savoy & McCann, 1978; Robson & Graham, 1981). The finding that spatial integration was similar for non-randomised and randomised gratings irrespective of

randomisation type indicates that spatial integration is not affected by parameter randomisation. Thus the area from which contrast information is collected, i.e. the sampling aperture (Burgess, 1990), does not depend on randomisation. However, spatial integration was more effective when the number of orientation components was 1 than 4 or 16, in agreement with the results described in Section 4.2.

The result that parameter randomisation reduced r.m.s. contrast sensitivity is in agreement with many previous uncertainty studies (e.g. Davis & Graham, 1981; Lappin & Uttal, 1976; Burgess & Ghandeharian, 1984a, b; Howard & Richardson, 1988). According to multichannel theories the uncertainty effect is due to attentional control over multiple channels. When the observer is uncertain of stimulus parameters she/he has to monitor many channels which results in reduced detectability of uncertain stimuli (e.g. Davis & Graham, 1981; Yager, Kramer, Shaw & Graham, 1984). Lappin and Uttal (1976) found that the detectability of a signal composed of dots in noise decreased when the number of alternative positions increased from 2 to 8. They concluded that the detection accuracy decreased because there were more opportunities for the noise to be confused with the signal when the number of possible positions increased. Their finding is consistent with the auto-correlation theory where detectability is determined by the structural characteristics of the stimulus pattern irrespective of observers' prior knowledge of the stimulus form. However, it has been suggested (Burgess & Ghandeharian, 1984a; Kersten, 1983; Howard & Richardson, 1988) that the reduction in observer performance when uncertainty is introduced to the task is consistent with a switch in observer strategy from cross-correlation to auto-correlation detection.

The effect of parameter randomisation on simple and compound non-randomised and randomised gratings was modelled according to the above suggestion (Burgess & Ghandeharian, 1984a; Kersten, 1983; Howard & Richardson, 1988). The detection of non-randomised gratings was mediated by a local matched filter described in detail in Sections 3.1 - 3.3 and the model for randomised gratings was described in Section 3.5.

The sensitivity reduction is due to the poor ability of the auto-correlation detector to reject visual noise. R.m.s. contrast sensitivity should reduce by a factor of  $\sqrt{2}$  according to the model. If the reduction is expressed as the ratio of measured contrast sensitivities in the randomised conditions divided by the corresponding sensitivities in the non-randomised conditions, it should be 0.71. The ratio was found to be on average 0.69 which implies that the introduced model is able to describe the effect of parameter randomisation very accurately. Thus, it is likely that human observers use different detection strategies depending on the task to be performed.

#### 5.4 CONCLUSIONS

The effects of parameter randomisation on r.m.s. contrast sensitivity, physical signal-to-noise ratio and spectral density of equivalent noise were studied in this chapter. Uncertainty of spatial location had no effect in peripheral vision because the accuracy of positional information is inherently poor, whereas in the fovea the effect of location uncertainty was compensated for by searching eye movements. Randomisation of aperture orientation reduced contrast sensitivity in the fovea, because in this case the effect of randomisation could not be compensated for. The finding that the spectral density of equivalent noise was constant across the randomisation range of aperture orientation gives experimental evidence that spatial uncertainty does not increase the amount of internal neural noise in the human visual system.

The finding that spatial integration was similar for non-randomised and randomised gratings irrespective of randomisation type indicates that spatial integration is not affected by parameter randomisation. Thus the area from which contrast information is collected, i.e. the sampling aperture (Burgess, 1990), does not depend on randomisation. The effect of randomisation on contrast sensitivity was modelled under the assumption that human

observers used different detection strategies depending on the task (e.g. Burgess & Ghandeharian, 1984a). When stimuli are known to the observer she/he uses a cross-correlation strategy where stimulus information is mediated by a local matched filter (Hauske et al., 1976). When stimulus uncertainty is introduced to the task, human observers seemed to change their observer strategy from cross-correlation to auto-correlation detection. Auto-correlation has a poorer ability to reject the noise, which is one of the limiting factors in the human visual system. This poor ability to reject noise results in reduced contrast sensitivity and, according to the model, contrast sensitivity for a randomised orientation and/or phase is 0.71 times the contrast sensitivity of a signal known exactly. When orientation and/or phase of the stimulus was completely random the sensitivity for randomised stimuli was on average 0.69 times the corresponding sensitivity for a signal known exactly. If the randomised aperture orientation data with and without external spatial noise from Section 5.2 is expressed by means of the same ratio, sensitivity for randomised stimuli was on average 0.56 times (ranging from 0.42 to 0.83) the sensitivity for non-randomised data when the randomisation range was  $180^\circ$  (i.e., complete). The marginal difference between ratios could be due to the fact that only six data points were measured at complete randomisation range in Section 5.2 whereas the average ratio in Section 5.3 is based on nearly 300 data points. Another possible explanation could be that parameter randomisation affects the perception of randomised gratings embedded in external spatial noise differently compared to randomised gratings without external noise. This is unlikely as it was found that randomisation affected gratings with and without external noise similarly in the experiments of Section 5.2.

The results of this section suggest that there are, however, limits to the conditions where human observers can benefit from the prior knowledge of the stimulus. If human observers are intrinsically uncertain of the stimulus, as in peripheral vision where positional accuracy is already poor, or if the effect of the uncertainty can be compensated for by eye movements, for example, the experimentally added uncertainty has little if any effect on

## Parameter uncertainty

performance. If the uncertainty effect exceeds the intrinsic uncertainty and it cannot be compensated for, the model proposed for the detection of randomised signals seems to be an appropriate mean. Before it is safe to say that the proposed model is one of the possible ways to describe the randomisation effect on detection in general, the applicability of the model has to be thoroughly tested with randomised gratings embedded in external noise.

## 6. OVERALL CONCLUSION

This thesis studied the effect of the number of grating components and parameter randomisation on r.m.s. contrast sensitivity and spatial integration. This final chapter provides an overview of the most important findings obtained in the experiments of this thesis.

Spatial integration for simple and complex stimuli was found to be similar with and without external noise. The critical area marking the saturation of spatial integration decreased with increasing number of orientation components, reaching a minimum when the number of components was 5 to 6, but increased again thereafter. Spatial integration was thus found to depend on the number of orientation components in complex stimuli and the dependence was similar with and without external noise. The dependence of the critical area on the number of orientation components seems to be based on the global Fourier structure of the stimulus rather than local structure.

The model of contrast detection (Rovamo et al., 1993b) was extended to include both simple and complex gratings. The model described in detail in Sections 3.2-3.4 was found to describe on average 93% of the experimental data and hence spatial integration for simple and a wide range of complex stimuli was described very accurately by the model.

In the second major part of the thesis, parameter uncertainty effects on r.m.s. contrast sensitivity were investigated. It was found that there are limits to the conditions where human observers can benefit from the prior knowledge of the stimulus. If human observers are intrinsically uncertain of the stimulus, as in peripheral vision where positional accuracy is already poor, or if the effect of the uncertainty can be compensated for by eye movements for instance, the experimentally added uncertainty has little if any effect on performance.

## Overall conclusion

If the uncertainty effect exceeds the intrinsic uncertainty or it cannot be compensated for, as in the foveal experiments of random aperture orientation and randomised orientation and/or phase of the grating components, r.m.s. contrast sensitivity for random visual signals is lower than sensitivity for exactly known signals. However, the shape of the spatial integration function was similar in both conditions. The model, where human observers use a cross-correlator in signal-known-exactly conditions and an auto-correlator in signal uncertainty conditions, predicts that r.m.s. contrast sensitivity for random visual signals is 0.71 times the corresponding sensitivity for signals known exactly. On average, the ratio between contrast sensitivity for random and known exactly stimuli was 0.63. Hence, the model described the data well.

Overall, the experiments of this thesis suggest that the detection mechanism of the human visual system is highly adaptive. The detection mechanism seems to adapt to the stimulus structure and it is generally able to benefit from prior knowledge of the stimulus. It also seems quite likely that human observers are able to use different detection strategies depending on the task to be performed.

## PUBLICATIONS AND PRESENTATIONS

### PUBLICATIONS

#### Papers

- 1) Rovamo, J., Ukkonen, O., Thompson, C., and Näsänen, R. (1994).  
Spatial integration for compound gratings with various number of orientation components. *Investigative Ophthalmology & Visual Science*, 35, 2611-2619.
- 2) Ukkonen, O. (1994).  
Colour vision. *The Journal of the Association of Optometry in Finland*, 1, 9-10.
- 3) Ukkonen, O., Rovamo, J., and Näsänen, R. (1995).  
The effect of location and orientation uncertainty on r.m.s. contrast sensitivity with and without noise in peripheral and foveal vision. *Optometry and Vision Science*, in press.
- 4) Rovamo, J., Ukkonen, O., and Näsänen, R. (1995).  
Spatial integration for compound gratings of two spatial frequencies in noise. In preparation.
- 5) Ukkonen, O., Rovamo, J., and Näsänen, R. (1995).  
Spatial integration for sums of orientation components in external noise. In preparation.

## Publications and presentations

- 6) Ukkonen, O., Rovamo, J., and Näsänen, R. (1995).  
Modelling the effect of orientation and/or phase randomisation on r.m.s. contrast sensitivity for simple and compound gratings. In preparation.

## Abstracts

- 1) Ukkonen, O., Thompson, C., Rovamo, J., and Näsänen, R. (1991).  
Effects of number of components and spatial frequency difference on contrast sensitivity to complex gratings, poster abstract, *Ophthalmic and Physiological Optics*, 11, 397.
- 2) Thompson, C., Rovamo, J., Näsänen, R., and Ukkonen, O. (1991).  
Effects of spatial frequency difference and number of components on the contrast sensitivity to complex gratings, poster abstract, *Perception*, 20, 82.
- 3) Rovamo, J., Thompson, C., Ukkonen, O., and Näsänen, R. (1991).  
Contrast sensitivity as a function of spatial frequency difference and number of components in complex gratings, poster abstract, *European Journal of Neuroscience*, Suppl. 4, 76.
- 4) Ukkonen, O., Thompson, C., Rovamo, J., and Näsänen, R. (1991).  
Effects of area and number of different orientations on contrast sensitivity to a sum of gratings, poster abstract, *OSA Annual meeting Technical Digest*, 17, 124.

## Publications and presentations

- 5) Ukkonen, O., Thompson, C., Rovamo, J., and Näsänen, R. (1992).  
The effect of area on contrast sensitivity for a sum of gratings with different orientation, poster abstract, *Perception*, 21, 92.
- 6) Ukkonen, O., Rovamo, J., and Näsänen, R. (1993).  
The effect of orientation randomization on simple and compound gratings, poster abstract, *Investigative Ophthalmology & Visual Science, Annual Meeting Abstract Issue*, 34, 781.
- 7) Ukkonen, O., Rovamo, J., and Näsänen, R. (1993).  
Aperture orientation reduces contrast sensitivity to gratings with and without external spatial noise, paper abstract, *Perception*, 22, 38.

## PRESENTATIONS

### Papers

- 1) Ukkonen, O. (1993).  
The effect of orientation randomisation on r.m.s. contrast sensitivity, internal seminar, Department of Vision Sciences, University of Aston, Birmingham, United Kingdom, 12 March.
- 2) Ukkonen, O., Rovamo, J., and Näsänen, R. (1993).  
Aperture orientation reduces contrast sensitivity to gratings with and without external spatial noise, European Conference On Visual Perception, Edinburgh, United Kingdom, 28 August.

## Publications and presentations

- 3) Ukkonen, O. (1993).  
Colour vision, Annual Meeting of Finnish Ophthalmic Opticians, Helsinki, Finland, 17 October.
- 4) Ukkonen, O. (1995).  
Detection of compound gratings in visual noise, internal seminar, Department of Vision Sciences, University of Aston, Birmingham, United Kingdom, 10 March.

## Posters

- 1) Ukkonen, O., Thompson, C., Rovamo, J., and Näsänen, R. (1991).  
Effects of number of components and spatial frequency difference on contrast sensitivity to complex gratings, Society of Experimental Optometry, Birmingham, United Kingdom, 15 - 16 July .
- 2) Ukkonen, O., Thompson, C., Rovamo, J., and Näsänen, R. (1991).  
Effects of area and number of different orientations on contrast sensitivity to a sum of gratings, Optical Society of America, San Jose, U.S.A., 3 - 8- November.
- 3) Ukkonen, O., Thompson, C., Rovamo, J., and Näsänen, R. (1992).  
The effect of area on contrast sensitivity for a sum of gratings with different orientation, European Conference on Visual Perception, Pisa, Italy, 30 August - 3 September.

## Publications and presentations

- 4) Ukkonen, O., Rovamo, J., and Näsänen, R. (1993).  
The effect of orientation randomization on simple and compound gratings,  
The Association for Research in Vision and Ophthalmology, Sarasota,  
U.S.A., 2 - 5 May.
- 5) Ukkonen, O., Rovamo, J., and Näsänen, R. (1995).  
Spatial integration for sums of two spatial frequencies, presented at The  
Association for Research in Vision and Ophthalmology Meeting, Miami,  
U.S.A., 14 - 19 May.
- 6) Ukkonen, O., Rovamo, J., and Näsänen, R. (1995).  
Spatial integration for sums of two spatial frequency components in external  
spatial noise, accepted to The European Conference on Visual Perception  
Meeting, Tübingen, Germany, 21 - 25 August.
- 7) Ukkonen, O., Rovamo, J., and Näsänen, R. (1995).  
The effect of orientation and/or phase uncertainty on simple and compound  
gratings, submitted to The Optical Society of America Meeting, Portland,  
U.S.A., 10 - 15 September.

**REFERENCES**

Artal, P. & Navarro, R. (1994). Monochromatic modulation transfer function of the human eye for different pupil diameters: an analytical expression. *Journal of Optical Society of America*. 11, 246-249.

Banks, M.S., Geisler, W.S. & Bennet, P.J. (1987). The physical limits of grating visibility. *Vision Research*, 27, 1915-1924.

Barlow, H.B. (1956). Retinal noise and absolute threshold. *Journal of the Optical Society of America*, 46, 634-639.

Bourbon, B. (1902). *La Perception Visuelle de L'Espace*, p.146. Scheicher, Paris.

Bracewell, R.N. (1978). *The Fourier Transform and Its Applications*. McGraw-Hill, New York, London.

Burgess, A. (1985). Visual signal detection. III. On Bayesian use of prior knowledge and cross correlation. *Journal of the Optical Society of America A*, 2, 1498-1507.

Burgess, A.E. (1990). High level decision efficiencies. In Blakemore, C. (Ed.), *Vision: Coding and Efficiency* (pp. 431-440). Cambridge University Press, New York.

Burgess, A. & Ghandeharian H. (1984a). Visual signal detection. I. Ability to use phase information. *Journal of the Optical Society of America A*, 1, 900-905.

## References

- Burgess, A.E. & Ghandeharian H. (1984b). Visual signal detection. II. Signal-location identification. *Journal of the Optical Society of America A*, 1, 906-910.
- Campbell, F.W. & Gubish, R.W. (1966). Optical quality of the human eye. *Journal of Physiology (London)*, 186, 558-578.
- Campbell, F.W., Kulikowski, J.J. & Levinson, J. (1966). The effect of orientation of the visual resolution of gratings. *Journal of Physiology (London)*, 187, 427-436.
- Campbell, F.W. & Robson, J.G. (1968). Application of Fourier analysis to the visibility of gratings. *Journal of Physiology (London)*, 197, 551-566.
- Carpenter, R.H.S. (1988). *The Movements of the Eyes*. Pion Limited, London.
- Cohen, R.W. (1978). Applying psychophysics to display design. *Photographic Science and Engineering*, 22, 56-59.
- Cohn, T.E. & Lasley, D.J. (1974). Detectability of a luminance increment: Effect of spatial uncertainty. *Journal of the Optical Society of America*, 64, 1715-1719.
- Cohn, T.E. & Wardlaw, J.C. (1985). Effect of large spatial uncertainty on foveal luminance increment detectability. *Journal of the Optical Society of America A*, 2, 820-825.
- Coltman, J.M. & Anderson, A.E. (1960). Noise limitations to resolving power in electronic imaging. *Proceedings of the IRE*, 48, 858-865

## References

- Cormack, R.H. & Blake, R. (1980). Do the two eyes constitute separate visual channels? *Science*, 207, 1100-1102.
- Cornsweet, T.N. (1970). *Visual Perception*. Academic Press, Orlando.
- Davis, E.T. (1981). Allocation of attention: Uncertainty effects when monitoring one or two visual gratings of noncontiguous spatial frequencies. *Perception & Psychophysics*, 29, 618-622.
- Davis, E.T. & Graham, N. (1981). Spatial frequency uncertainty effects in the detection of sinusoidal gratings. *Vision Research*, 21, 705-712.
- Davis, E.T., Kramer, P. & Graham, N. (1983). Uncertainty about spatial frequency, spatial position, or contrast of visual patterns. *Perception & Psychophysics*, 33, 20-28.
- Deeley, R.J., Drasdo, N. & Charman, W.N. (1991). A simple parametric model of the human ocular modulation transfer function. *Ophthalmic & Physiological Optics*, 11, 91-93.
- DePalma, J.J. & Lowry, E.M. (1962). Sine-wave response of the visual system. II. Sine-wave and square-wave contrast sensitivity. *Journal of the Optical Society of America*, 52, 328-335.
- De Valois, R.L., Albrecht, D.G. & Thorell, L.G. (1982). Spatial frequency selectivity of cells in macaque visual cortex. *Vision Research*, 22, 545-559.

## References

- Elliot, P.B. (1964). Forced choice tables (Appendix 1). In Swets, J.A. (Ed.), *Signal Detection and Recognition by Human Observers*, (pp. 679-684). John Wiley and Sons, New York.
- Estevez, O. & Cavonius, C.R. (1976). Low-frequency attenuation in the detection of gratings: sorting out the artefacts. *Vision Research*, 16, 497-500.
- Findlay, J.M. (1969). A spatial integration effect in visual acuity. *Vision Research*, 9, 157-166.
- Graham, N. (1989). *Visual Pattern Analyzers*. Oxford University Press, New York.
- Graham, N. & Nachmias, J. (1971). Detection of grating patterns containing two spatial frequencies: A comparison of single-channel and multiple-channels models. *Vision Research*, 11, 251-259.
- Graham, N. & Robson, J.G. (1987). Summation of very close spatial frequencies: The importance of spatial probability summation. *Vision Research*, 27, 1997-2007.
- Graham, N., Robson, J.G. & Nachmias, J. (1978). Grating summation in fovea and periphery. *Vision Research*, 18, 815-825.
- Green, D.M. & Swets, J.A. (1966). *Signal Detection Theory and Psychophysics*. John Wiley and Sons, New York.
- Greenhouse, D.S. & Cohn, T.E. (1978). Effect of chromatic uncertainty on detectability of a visual stimulus. *Journal of the Optical Society of America*, 68, 266-267.

## References

- Grindley, G.C. & Townsend, V. (1968). Voluntary attention in peripheral vision and its effects on acuity and differential thresholds. *Quarterly Journal of Experimental Psychology*, 20, 11-19.
- Hartmann, E., Lachenmayr, B. & Brettel, H. (1979). The peripheral critical flicker frequency. *Vision Research*, 19, 1019-1023.
- Hauske, G., Wolf, W. & Lupp, U. (1976). Matched filters in human vision. *Biological Cybernetics*, 22, 181-188.
- Hess, R. F. & Field, D. (1993). Is the increased spatial uncertainty in the normal periphery due to spatial undersampling or uncalibrated disarray? *Vision Research*, 33, 2663-2670.
- Hoekstra, J., van der Goot, D.P.J., van den Brink, G. & Bilsen, F.A. (1974). The influence of the number of cycles upon the visual contrast threshold for spatial sine wave patterns. *Vision Research*, 14, 365-368.
- Howard, J.H. & Richardson, K.H. (1988). Absolute phase uncertainty in sinusoidal grating detection. *Perception & Psychophysics*, 43, 38-44.
- Howarth, C.I. & Lowe, G. (1966). Statistical detection theory of Piper's law. *Nature*, 212, 324-326.
- Howell, E.R. & Hess, R.F. (1978). The functional area for summation to threshold for sinusoidal gratings. *Vision Research*, 18, 369-374.

## References

Hubel, D.H. & Wiesel, T.N. (1968). Receptive fields and functional architecture of monkey striate cortex. *Journal of Physiology (London)*, 195, 215-243.

Ijspeert, J.K., van den Berg, T.J.T.P. & Spekreijse, H. (1993). An improved mathematical description of the foveal visual point spread function with parameters for age, pupil size and pigmentation. *Vision Research*, 33, 15-20.

Kelly, D.H. & Magnuski, H.S. (1975). Pattern detection and the two-dimensional Fourier transform: Circular targets. *Vision Research*, 15, 911-915.

Kersten, D. (1983). A comparison of human and ideal performance for detection of visual pattern. Ph.D. dissertation, University of Minnesota, Minneapolis, Minnesota.

Kersten, D. (1984). Spatial summation in visual noise. *Vision Research*, 24, 1977-1990.

Kukkonen, H., Näsänen, R. & Rovamo, J. (1994). Detection efficiency of circular gratings and band-pass filtered points with randomized phase spectra. *Investigative Ophthalmology & Visual Science*, 35, 3111-3118.

Kukkonen, H, Rovamo, J & Näsänen, R. (1995). Masking potency and whiteness of noise at various noise check sizes. *Investigative Ophthalmology & Visual Science*, 36, 513-518.

Kulikowski, J.J. & King-Smith, P.E. (1973). Spatial arrangement of line, edge and grating detectors revealed by subthreshold summation. *Vision Research*, 13, 1455-1478.

## References

- Lappin, J.S. & Uttal, W.R. (1976). Does prior knowledge facilitate the detection of visual targets in random noise? *Perception & Psychophysics*, 20, 367-374.
- Lasley, D.J. & Cohn, T. (1981). Detection of a luminance increment: Effect of temporal uncertainty. *Journal of the Optical Society of America*, 71, 845-850.
- Legge, G.E., Kersten, D. & Burgess, A.E. (1987). Contrast discrimination in noise. *Journal of the Optical Society of America A*, 4, 391-404.
- Levi, D.M., Klein, S.A. & Yap, Y.L. (1987). Positional uncertainty in peripheral and amblyopic vision. *Vision Research*, 27, 581-597.
- Lindblom, B. & Westheimer, G. (1992). Uncertainty effects in orientation discrimination of foveally seen lines in human observers. *Journal of Physiology (London)*, 454, 1-8.
- Lowe, G. (1967). Interval of time uncertainty in visual detection. *Perception & Psychophysics*, 2, 278-280.
- Luntinen, O., Rovamo, J. & Näsänen, R. (1995). Contrast sensitivity as a function of grating area and spectral density of external spatial noise. *Vision Research*, under revision.
- McCann, J.J. (1978). Visibility of gradients and low spatial frequency sinusoids: Evidence for a distance constancy mechanism. *Photographic Science and Engineering*, 22, 64-68.
- van Meeteren, A. & Barlow, H.B. (1981). The statistical efficiency for detecting sinusoidal modulation of average dot density in random figures. *Vision Research*, 21, 765-777.

## References

- van Meeteren, A. & Valetton, J.M. (1988). Effects of pictorial noise interfering with visual detection. *Journal of the Optical Society of America A*, 5, 438-444.
- Mertens, J.J. (1956). Influence of knowledge of target location upon the probability of observation of peripherally observable test flashes. *Journal of the Optical Society of America*, 46, 1069-1070.
- Mostafavi, H. & Sakrison, D.J. (1976). Structure and properties of a single channel in the human visual system. *Vision Research*, 16, 957-968.
- Moulden, B., Kingdom, F. & Gatley, L.F. (1990). The standard deviation of luminance as a metric for contrast in random-dot images. *Perception*, 19, 79-101.
- Movshon, J.A., Thompson, I.D. & Tolhurst, D.J. (1978). Spatial summation in the receptive fields of simple cells in the cat's striate cortex. *Journal of Physiology (London)*, 283, 53-77.
- Mustonen, J., Rovamo, J. & Näsänen, R. (1993). The effects of grating area and spatial frequency on contrast sensitivity as a function of light level. *Vision Research*, 33, 2065-2072.
- Nachmias, J. (1968). Visual resolution of two-bar patterns and square-wave gratings. *Journal of the Optical Society of America*, 58, 9-13.
- Nagaraja, N.S. (1964). Effect of luminance noise on contrast thresholds. *Journal of the Optical Society of America*, 54, 950-955.

## References

- Näsänen, R., Kukkonen, H. & Rovamo, J. (1993). Spatial integration of band-pass filtered patterns in noise. *Vision Research*, 33, 903-911.
- Näsänen, R., Kukkonen, H. & Rovamo, J. (1994). Relationship between spatial integration and spatial spread of contrast energy in detection. *Vision Research*, 34, 949-954.
- Pantle, A. (1973). Visual effects of sinusoidal components of complex gratings: Independent or additive. *Vision Research*, 13, 2195-2204.
- Pelli, D.G. (1981). Effects of visual noise. Ph.D. dissertation, Cambridge University, Cambridge.
- Pelli, D.G. (1984). Intrinsic uncertainty in visual detection. *Perception*, 13, 1, A14.
- Pelli, D. G. (1990). The quantum efficiency of vision. In Blakemore, C. (Ed.), *Vision: Coding and Efficiency* (pp. 3-24). Cambridge University Press, Cambridge.
- Pelli, D.G. & Zhang, L. (1991). Accurate control of contrast on microcomputer displays. *Vision Research*, 31, 1337-1350.
- Piper, H. (1903). Die Abhängigkeit des Reizwertes leuchtender Objekte von ihrer Flächenbesw. Winkelgröfse. *Zeitschrift für Psychologie und Physiologie der Sinneorgane*, 32, 98-112.
- Pollehn, H. & Roehrig, H. (1970). Effect of noise on the modulation transfer function of the visual channel. *Journal of the Optical Society of America*, 60, 842-848.

## References

- Posner, M.I., Nissen, M.J. & Ogden, W.C. (1978). Attended and unattended processing modes: The role of set for spatial location. In Pick, H. L. & Saltzman, E. (Eds.), *Modes of Perceiving and Processing Information* (pp. 137-157). Lawrence Erlbaum Associates, Hillsdale, New Jersey
- Quick, R.F., Hamerly, J.R. & Reichert, T.A. (1976). The absence of a measurable "critical band" at low suprathreshold contrasts. *Vision Research*, 16, 351-355.
- Quick, R.F., Mullins, W.W. & Reichert, T.A. (1978). Spatial summation effects on two-component grating thresholds. *Journal of the Optical Society of America*, 68, 116-121.
- Quick, R.F. & Reichert, T.A. (1975). Spatial-frequency selectivity in contrast detection. *Vision Research*, 15, 637-643.
- Ratliff, F. & Hartline, H.K. (1959). The responses of limulus optic nerve fibers to patterns of illumination on the receptor mosaic. *Journal of General Physiology*, 42, 1241-1255.
- Robson, J.G. & Graham, N. (1981). Probability summation and regional variation in contrast sensitivity across the visual field. *Vision Research*, 21, 409-418.
- Ross, J. & Johnstone, J.R. (1980). Phase and detection of compound gratings. *Vision Research*, 20, 189-192.
- Rovamo, J., Franssila, R. & Näsänen, R. (1992). Contrast sensitivity as a function of spatial frequency, viewing distance and eccentricity with and without spatial noise. *Vision Research*, 32, 631-637.

## References

- Rovamo, J., Kukkonen, H., Tiippana, K. & Näsänen, R. (1993a). Effects of luminance and exposure time on contrast sensitivity in spatial noise. *Vision Research*, 33, 1123-1129.
- Rovamo, J., Luntinen, O. & Näsänen, R. (1993b). Modelling the dependence of contrast sensitivity on grating area and spatial frequency. *Vision Research*, 33, 2773-2788.
- Rovamo, J., Mustonen, J. & Näsänen, R. (1994a). Modelling contrast sensitivity as a function of retinal illuminance and grating area. *Vision Research*, 34, 1301-1314.
- Rovamo, J., Mustonen, J. & Näsänen, R. (1994b). Two simple psychophysical methods for determining the optical modulation function of the human eye. *Vision Research*, 34, 2493-2502.
- Rovamo, J., Mustonen, J. & Näsänen, R. (1995). Neural modulation transfer function of the human visual system at various eccentricities. *Vision Research*, 35, 767-774.
- Rovamo, J. & Raninen, A. (1984). Critical flicker frequency and M-scaling of stimulus size and retinal illuminance. *Vision Research*, 24, 1127-1131.
- Sachs, M.B., Nachmias, J. & Robson, J.G. (1971). Spatial frequency channels in human vision. *Journal of the Optical Society of America*, 61, 1176-1186.
- Santamaria, J., Artal, P. & Bescos, J. (1987). Determination of the point-spread function of the human eyes using a hybrid optical-digital method. *Journal of the Optical Society of America A*, 4, 1109-1114.

## References

- Savoy, R.L. & McCann, J.J. (1975). Visibility of low-spatial-frequency sine-wave targets: Dependence on number of cycles. *Journal of the Optical Society of America*, 65, 343-350.
- Schade, O.H. (1956). Optical and photoelectric analog of the eye. *Journal of the Optical Society of America*, 46, 721-739.
- Schober, H.A.W. & Hilz, R. (1965). Contrast sensitivity of the human eye for square-wave gratings. *Journal of the Optical Society of America*, 55, 1086-1091.
- Schuckman, H. (1963). Attention and visual threshold. *American Journal of Optometry and Archives of American Academy of Optometry*, 40, 284-291
- Sekuler, R. & Ball, K. (1977). Mental set alters visibility of moving targets. *Science*, 198, 60-62.
- Shiffrin, R.M. & Gardner, G.T. (1972). Visual processing capacity and attentional control. *Journal of Experimental Psychology*, 93, 72-82.
- Shiffrin, R.M., McKay, D.P. & Shaffer, W.O. (1976). Attending to forty-nine spatial positions at once. *Journal of Experimental Psychology: Human Perception and Performance*, 2, 15-22.
- Tanner, W.P. & Birdsall, T.G. (1958). Definitions of  $d'$  and  $\eta$  as psychophysical measures. *The Journal of the Acoustical Society of America*, 30, 922-928.

## References

- Tiippana, K., Näsänen, R. & Rovamo, J. (1994). Contrast matching of two-dimensional compound gratings. *Vision Research*, 34, 1157-1163.
- Verghese, P. & Pelli, D.G. (1992). The information capacity of visual attention. *Vision Research*, 32, 983-995.
- Virsu, V. & Rovamo, J. (1979). Visual resolution, contrast sensitivity, and the cortical magnification factor. *Experimental Brain Research*, 37, 475-494.
- Westheimer, G. (1982). The spatial grain of the perifoveal visual field. *Vision Research*, 22, 157-162.
- Wetherill, G.B. & Levitt, H. (1965). Sequential estimation of points on a psychometric function. *The British Journal of Mathematical and Statistical Psychology*, 18, 1-10.
- Yager, D., Kramer, P., Shaw, M. & Graham, N. (1984). Detection and identification of spatial frequency: Models and data. *Vision Research*, 24, 1021-1035.

## APPENDIX 1

## TABLES OF THE EXPERIMENTAL DATA OF THE THESIS

Figure 4.2 (A)

Area deg <sup>2</sup>	R.m.s. contrast sensitivity 1 component 0.25 c/deg JM solid circles	R.m.s. contrast sensitivity 2 components 0.25 c/deg JM solid squares	R.m.s. contrast sensitivity 3 components 0.25 c/deg JM solid triangles	R.m.s. contrast sensitivity 4 components 0.25 c/deg JM solid circles	R.m.s. contrast sensitivity 5 components 0.25 c/deg JM open circles	R.m.s. contrast sensitivity 6 components 0.25 c/deg JM open squares	R.m.s. contrast sensitivity 8 components 0.25 c/deg JM open triangles	R.m.s. contrast sensitivity 16 components 0.25 c/deg JM open circles
12.60	107.9	112.5	116.0	116.5	111.3	109.0	141.8	120.3
50.27	153.5	145.9	167.7	203.7	157.5	176.2	182.1	169.4
199.1	283.4	250.4	198.8	262.1	158.9	209.1	245.0	314.7
767.2	424.6	551.9	236.0	201.8	248.3	246.8	297.1	345.7

Figure 4.2 (B)

Area deg <sup>2</sup>	R.m.s. contrast sensitivity 1 component 0.25 c/deg OU solid circles	R.m.s. contrast sensitivity 2 components 0.25 c/deg OU solid squares	R.m.s. contrast sensitivity 3 components 0.25 c/deg OU solid triangles	R.m.s. contrast sensitivity 4 components 0.25 c/deg OU solid circles	R.m.s. contrast sensitivity 5 components 0.25 c/deg OU open circles	R.m.s. contrast sensitivity 6 components 0.25 c/deg OU open squares	R.m.s. contrast sensitivity 8 components 0.25 c/deg OU open triangles	R.m.s. contrast sensitivity 16 components 0.25 c/deg OU open circles
12.60	109.5	91.52	92.91	74.24	104.0	80.02	123.8	134.0
50.27	164.7	112.4	126.5	138.7	149.2	144.4	202.8	247.0
199.1	236.3	175.1	153.7	163.8	176.8	198.5	279.5	327.4
767.2	369.5	242.3	206.8	210.5	217.0	224.4	221.9	486.4

Figure 4.3 (A)

Area deg <sup>2</sup>	R.m.s. contrast sensitivity 1 component 1 c/deg CT solid circles	R.m.s. contrast sensitivity 2 components 1 c/deg CT solid squares	R.m.s. contrast sensitivity 3 components 1 c/deg CT solid triangles	R.m.s. contrast sensitivity 4 components 1 c/deg CT solid circles	R.m.s. contrast sensitivity 5 components 1 c/deg CT open circles	R.m.s. contrast sensitivity 6 components 1 c/deg CT open squares	R.m.s. contrast sensitivity 8 components 1 c/deg CT open triangles	R.m.s. contrast sensitivity 16 components 1 c/deg CT open circles
0.7935	148.4	173.8	173.8	177.5	185.9	125.7	158.9	174.4
3.174	273.5	234.5	234.5	250.4	305.9	238.7	238.0	309.3
12.69	522.3	408.3	408.3	266.2	294.6	332.3	393.3	437.8
50.62	654.7	467.8	467.8	390.7	376.6	390.4	318.2	684.8
200.5	729.6	596.5	596.5	482.0	488.0	412.4	462.9	664.8

Figure 4.3 (B)

Area deg <sup>2</sup>	R.m.s. contrast sensitivity 1 component 1 c/deg OU solid circles	R.m.s. contrast sensitivity 2 components 1 c/deg OU solid squares	R.m.s. contrast sensitivity 3 components 1 c/deg OU solid triangles	R.m.s. contrast sensitivity 4 components 1 c/deg OU solid circles	R.m.s. contrast sensitivity 5 components 1 c/deg OU open circles	R.m.s. contrast sensitivity 6 components 1 c/deg OU open squares	R.m.s. contrast sensitivity 8 components 1 c/deg OU open triangles	R.m.s. contrast sensitivity 16 components 1 c/deg OU open circles
0.7935	135.7	154.1	125.7	132.1	151.1	149.0	116.9	135.0
3.174	246.1	190.3	209.2	263.4	273.4	259.2	250.0	277.8
12.69	417.5	255.4	237.6	268.8	230.1	283.9	335.5	409.4
50.62	691.7	389.9	372.9	346.0	332.5	392.2	353.2	576.8
200.5	738.7	500.6	378.5	349.2	407.0	370.7	367.8	449.7

Figure 4.4 (A)

Area deg <sup>2</sup>	R.m.s. contrast sensitivity 1 component 4 c/deg CT solid circles	R.m.s. contrast sensitivity 2 components 4 c/deg CT solid squares	R.m.s. contrast sensitivity 3 components 4 c/deg CT solid triangles	R.m.s. contrast sensitivity 4 components 4 c/deg CT solid circles	R.m.s. contrast sensitivity 5 components 4 c/deg CT open circles	R.m.s. contrast sensitivity 6 components 4 c/deg CT open squares	R.m.s. contrast sensitivity 8 components 4 c/deg CT open triangles	R.m.s. contrast sensitivity 16 components 4 c/deg CT open circles
0.0496	125.9	131.7	104.5	126.1	139.7	113.6	123.7	136.8
0.1984	225.3	167.4	169.1	209.7	226.5	250.5	235.0	227.8
0.7935	404.4	325.0	324.7	296.0	281.7	367.4	412.5	370.3
3.174	544.0	436.2	346.7	377.9	346.2	369.8	421.1	545.5
12.69	810.9	485.4	483.7	478.0	423.2	396.0	363.3	575.1

Figure 4.4 (B)

Area deg <sup>2</sup>	R.m.s. contrast sensitivity 1 component 4 c/deg OU solid circles	R.m.s. contrast sensitivity 2 components 4 c/deg OU solid squares	R.m.s. contrast sensitivity 3 components 4 c/deg OU solid triangles	R.m.s. contrast sensitivity 4 components 4 c/deg OU solid circles	R.m.s. contrast sensitivity 5 components 4 c/deg OU open circles	R.m.s. contrast sensitivity 6 components 4 c/deg OU open squares	R.m.s. contrast sensitivity 8 components 4 c/deg OU open triangles	R.m.s. contrast sensitivity 16 components 4 c/deg OU open circles
0.0496	113.2	151.0	142.2	133.0	126.9	139.6	110.1	109.6
0.1984	263.0	239.0	216.2	224.5	255.1	294.7	241.7	291.3
0.7935	487.7	329.4	314.3	263.5	273.1	324.4	438.9	454.3
3.174	593.5	393.0	387.3	361.8	377.3	382.1	409.3	647.4
12.69	649.8	504.3	425.3	398.5	440.8	420.0	407.9	522.3

Figure 4.5

Number of components	A <sub>c</sub> 0.25 c/deg JM open triangles	A <sub>c</sub> 0.25 c/deg OU solid triangles	A <sub>c</sub> 1 c/deg CT open circles	A <sub>c</sub> 1 c/deg OU solid circles	A <sub>c</sub> 4 c/deg CT open squares	A <sub>c</sub> 4 c/deg OU solid squares
1	279.6	165.9	20.66	30.47	2.388	1.356
2	615.9	86.12	9.022	7.800	0.7517	0.4881
3	39.54	50.09	4.739	6.947	1.082	0.4193
4	44.81	87.00	7.588	3.866	0.6662	0.3889
5	48.19	42.03	3.798	3.813	0.3777	0.4460
6	52.49	96.78	7.505	4.342	0.4467	0.2908
8	44.45	48.76	5.743	5.808	0.5232	0.6030
16	126.7	180.6	13.44	11.97	1.025	1.083

Figure 4.6

Number of components	$S_{\max}$ 0.25 c/deg JM open triangles	$S_{\max}$ 0.25 c/deg OU solid triangles	$S_{\max}$ 1 c/deg CT open circles	$S_{\max}$ 1 c/deg OU solid circles	$S_{\max}$ 4 c/deg CT open squares	$S_{\max}$ 4 c/deg OU solid squares
1	474.6	380.9	786.0	823.1	832.5	721.6
2	701.3	236.3	559.9	455.3	481.8	467.7
3	230.9	196.9	435.6	377.3	475.9	413.3
4	265.9	215.9	434.4	352.7	451.6	382.7
5	233.7	210.5	440.3	375.2	392.9	420.9
6	248.0	240.9	421.0	382.8	421.9	413.8
8	286.6	282.3	441.6	387.2	460.5	490.1
16	380.6	517.2	714.3	580.2	601.7	684.9

Figure 4.7 (0.25 c/deg)

A/A <sub>c</sub> 0.25 c/deg JM	Energy threshold 0.25 c/deg JM open triangles	A/A <sub>c</sub> 0.25 c/deg OU	Energy threshold 0.25 c/deg OU solid triangles
0.04505	1.083e-03	0.07596	1.050e-03
0.1798	2.134e-03	0.3031	1.854e-03
0.7122	2.479e-03	1.201	3.568e-03
2.744	4.256e-03	4.626	5.619e-03
0.02045	9.956e-04	0.1463	1.504e-03
0.08162	2.361e-03	0.5837	3.977e-03
0.3233	3.175e-03	2.312	6.498e-03
1.246	2.519e-03	8.909	1.307e-02
0.3186	9.360e-04	0.2515	1.459e-03
1.271	1.788e-03	1.003	3.140e-03
5.036	5.040e-03	3.975	8.432e-03
19.40	1.378e-02	15.32	1.795e-02
0.2812	9.289e-04	0.1448	2.286e-03
1.122	1.211e-03	0.5778	2.613e-03
4.444	2.900e-03	2.289	7.423e-03
17.12	1.883e-02	8.818	1.732e-02
0.2614	1.017e-03	0.2997	1.165e-03
1.043	2.026e-03	1.196	2.257e-03
4.132	7.884e-03	4.738	6.374e-03
15.92	1.244e-02	18.25	1.630e-02
0.2400	1.060e-03	0.1302	1.968e-03
0.9577	1.618e-03	0.5194	2.412e-03
3.794	4.555e-03	2.058	5.055e-03
14.62	1.260e-02	7.927	1.524e-02
0.2834	6.264e-04	0.2584	8.220e-04
1.131	1.515e-03	1.031	1.223e-03
4.480	3.317e-03	4.084	2.548e-03
17.26	8.692e-03	15.73	1.558e-02
0.09942	8.711e-04	0.06977	7.020e-04
0.3967	1.752e-03	0.2784	8.240e-04
1.572	2.011e-03	1.103	1.858e-03
6.055	6.418e-03	4.249	3.243e-03

Figure 4.7 (1 c/deg)

A/A <sub>c</sub> 1 c/deg CT	Energy threshold 1 c/deg CT open circles	A/A <sub>c</sub> 1 c/deg OU	Energy threshold 1 c/deg OU solid circles
0.03842	3.601e-05	0.02604	4.307e-05
0.1536	4.242e-05	0.1042	5.238e-05
0.6142	4.650e-05	0.4164	7.278e-05
2.451	1.181e-04	1.661	1.058e-04
9.708	3.767e-04	6.581	3.675e-04
0.08795	2.628e-05	0.1017	3.342e-05
0.3518	5.771e-05	0.4069	8.762e-05
1.406	7.614e-05	1.626	1.945e-04
5.611	2.313e-04	6.490	3.331e-04
22.23	5.636e-04	25.71	8.001e-04
0.1674	2.519e-05	0.1142	5.023e-05
0.6696	5.063e-05	0.4568	7.249e-05
2.677	1.791e-04	1.826	2.247e-04
10.68	3.317e-04	7.287	3.641e-04
42.31	8.630e-04	28.86	1.400e-03
0.1046	6.996e-05	0.2053	4.547e-05
0.4183	4.547e-05	0.8209	4.574e-05
1.672	1.067e-04	3.282	1.756e-04
6.672	3.797e-04	13.09	4.228e-04
26.43	1.045e-03	51.87	1.644e-03
0.2089	2.295e-05	0.2081	3.474e-05
0.8356	3.393e-05	0.8323	4.246e-05
3.340	1.462e-04	3.327	2.397e-04
13.33	3.569e-04	13.28	4.580e-04
52.79	8.421e-04	52.59	1.211e-03
0.1057	5.024e-05	0.1828	3.575e-05
0.4229	5.571e-05	0.7309	4.723e-05
1.691	1.149e-04	2.922	1.574e-04
6.746	3.321e-04	11.66	3.291e-04
26.72	1.179e-03	46.18	1.459e-03
0.1382	3.141e-05	0.1366	5.804e-05
0.5526	5.602e-05	0.5464	5.079e-05
2.209	8.203e-05	2.184	1.127e-04
8.815	5.000e-04	8.716	4.057e-04
34.92	9.357e-04	34.53	1.482e-03
0.05906	2.609e-05	0.06629	4.352e-05
0.2362	3.317e-05	0.2651	4.112e-05
0.9443	6.620e-05	1.060	7.571e-05
3.768	1.079e-04	4.229	1.521e-04
14.93	4.537e-04	16.75	9.917e-04

Figure 4.7 (4 c/deg)

A/A <sub>c</sub> 4 c/deg CT	Energy threshold 4 c/deg CT open squares	A/A <sub>c</sub> 4 c/deg OU	Energy threshold 4 c/deg OU solid squares
0.02077	3.129e-06	0.03657	3.867e-06
0.08309	3.908e-06	0.1463	2.869e-06
0.3323	4.853e-06	0.5851	3.337e-06
1.329	1.072e-05	2.340	9.009e-06
5.313	1.929e-05	9.354	3.004e-05
0.06598	2.858e-06	0.1016	2.175e-06
0.2639	7.079e-06	0.4065	3.474e-06
1.056	7.513e-06	1.626	7.312e-06
4.222	1.668e-05	6.503	2.055e-05
16.88	5.384e-05	25.99	4.989e-05
0.04583	4.540e-06	0.1183	2.453e-06
0.1833	6.942e-06	0.4731	4.244e-06
0.7333	7.529e-06	1.892	8.033e-06
2.933	2.641e-05	7.569	2.116e-05
11.72	5.422e-05	30.26	7.014e-05
0.07445	3.118e-06	0.1287	2.803e-06
0.2978	4.512e-06	0.5150	3.935e-06
1.191	9.060e-06	2.060	1.143e-05
4.764	2.223e-05	8.238	2.424e-05
19.04	5.553e-05	32.93	7.990e-05
0.1313	2.540e-06	0.1112	3.078e-06
0.5252	3.866e-06	0.4449	3.047e-06
2.101	9.998e-06	1.779	1.064e-05
8.402	2.648e-05	7.116	2.230e-05
33.59	7.082e-05	28.45	6.528e-05
0.1110	3.841e-06	0.1706	2.544e-06
0.4441	3.163e-06	0.6822	2.284e-06
1.776	5.878e-06	2.729	7.542e-06
7.105	2.321e-05	10.91	2.174e-05
28.40	8.090e-05	43.63	7.190e-05
0.09479	3.241e-06	0.08225	4.095e-06
0.3792	3.593e-06	0.3290	3.395e-06
1.517	4.663e-06	1.316	4.120e-06
6.066	1.789e-05	5.263	1.895e-05
24.25	9.614e-05	21.04	7.624e-05
0.04839	2.651e-06	0.04580	4.131e-06
0.1936	3.822e-06	0.1832	2.338e-06
0.7742	5.786e-06	0.7328	3.844e-06
3.096	1.067e-05	2.931	7.572e-06
12.38	3.836e-05	11.72	4.651e-05

Figure 4.8

Spatial frequency c/deg	$E_0$
0.25	9.800e-04
1	3.277e-05
4	2.678e-06

Figure 4.9

Number of components	$S_{\max}^{-2}A_c$ 0.25 c/deg JM open triangles	$S_{\max}^{-2}A_c$ 0.25 c/deg OU solid triangles	$S_{\max}^{-2}A_c$ 1 c/deg CT open circles	$S_{\max}^{-2}A_c$ 1 c/deg OU solid circles	$S_{\max}^{-2}A_c$ 4 c/deg CT open squares	$S_{\max}^{-2}A_c$ 4 c/deg OU solid squares
1	1.241e-03	1.143e-03	3.344e-05	4.498e-05	3.445e-06	2.604e-06
2	1.252e-03	1.543e-03	2.878e-05	3.762e-05	3.238e-06	2.231e-06
3	7.414e-04	1.292e-03	2.498e-05	4.881e-05	4.778e-06	2.454e-06
4	6.337e-04	1.866e-03	4.021e-05	3.107e-05	3.266e-06	2.655e-06
5	8.823e-04	9.484e-04	1.959e-05	2.709e-05	2.447e-06	2.517e-06
6	8.531e-04	1.668e-03	4.235e-05	2.963e-05	2.510e-06	1.698e-06
8	5.412e-04	6.116e-04	2.945e-05	3.875e-05	2.468e-06	2.511e-06
16	8.749e-04	6.751e-04	2.634e-05	3.556e-05	2.831e-06	2.308e-06

Figure 4.11 (A)

Square cycles $Af^2$	R.m.s. contrast sensitivity cosine 1 c/deg OU circles	R.m.s. contrast sensitivity sine 1 c/deg OU squares	R.m.s. contrast sensitivity cosine+sine 1 c/deg OU diamonds	R.m.s. contrast sensitivity random orientation 1 c/deg OU triangles	R.m.s. contrast sensitivity random phase 1 c/deg OU inverted triangles	R.m.s. contrast sensitivity random orientation+ phase 1 c/deg OU crosses
0.7935	21.77	16.55	20.11	21.16	16.52	20.04
3.174	30.24	18.20	19.48	23.87	17.59	32.14
12.69	29.19	22.41	32.06	30.71	29.37	31.87
50.62	36.64	39.63	38.65	41.30	40.49	40.50
200.5	37.99	50.09	51.53	50.78	43.80	44.45

Figure 4.11 (B)

Square cycles $Af^2$	R.m.s. contrast sensitivity cosine 4 c/deg HK circles	R.m.s. contrast sensitivity sine 4 c/deg HK squares	R.m.s. contrast sensitivity cosine+sine 4 c/deg HK diamonds	R.m.s. contrast sensitivity random orientation 4 c/deg HK triangles	R.m.s. contrast sensitivity random phase 4 c/deg HK inverted triangles	R.m.s. contrast sensitivity random orientation+phase 4 c/deg HK crosses
0.7935	17.51	11.36	13.28	16.09	9.081	10.58
3.174	18.22	15.85	17.47	23.33	15.89	23.37
12.69	26.99	24.59	31.58	27.17	32.35	30.53
50.62	48.47	34.15	37.10	33.96	41.36	29.47
200.5	43.08	47.86	50.48	43.69	41.71	36.87

Figure 4.12 (A)

Square cycles $Af^2$	R.m.s. contrast sensitivity cosine 1 c/deg OU circles	R.m.s. contrast sensitivity sine 1 c/deg OU squares	R.m.s. contrast sensitivity cosine+sine 1 c/deg OU diamonds	R.m.s. contrast sensitivity random orientation 1 c/deg OU triangles	R.m.s. contrast sensitivity random phase 1 c/deg OU inverted triangles	R.m.s. contrast sensitivity random orientation+phase 1 c/deg OU crosses
0.7935	31.24	29.88	34.44	33.48	41.12	25.62
3.174	50.19	35.01	35.28	40.74	40.17	36.28
12.69	70.97	42.52	42.68	46.42	55.78	48.88
50.62	59.53	63.66	78.41	61.82	64.68	65.54
200.5	72.29	79.01	73.74	81.08	90.59	94.00

Figure 4.12 (B)

Square cycles $Af^2$	R.m.s. contrast sensitivity cosine 2 c/deg HK circles	R.m.s. contrast sensitivity sine 2 c/deg HK squares	R.m.s. contrast sensitivity cosine+sine 2 c/deg HK diamonds	R.m.s. contrast sensitivity random orientation 2 c/deg HK triangles	R.m.s. contrast sensitivity random phase 2 c/deg HK inverted triangles	R.m.s. contrast sensitivity random orientation+phase 2 c/deg HK crosses
0.7935	22.59	18.66	13.13	28.33	49.11	22.39
3.174	37.18	36.30	24.71	29.15	33.35	28.94
12.69	46.39	29.01	29.87	38.26	56.04	31.40
50.62	40.53	47.51	46.95	47.48	80.45	47.65
200.5	48.23	49.23	38.49	66.86	105.1	55.51

Figure 4.13 (A)

Square cycles $Af^2$	R.m.s. contrast sensitivity cosine 0.5 c/deg TH circles	R.m.s. contrast sensitivity sine 0.5 c/deg TH squares	R.m.s. contrast sensitivity cosine+sine 0.5 c/deg TH diamonds	R.m.s. contrast sensitivity random orientation 0.5 c/deg TH triangles	R.m.s. contrast sensitivity random phase 0.5 c/deg TH inverted triangles	R.m.s. contrast sensitivity random orientation+phase 0.5 c/deg TH crosses
0.7935	11.16	10.25	16.79	22.06	21.28	16.94
3.174	25.50	18.11	46.06	35.74	21.70	18.91
12.69	42.49	24.90	46.51	44.81	33.92	40.45
50.62	64.09	52.50	57.09	60.14	69.91	55.62
200.5	52.93	42.45	71.21	66.80	64.27	63.23

Figure 4.13 (B)

Square cycles $Af^2$	R.m.s. contrast sensitivity cosine 1 c/deg OU circles	R.m.s. contrast sensitivity sine 1 c/deg OU squares	R.m.s. contrast sensitivity cosine+sine 1 c/deg OU diamonds	R.m.s. contrast sensitivity random orientation 1 c/deg OU triangles	R.m.s. contrast sensitivity random phase 1 c/deg OU inverted triangles	R.m.s. contrast sensitivity random orientation+phase 1 c/deg OU crosses
0.7935	41.15	27.79	40.32	31.58	34.54	42.50
3.174	74.51	45.04	67.20	44.45	44.87	47.66
12.69	97.04	71.18	67.82	79.97	64.68	64.70
50.62	123.2	113.1	109.9	82.91	89.33	84.58
200.5	109.3	112.7	133.3	116.6	126.0	103.7

Figure 4.14

Number of components	$A_c f^2$ open	$A_c f^2$ solid
1	21.34	
2	10.54	
3	5.562	5.917
4	5.563	
5	4.127	
6	5.273	3.870
8	5.325	
16	12.64	10.160

Figure 4.15

Stimulus type	$S^2_{\max N_e f^2}$ 3 components 1 c/deg OU circles	$S^2_{\max N_e f^2}$ 3 components 4 c/deg HK squares	$S^2_{\max N_e f^2}$ 6 components 1 c/deg OU circles	$S^2_{\max N_e f^2}$ 6 components 2 c/deg HK squares	$S^2_{\max N_e f^2}$ 16 components 0.5 c/deg TH squares	$S^2_{\max N_e f^2}$ 16 components 1 c/deg OU circles
Cosine	0.8543	1.640	0.8341	1.110	1.303	1.271
Sine	0.6481	1.140	0.6152	0.9073	0.7500	0.7680
Cosine+ sine	0.8319	1.472	0.4803	0.6169	1.387	1.084
Random orientation	0.9241	1.531	0.7075	1.240	1.370	0.7542
Random phase	0.6803	1.189	0.6077	0.7025	1.035	0.7659
Random orientation +phase	0.9723	1.198	0.4673	0.9665	0.8699	0.7716

Figure 4.16 (A)

Square cycles $Af^2/g(n)$	Efficiency cosine 1 c/deg OU circles	Efficiency sine 1 c/deg OU squares	Efficiency cosine+ sine 1 c/deg OU diamonds	Efficiency random orientation 1 c/deg OU triangles	Efficiency random phase 1 c/deg OU inverted triangles	Efficiency random orientation+ phase 1 c/deg OU crosses
3.009	5.194e-01	3.004e-01	4.435e-01	4.910e-01	2.992e-01	4.402e-01
12.03	2.507e-01	9.083e-02	1.409e-01	1.562e-01	8.480e-02	2.832e-01
48.10	5.844e-02	3.444e-02	7.503e-02	6.469e-02	5.916e-02	6.964e-02
191.9	2.307e-02	2.699e-02	2.568e-02	2.932e-02	2.817e-02	3.082e-02
760.3	6.262e-03	1.089e-02	1.152e-02	1.189e-02	8.326e-03	8.573e-03

Figure 4.16 (B)

Square cycles $Af^2/g(n)$	Efficiency cosine 4 c/deg HK circles	Efficiency sine 4 c/deg HK squares	Efficiency cosine+ sine 4 c/deg HK diamonds	Efficiency random orientation 4 c/deg HK triangles	Efficiency random phase 4 c/deg HK inverted triangles	Efficiency random orientation+ phase 4 c/deg HK crosses
3.009	7.563e-01	3.186e-01	4.353e-01	6.384e-01	2.034e-01	2.762e-01
12.03	2.048e-01	1.549e-01	1.882e-01	3.357e-01	1.557e-01	3.463e-01
48.10	1.123e-01	9.324e-02	1.538e-01	1.138e-01	1.614e-01	1.437e-01
191.9	9.058e-02	4.495e-02	5.308e-02	4.447e-02	6.596e-02	3.348e-02
760.3	1.790e-02	2.209e-02	2.458e-02	1.841e-02	1.678e-02	1.311e-02

Figure 4.17 (A)

Square cycles $Af^2/g(n)$	Efficiency cosine 1 c/deg OU circles	Efficiency sine 1 c/deg OU squares	Efficiency cosine+ sine 1 c/deg OU diamonds	Efficiency random orientation 1 c/deg OU triangles	Efficiency random phase 1 c/deg OU inverted triangles	Efficiency random orientation+ phase 1 c/deg OU crosses
3.408	3.853e-01	3.524e-01	3.251e-01	4.424e-01	4.634e-01	1.799e-01
13.63	2.486e-01	1.210e-01	8.533e-02	1.638e-01	1.106e-01	9.024e-02
54.48	1.244e-01	4.464e-02	3.116e-02	5.320e-02	5.334e-02	4.096e-02
217.4	2.193e-02	2.507e-02	2.642e-02	2.364e-02	1.798e-02	1.846e-02
861.2	8.163e-03	9.752e-03	5.899e-03	1.027e-02	8.902e-03	9.584e-03

Figure 4.17 (B)

Square cycles $Af^2/g(n)$	Efficiency cosine 2 c/deg HK circles	Efficiency sine 2 c/deg HK squares	Efficiency cosine+ sine 2 c/deg HK diamonds	Efficiency random orientation 2 c/deg HK triangles	Efficiency random phase 2 c/deg HK inverted triangles	Efficiency random orientation+ phase 2 c/deg HK crosses
3.408	4.185e-01	3.818e-01	1.892e-01	4.908e-01	6.611e-01	5.497e-01
13.63	3.790e-01	3.963e-01	1.674e-01	2.330e-01	7.621e-02	2.296e-01
54.48	1.475e-01	7.745e-02	6.114e-02	1.003e-01	5.382e-02	6.759e-02
217.4	2.549e-02	3.871e-02	3.780e-02	3.865e-02	2.774e-02	3.892e-02
861.2	9.994e-03	1.413e-02	6.365e-03	1.921e-02	1.186e-02	1.324e-02

Figure 4.18 (A)

Square cycles $Af^2/g(n)$	Efficiency cosine 0.5 c/deg TH circles	Efficiency sine 0.5 c/deg TH squares	Efficiency cosine+ sine 0.5 c/deg TH diamonds	Efficiency random orientation 0.5 c/deg TH triangles	Efficiency random phase 0.5 c/deg TH inverted triangles	Efficiency random orientation+ phase 0.5 c/deg TH crosses
1.577	1.398e-01	1.181e-01	2.026e-01	3.498e-01	3.254e-01	2.064e-01
6.306	1.828e-01	9.217e-02	3.815e-01	2.297e-01	8.468e-02	6.430e-02
25.21	1.271e-01	4.364e-02	9.748e-02	9.049e-02	5.185e-02	7.374e-02
100.6	7.302e-02	4.900e-02	3.708e-02	4.137e-02	5.560e-02	3.519e-02
398.5	1.292e-02	8.314e-03	1.497e-02	1.280e-02	1.220e-02	1.181e-02

Figure 4.18 (B)

Square cycles Af <sup>2</sup> /g(n)	Efficiency cosine 1 c/deg OU circles	Efficiency sine 1 c/deg OU squares	Efficiency cosine+ sine 1 c/deg OU diamonds	Efficiency random orientation 1 c/deg OU triangles	Efficiency random phase 1 c/deg OU inverted triangles	Efficiency random orientation+ phase 1 c/deg OU crosses
1.577	2.971e-01	1.355e-01	2.852e-01	1.750e-01	2.093e-01	3.168e-01
6.306	2.435e-01	8.901e-02	1.981e-01	8.667e-02	8.830e-02	9.963e-02
25.21	1.033e-01	5.560e-02	5.047e-02	7.018e-02	4.591e-02	4.549e-02
100.6	4.174e-02	3.519e-02	3.319e-02	1.890e-02	2.194e-02	1.967e-02
398.5	8.291e-03	8.812e-03	1.233e-02	9.442e-03	1.103e-02	7.462e-03

Figure 4.20 (A)

Area deg <sup>2</sup>	R.m.s. contrast sensitivity cosine 0.5+1.5 c/deg AS solid squares	R.m.s. contrast sensitivity sine 0.5+1.5 c/deg AS open squares	R.m.s. contrast sensitivity cosine 1+3 c/deg OU solid circles	R.m.s. contrast sensitivity sine 1+3 c/deg OU open circles	R.m.s. contrast sensitivity cosine 2+6 c/deg KL solid diamonds	R.m.s. contrast sensitivity sine 2+6 c/deg KL open diamonds
3.137	23.28	20.24				
5.576	24.04	26.59				
22.28	37.98	36.12				
88.73	55.52	59.57				
349.0	84.92	85.93				
0.7843			31.24	27.75		
1.394			34.83	35.61		
5.576			57.49	57.99		
22.28			106.2	116.0		
88.73			166.8	180.8		
0.1961					23.23	25.95
0.3486					34.38	25.93
1.394					43.12	51.42
5.576					77.74	87.53
22.28					116.1	108.2

Figure 4.20 (B)

Area deg <sup>2</sup>	R.m.s. contrast sensitivity cosine 0.5+1.5 c/deg AS solid squares	R.m.s. contrast sensitivity sine 0.5+1.5 c/deg AS open squares	R.m.s. contrast sensitivity cosine 1+3 c/deg OU solid circles	R.m.s. contrast sensitivity sine 1+3 c/deg OU open circles	R.m.s. contrast sensitivity cosine 2+6 c/deg KL solid diamonds	R.m.s. contrast sensitivity sine 2+6 c/deg KL open diamonds
3.137	24.78	18.65				
5.576	25.60	25.02				
22.28	38.79	45.39				
88.73	54.68	52.66				
349.0	79.41	79.60				
0.7843			25.43	33.29		
1.394			30.50	47.10		
5.576			53.85	56.87		
22.28			85.26	114.6		
88.73			154.8	186.3		
0.1961					23.74	25.15
0.3486					36.13	28.27
1.394					42.23	45.32
5.576					76.68	96.55
22.28					84.14	97.54

Figure 4.20 (C)

Area deg <sup>2</sup>	R.m.s. contrast sensitivity cosine 0.5+1.5 c/deg AS solid squares	R.m.s. contrast sensitivity sine 0.5+1.5 c/deg AS open squares	R.m.s. contrast sensitivity cosine 1+3 c/deg OU solid circles	R.m.s. contrast sensitivity sine 1+3 c/deg OU open circles	R.m.s. contrast sensitivity cosine 2+6 c/deg KL solid diamonds	R.m.s. contrast sensitivity sine 2+6 c/deg KL open diamonds
3.137	21.79	18.38				
5.576	25.02	29.68				
22.28	33.75	34.45				
88.73	52.10	53.31				
349.0	57.65	65.15				
0.7843			24.97	27.03		
1.394			33.49	30.61		
5.576			49.14	53.45		
22.28			80.55	72.20		
88.73			114.4	134.3		
0.1961					20.98	16.97
0.3486					23.91	26.96
1.394					35.60	30.84
5.576					50.77	77.71
22.28					68.80	77.25

Figure 4.20 (D)

Area deg <sup>2</sup>	R.m.s. contrast sensitivity cosine 0.5+1.5 c/deg AS solid squares	R.m.s. contrast sensitivity sine 0.5+1.5 c/deg AS open squares	R.m.s. contrast sensitivity cosine 1+3 c/deg OU solid circles	R.m.s. contrast sensitivity sine 1+3 c/deg OU open circles	R.m.s. contrast sensitivity cosine 2+6 c/deg KL solid diamonds	R.m.s. contrast sensitivity sine 2+6 c/deg KL open diamonds
3.137	22.58	14.93				
5.576	23.86	21.59				
22.28	32.51	31.49				
88.73	47.84	53.02				
349.0	68.14	63.02				
0.7843			24.57	30.36		
1.394			35.32	30.40		
5.576			50.17	53.22		
22.28			70.54	83.99		
88.73			109.3	102.9		
0.1961					20.73	14.63
0.3486					22.82	24.40
1.394					33.27	36.79
5.576					45.91	56.51
22.28					53.67	61.92

Figure 4.20 (E)

Area deg <sup>2</sup>	R.m.s. contrast sensitivity cosine 0.5+1.5 c/deg AS solid squares	R.m.s. contrast sensitivity sine 0.5+1.5 c/deg AS open squares	R.m.s. contrast sensitivity cosine 1+3 c/deg OU solid circles	R.m.s. contrast sensitivity sine 1+3 c/deg OU open circles	R.m.s. contrast sensitivity cosine 2+6 c/deg KL solid diamonds	R.m.s. contrast sensitivity sine 2+6 c/deg KL open diamonds
0.3486	10.01	9.834				
1.394	17.58	15.35				
3.137	19.61	17.46				
5.576	23.70	21.58				
22.28	33.71	33.05				
88.73	47.97	43.08				
349.0	69.80	70.02				
0.08715			14.71	14.38		
0.3486			23.48	23.82		
0.7843			29.77	23.64		
1.394			38.89	42.74		
5.576			53.15	61.49		
22.28			69.14	84.26		
88.73			107.3	108.5		
0.02179					10.29	9.623
0.08715					14.33	16.97
0.1961					18.48	16.25
0.3486					19.50	24.30
1.394					31.00	38.99
5.576					51.27	68.93
22.28					54.13	65.03

Figure 4.21

Relative contrast of the third harmonic	A <sub>c</sub> 0.5+1.5 c/deg AS squares	A <sub>c</sub> 1+3 c/deg OU circles	A <sub>c</sub> 2+6 c/deg KL diamonds
0	91.82	22.96	5.739
0.25	66.78	16.70	4.174
0.50	47.17	11.72	2.948
0.75	41.14	10.29	2.571
1	18.23	4.56	1.140

Figure 4.22

Relative contrast of the third harmonic	$S_{\max}$ 0.5+1.5 c/deg AS squares	$S_{\max}$ 1+3 c/deg OU circles	$S_{\max}$ 2+6 c/deg KL diamonds
0	99.42	157.2	121.5
0.25	86.29	138.1	105.5
0.50	70.34	102.9	73.04
0.75	63.50	97.56	62.95
1	55.51	87.50	55.43

Figure 4.23

Square cycles for grating sums $n^{2a}Af^2$	Normalised r.m.s. contrast sensitivity $Sn^af$ cosine 0.5+1.5 c/deg AS solid squares	Normalised r.m.s. contrast sensitivity $Sn^af$ sine 0.5+1.5 c/deg AS open squares	Normalised r.m.s. contrast sensitivity $Sn^af$ cosine 1+3 c/deg OU solid circles	Normalised r.m.s. contrast sensitivity $Sn^af$ sine 1+3 c/deg OU open circles	Normalised r.m.s. contrast sensitivity $Sn^af$ cosine 2+6 c/deg KL solid diamonds	Normalised r.m.s. contrast sensitivity $Sn^af$ cosine 2+6 c/deg KL open diamonds
0.7843	11.64	10.12	31.24	27.75	46.47	51.90
1.394	12.02	13.29	34.83	35.61	68.76	51.87
5.576	18.99	18.06	57.49	57.99	86.24	102.8
22.28	27.76	29.79	106.2	116.0	155.5	175.1
88.73	42.46	42.97	166.8	180.8	232.1	216.3
1.358	16.30	12.27	33.47	43.82	62.48	66.21
2.415	16.85	16.46	40.15	61.99	95.10	74.41
9.657	25.52	29.87	70.87	74.85	111.1	119.3
38.59	35.98	34.65	112.2	150.9	201.8	254.1
153.7	52.25	52.38	203.8	245.2	221.5	256.7
2.353	18.87	15.92	43.25	46.82	72.69	58.80
4.183	21.67	25.70	58.01	53.02	82.81	93.39
16.73	29.23	29.84	85.11	92.57	123.3	106.8
66.84	45.12	46.16	139.5	125.1	175.9	269.2
266.2	49.92	56.42	198.2	232.7	238.3	267.6
4.075	25.73	17.01	56.01	69.20	94.53	66.70
7.245	27.19	24.61	80.51	69.29	104.1	111.2
28.97	37.05	35.89	114.4	121.3	151.7	167.7
115.8	54.52	60.43	160.8	191.4	209.3	257.6
461.1	77.67	71.83	249.1	234.5	244.7	282.3
0.7844	15.02	14.75	44.14	43.13	61.75	57.74
3.137	26.36	23.02	70.43	71.47	85.97	101.8
7.059	29.42	26.19	89.30	70.93	110.9	97.51
12.55	35.55	32.36	116.7	128.2	117.0	145.8
50.18	50.56	49.57	159.4	184.5	186.0	233.9
200.5	71.96	64.62	207.4	252.8	307.6	413.6
798.6	104.7	105.0	322.0	325.6	324.8	390.2

Figure 4.24

Square cycles for grating sums $n^{2a}Af^2$	Energy threshold cosine 0.5+1.5 c/deg AS solid squares	Energy threshold sine 0.5+1.5 c/deg AS open squares	Energy threshold cosine 1+3 c/deg OU solid circles	Energy threshold sine 1+3 c/deg OU open circles	Energy threshold cosine 2+6 c/deg KL solid diamonds	Energy threshold cosine 2+6 c/deg KL open diamonds
0.7843	5.787e-03	7.661e-03	8.034e-04	1.019e-03	3.633e-04	2.911e-04
1.394	9.648e-03	7.888e-03	1.150e-03	1.100e-03	2.950e-04	5.183e-04
5.576	1.545e-02	1.708e-02	1.687e-03	1.658e-03	7.499e-04	5.273e-04
22.28	2.878e-02	2.500e-02	1.976e-03	1.657e-03	9.225e-04	7.277e-04
88.73	4.838e-02	4.726e-02	3.182e-03	2.716e-03	1.654e-03	1.904e-03
1.358	5.110e-03	9.020e-03	1.212e-03	7.075e-04	3.481e-04	3.099e-04
2.415	8.508e-03	8.907e-03	1.498e-03	6.285e-04	2.671e-04	4.361e-04
9.657	1.481e-02	1.081e-02	1.923e-03	1.724e-03	7.819e-04	6.788e-04
38.59	2.967e-02	3.200e-02	3.065e-03	1.696e-03	9.482e-04	5.981e-04
153.7	5.534e-02	5.508e-02	3.701e-03	2.556e-03	3.147e-03	2.342e-03
2.353	6.609e-03	9.282e-03	1.258e-03	1.074e-03	4.454e-04	6.806e-04
4.183	8.906e-03	6.330e-03	1.243e-03	1.488e-03	6.100e-04	4.796e-04
16.73	1.956e-02	1.877e-02	2.309e-03	1.952e-03	1.100e-03	1.466e-03
66.84	3.269e-02	3.123e-02	3.434e-03	4.273e-03	2.164e-03	9.234e-04
266.2	1.050e-01	8.222e-02	6.776e-03	4.918e-03	4.707e-03	3.733e-03
4.075	6.154e-03	1.408e-02	1.299e-03	8.510e-04	4.561e-04	9.161e-04
7.245	9.796e-03	1.196e-02	1.118e-03	1.509e-03	6.692e-04	5.856e-04
28.97	2.108e-02	2.247e-02	2.215e-03	1.969e-03	1.260e-03	1.030e-03
115.8	3.878e-02	3.157e-02	4.477e-03	3.158e-03	2.660e-03	1.746e-03
461.1	7.515e-02	8.787e-02	7.430e-03	8.388e-03	7.735e-03	5.810e-03
0.7844	3.477e-03	3.605e-03	4.025e-04	4.217e-04	2.057e-04	2.357e-04
3.137	4.514e-03	5.920e-03	6.324e-04	6.142e-04	3.994e-04	3.027e-04
7.059	8.157e-03	1.030e-02	8.851e-04	1.403e-03	1.199e-03	7.424e-04
12.55	9.925e-03	1.198e-02	9.218e-04	7.631e-04	6.326e-04	5.902e-04
50.18	1.961e-02	2.040e-02	1.974e-03	1.475e-03	1.782e-03	9.173e-04
200.5	3.856e-02	4.781e-02	4.660e-03	3.138e-03	2.121e-03	1.173e-03
798.6	7.162e-02	7.117e-02	7.702e-03	7.531e-03	7.604e-03	5.268e-03

Figure 4.25

Square cycles for grating sums $n^{2a}Af^2$	Efficiency cosine 0.5+1.5 c/deg AS solid squares	Efficiency sine 0.5+1.5 c/deg AS open squares	Efficiency cosine 1+3 c/deg OU solid circles	Efficiency sine 1+3 c/deg OU open circles	Efficiency cosine 2+6 c/deg KL solid diamonds	Efficiency cosine 2+6 c/deg KL open diamonds
0.7843	3.804e-01	2.874e-01	1.713e-01	1.351e-01	3.788e-01	4.726e-01
1.394	2.309e-01	2.791e-01	1.197e-01	1.251e-01	4.665e-01	2.655e-01
5.576	1.443e-01	1.289e-01	8.157e-02	8.300e-02	1.835e-01	2.609e-01
22.28	7.741e-02	8.806e-02	6.962e-02	8.304e-02	1.492e-01	1.891e-01
88.73	4.550e-02	4.659e-02	4.316e-02	5.067e-02	8.319e-02	7.226e-02
1.358	4.308e-01	2.470e-01	1.340e-01	1.945e-01	3.953e-01	4.440e-01
2.415	2.588e-01	2.502e-01	9.183e-02	2.189e-01	5.152e-01	3.155e-01
9.657	1.487e-01	2.036e-01	7.156e-02	7.983e-02	1.760e-01	2.027e-01
38.59	7.419e-02	6.963e-02	4.489e-02	8.114e-02	1.451e-01	2.300e-01
153.7	3.978e-02	3.997e-02	3.718e-02	5.384e-02	4.373e-02	5.876e-02
2.353	3.331e-01	2.372e-01	1.094e-01	1.282e-01	3.089e-01	2.022e-01
4.183	2.472e-01	3.478e-01	1.107e-01	9.247e-02	2.256e-01	2.869e-01
16.73	1.126e-01	1.173e-01	5.959e-02	7.049e-02	1.251e-01	9.387e-02
66.84	6.735e-02	7.050e-02	4.145e-02	3.220e-02	6.360e-02	1.490e-01
266.2	2.097e-02	2.678e-02	2.031e-02	2.798e-02	2.923e-02	3.686e-02
4.075	3.578e-01	1.564e-01	1.059e-01	1.617e-01	3.017e-01	1.502e-01
7.245	2.302e-01	1.841e-01	1.231e-01	9.118e-02	2.056e-01	2.350e-01
28.97	1.070e-01	9.798e-02	6.212e-02	6.990e-02	1.092e-01	1.335e-01
115.8	5.815e-02	6.975e-02	3.073e-02	4.357e-02	5.200e-02	7.882e-02
461.1	2.930e-02	2.506e-02	1.852e-02	1.640e-02	1.779e-02	2.368e-02
0.7844	6.331e-01	6.107e-01	3.419e-01	3.263e-01	6.690e-01	5.837e-01
3.137	4.877e-01	3.764e-01	2.176e-01	2.240e-01	3.445e-01	4.545e-01
7.059	2.732e-01	2.139e-01	1.555e-01	9.807e-02	1.148e-01	1.853e-01
12.55	2.245e-01	1.838e-01	1.493e-01	1.803e-01	2.175e-01	2.332e-01
50.18	1.136e-01	1.092e-01	6.971e-02	7.784e-02	7.721e-02	1.500e-01
200.5	5.779e-02	4.660e-02	2.953e-02	4.385e-02	6.485e-02	1.173e-01
798.6	3.074e-02	3.131e-02	1.786e-02	1.827e-02	1.807e-02	2.612e-02

Figure 5.4

Exposure duration	R.m.s. contrast sensitivity non-random TH open	R.m.s. contrast sensitivity random TH solid	R.m.s. contrast sensitivity non-random OU open	R.m.s. contrast sensitivity random OU solid
33.3	11.2	14.6	9.36	9.24
133	17.1	14.2	10.7	12.6
533	14.5	13.9	9.47	9.45

Figure 5.5

Exposure duration ms	Signal-to-noise ratio non-random TH open	Signal-to-noise ratio random TH solid	Signal-to-noise ratio non-random OU open	Signal-to-noise ratio random OU solid
33.3	21.8	26.1	16.8	26.5
133	14.4	22.9	17.2	19.4
533	16.9	25.8	17.6	25.9

Figure 5.6

Randomisation range deg	R.m.s. contrast sensitivity without noise KT open	R.m.s. contrast sensitivity with noise KT solid	R.m.s. contrast sensitivity without noise OU open	R.m.s. contrast sensitivity with noise OU solid
0	57.7	15.1	87.0	11.3
2.6	44.8	8.73	71.2	10.1
5.2	55.4	7.98	54.2	10.3
7.8	49.7	8.01	51.8	9.64

Figure 5.7

Randomisation range deg	Signal-to-noise ratio KT	Signal-to-noise ratio OU
0	3.42	4.58
2.6	5.90	5.11
5.2	6.46	4.98
7.8	6.44	5.35

Figure 5.8

Randomisation range deg	Equivalent noise KT	Equivalent noise OU
0	4.264e-05	9.912e-06
2.6	2.292e-05	1.189e-05
5.2	1.231e-05	2.197e-05
7.8	1.551e-05	2.086e-05

Figure 5.9

Orientation range deg	R.m.s. contrast sensitivity without noise 0.5 c/deg OL open	R.m.s. contrast sensitivity with noise 0.5 c/deg OL solid	R.m.s. contrast sensitivity without noise 2 c/deg OU open	R.m.s. contrast sensitivity with noise 2 c/deg OU solid	R.m.s. contrast sensitivity without noise 8 c/deg JM open	R.m.s. contrast sensitivity with noise 8 c/deg JM solid
0	584.9	85.06	490.3	83.80	128.5	34.31
11.25	434.4	70.61	323.8	72.76	101.9	35.12
22.5	371.4	60.78	344.1	74.18	92.11	31.17
45	321.4	54.88	302.2	68.13	97.59	26.59
90	232.2	40.38	276.8	53.49	90.65	28.60
180	249.7	38.06	258.2	47.68	77.83	28.60

Figure 5.10

Orientation range deg	Signal-to-noise ratio 0.5 c/deg OL	Signal-to-noise ratio 2 c/deg OU	Signal-to-noise ratio 8 c/deg JM
0	3.66	3.81	4.65
11.25	4.41	4.38	4.55
22.5	5.13	4.30	5.12
45	5.68	4.68	6.01
90	7.72	5.96	5.58
180	8.19	6.69	5.58

Figure 5.11

Orientation range deg	Equivalent noise 0.5 c/deg OL	Equivalent noise 2 c/deg OU	Equivalent noise 8 c/deg JM
0	1.344e-05	1.485e-06	7.457e-07
11.25	1.688e-05	2.082e-06	1.307e-06
22.5	1.712e-05	1.908e-06	1.255e-06
45	1.868e-05	2.098e-06	7.781e-07
90	1.939e-05	1.519e-06	1.073e-06
180	1.479e-05	1.383e-06	1.515e-06

Figure 5.13

Square cycles $Af^2$	R.m.s. contrast sensitivity non-random 0.5 c/deg KT open circles	R.m.s. contrast sensitivity random orientation 0.5 c/deg KT solid circles	R.m.s. contrast sensitivity non-random 0.5 c/deg PR open squares	R.m.s. contrast sensitivity random phase 0.5 c/deg PR solid squares	R.m.s. contrast sensitivity non-random 0.5 c/deg PR open triangles	R.m.s. contrast sensitivity random orientation+ phase 0.5 c/deg PR solid triangles
0.7936	104.3	83.21	106.2	78.02	106.2	79.48
3.174	262.9	144.7	161.1	110.2	161.1	119.9
12.69	352.4	239.4	285.4	207.2	285.4	200.6
50.75	657.6	412.0	396.0	299.9	396.0	313.7
202.5	869.0	451.8	494.8	388.4	494.8	379.2

Figure 5.14

Square cycles $Af^2$	R.m.s. contrast sensitivity non-random 2 c/deg OU open circles	R.m.s. contrast sensitivity random orientation 2 c/deg OU solid circles	R.m.s. contrast sensitivity non-random 2 c/deg OU open squares	R.m.s. contrast sensitivity random phase 2 c/deg OU solid squares	R.m.s. contrast sensitivity non-random 2 c/deg OU open triangles	R.m.s. contrast sensitivity random orientation+ phase 2 c/deg OU solid triangles
0.7936	187.3	113.0	187.3	144.9	187.3	93.51
3.174	286.7	185.2	286.7	225.2	286.7	165.0
12.69	472.9	287.8	472.9	335.0	472.9	275.4
50.75	555.0	429.6	555.0	493.0	555.0	372.8
202.5	607.5	455.3	607.5	594.1	607.5	451.8

Figure 5.15

Square cycles $Af^2$	R.m.s. contrast sensitivity non-random 8 c/deg JM open circles	R.m.s. contrast sensitivity random orientation 8 c/deg JM solid circles	R.m.s. contrast sensitivity non-random 8 c/deg OU open squares	R.m.s. contrast sensitivity random phase 8 c/deg OU solid squares	R.m.s. contrast sensitivity non-random 8 c/deg OU open triangles	R.m.s. contrast sensitivity random orientation+ phase 8 c/deg OU solid triangles
0.7936	37.26	26.58	32.11	25.93	32.11	18.69
3.174	88.01	55.06	65.52	58.43	65.52	40.19
12.69	189.1	88.97	144.4	106.0	144.4	71.93
50.75	305.8	165.0	183.4	187.0	183.4	126.3
202.5	382.4	201.0	308.6	242.3	308.6	171.1

Figure 5.16

Square cycles $Af^2$	R.m.s. contrast sensitivity non-random 0.5 c/deg HN open circles	R.m.s. contrast sensitivity random orientation 0.5 c/deg HN solid circles	R.m.s. contrast sensitivity non-random 0.5 c/deg PR open squares	R.m.s. contrast sensitivity random phase 0.5 c/deg PR solid squares	R.m.s. contrast sensitivity non-random 0.5 c/deg PR open triangles	R.m.s. contrast sensitivity random orientation+ phase 0.5 c/deg PR solid triangles
0.7936	78.986	53.952	123.94	101.45	123.94	65.292
3.174	136.19	82.501	215.94	121.93	215.94	120.69
12.69	167.60	124.34	209.32	169.90	209.32	200.30
50.75	207.26	184.97	272.94	252.93	272.94	274.39
202.5	265.80	254.03	398.42	317.70	398.42	314.30

Figure 5.17

Square cycles $Af^2$	R.m.s. contrast sensitivity non-random 2 c/deg OU open circles	R.m.s. contrast sensitivity random orientation 2 c/deg OU solid circles	R.m.s. contrast sensitivity non-random 2 c/deg OU open squares	R.m.s. contrast sensitivity random phase 2 c/deg OU solid squares	R.m.s. contrast sensitivity non-random 2 c/deg OU open triangles	R.m.s. contrast sensitivity random orientation+ phase 2 c/deg OU solid triangles
0.7936	149.77	86.868	143.06	115.04	143.06	120.52
3.174	279.94	191.15	310.11	177.36	310.11	172.87
12.69	315.63	231.00	385.61	236.24	385.61	237.34
50.75	436.58	278.55	370.16	287.13	370.16	332.14
202.5	412.83	334.14	409.01	330.17	409.01	449.49

Figure 5.18

Square cycles $Af^2$	R.m.s. contrast sensitivity non-random 8 c/deg HN open circles	R.m.s. contrast sensitivity random orientation 8 c/deg HN solid circles	R.m.s. contrast sensitivity non-random 8 c/deg MK open squares	R.m.s. contrast sensitivity random phase 8 c/deg MK solid squares	R.m.s. contrast sensitivity non-random 8 c/deg MK open triangles	R.m.s. contrast sensitivity random orientation+ phase 8 c/deg MK solid triangles
0.7936	60.098	44.107	24.194	12.448	24.194	11.615
3.174	146.47	87.927	42.294	20.334	42.294	28.537
12.69	176.58	114.56	72.231	36.940	72.231	30.623
50.75	248.30	158.71	70.499	48.845	70.499	50.999
202.5	391.06	256.04	89.282	62.194	89.282	59.789

Figure 5.19

Square cycles $Af^2$	R.m.s. contrast sensitivity non-random 0.5 c/deg KT open circles	R.m.s. contrast sensitivity random orientation 0.5 c/deg KT solid circles	R.m.s. contrast sensitivity non-random 0.5 c/deg PR open squares	R.m.s. contrast sensitivity random phase 0.5 c/deg PR solid squares	R.m.s. contrast sensitivity non-random 0.5 c/deg PR open triangles	R.m.s. contrast sensitivity random orientation+ phase 0.5 c/deg PR solid triangles
0.7936	114.53	108.48	122.02	88.522	122.02	121.76
3.174	240.91	183.30	242.34	150.61	242.34	136.85
12.69	384.16	278.44	370.03	226.89	370.03	218.70
50.75	439.21	329.80	462.89	233.29	462.89	253.91
202.5	431.42	349.50	429.96	292.28	429.96	303.79

Figure 5.20

Square cycles $Af^2$	R.m.s. contrast sensitivity non-random 2 c/deg OU open circles	R.m.s. contrast sensitivity random orientation 2 c/deg OU solid circles	R.m.s. contrast sensitivity non-random 2 c/deg OU open squares	R.m.s. contrast sensitivity random phase 2 c/deg OU solid squares	R.m.s. contrast sensitivity non-random 2 c/deg OU open triangles	R.m.s. contrast sensitivity random orientation+ phase 2 c/deg OU solid triangles
0.7936	185.94	130.86	185.94	120.44	185.94	135.74
3.174	308.25	184.25	308.25	206.92	308.25	226.32
12.69	432.85	327.28	432.85	256.05	432.85	330.83
50.75	573.17	370.88	573.17	319.81	573.17	342.03
202.5	583.07	431.70	583.07	402.32	583.07	351.18

Figure 5.21

Square cycles $Af^2$	R.m.s. contrast sensitivity non-random 8 c/deg JM open circles	R.m.s. contrast sensitivity random orientation 8 c/deg JM solid circles	R.m.s. contrast sensitivity non-random 8 c/deg MK open squares	R.m.s. contrast sensitivity random phase 8 c/deg MK solid squares	R.m.s. contrast sensitivity non-random 8 c/deg MK open triangles	R.m.s. contrast sensitivity random orientation+ phase 8 c/deg MK solid triangles
0.7936	48.743	40.974	27.061	22.275	27.061	23.469
3.174	81.678	61.155	50.856	37.612	50.856	33.128
12.69	157.54	113.19	84.200	54.866	84.200	57.567
50.75	220.16	144.96	121.34	67.410	121.34	66.867
202.5	228.92	174.98	105.49	97.830	105.49	89.890